

RECEIVED
FEB 14 1939

Library *L. M. a L.*

Copy 2

TECHNICAL NOTES

NATIONAL ADVISORY COMMITTEE FOR AERONAUTICS

No. 684

43.1.3
4.2
4.2

EXPERIMENTAL STUDY OF DEFORMATION AND OF EFFECTIVE WIDTH
IN AXIALLY LOADED SHEET-STRINGER PANELS

By Walter Ramberg, Albert E. McPherson, and Sam Levy
National Bureau of Standards

Washington
February 1939

NATIONAL ADVISORY COMMITTEE FOR AERONAUTICS

TECHNICAL NOTE NO. 684

EXPERIMENTAL STUDY OF DEFORMATION AND OF EFFECTIVE WIDTH
IN AXIALLY LOADED SHEET-STRINGER PANELS

By Walter Ramberg, Albert E. McPherson, and Sam Levy

SUMMARY

The deformation of two sheet-stringer panels subjected to end compression under carefully controlled end conditions was measured at a number of points and at a number of loads, most of which were above the load at which the sheet had begun to buckle. The two panels were identical except for the sheet, which was 0.070-inch 24ST Alclad for specimen 1 and 0.025-inch 24ST aluminum alloy for specimen 6. A technique was developed for attaching Tuckerman optical strain gages to the sheet without disturbing the strain distribution in the sheet by the method of attachment. This technique was used to explore the strain distribution in the sheet at various loads. The twisting and the bending of the stringers were measured by means of pointers attached to the stringers. The shape of the buckles in the sheet of specimen 6 was recorded at two loads by means of plaster casts.

The sheet and the stringer loads at failure are compared with the corresponding loads for five similar panels tested at the Navy Model Basin. A detailed comparison is made between the measured deformation of the buckled sheet and the deformation calculated from approximate theories for the deformation in a rectangular sheet with freely supported edges buckling under end compression advanced by Timoshenko, Frankland, and Marguerre. The measured effective width for the specimens is compared with the effective width given by nine different relations for effective width as a function of the edge stress σ divided by the buckling stress σ_{cr} of the sheet.

The analysis of the measured stringer deformation is confined to an application of Southwell's method of plotting deformation against deformation over load. If the stringer approaches instability in accordance with Southwell's relation, the deformation will be a linear function

of the deformation divided by the load and the slope of the straight line obtained will be equal to the elastic buckling load. A good check with the observed ultimate load was obtained from a plot of the twisting deformation and of bending deformation as indicated by the pointer readings and of bending deformation as measured by differences in extreme fiber strains in those cases in which all observed points could be brought to scatter about a common straight line. It was concluded that the stringer failure in both specimens was due to an instability in which the stringer was simultaneously twisted and bent as a column.

INTRODUCTION

The strength of sheet-stringer panels in end compression has become a problem of importance with the increasing use of stiffened sheet to carry compressive loads in box beams for airplane wings and in other types of monocoque construction.

The buckling of the sheet between stringers in a panel under end compression, the strain distribution in the sheet, and the effective width of the sheet as a function of the stringer stress, have been considered from a theoretical point of view by a number of authors (references 1 to 24). Experimental studies confirming this theoretical work have been few in number and restricted in scope (references 25 to 30). The present paper gives the results of an experimental study under carefully controlled end conditions of two sheet-stringer panels in end compression, which was carried out at the National Bureau of Standards for the Bureau of Aeronautics of the Navy Department.

The tests had as their purpose (1) a determination of the strain-distribution in these panels, (2) a comparison of their strength with the strength of similar panels tested at the Navy Model Basin, and (3) a comparison of the observed deformations with those predicted from existing methods of analysis.

In connection with this study, convenient procedures were developed for measuring the strains in the buckled sheet, for observing the shape of the buckles, and for following the deformation of the stringers. The observed

results were compared with various theories. The comparison suggests certain modifications in the theoretical attack that would probably lead to better agreement between the calculated and the observed deformations of the sheet.

The authors are indebted to the Navy Department for permission to publish this work. They also acknowledge with pleasure the close cooperation with members of the Structures Section of the Bureau of Aeronautics and the experimental model basin of the Bureau of Construction and Repair, Navy Department, and, in particular, the many valuable suggestions received from Dr. J. M. Frankland of the Structures Section.

SPECIMENS

The two test specimens are described in table I and in figure 1.

Young's modulus, the yield strength in tension, and the tensile strength of each sheet and of each one of the six stringers, had been obtained by the Navy Department with Huggenberger extensometers. They are summarized in table II.

The properties of sheets and stringers are seen to be nearly uniform except the low value of Young's modulus for the Alclad sheet of specimen 1, which is, however, in agreement with published data (reference 31).

In addition to the tensile test, flat-end-column tests were made at the model basin on four stringers ranging in length from 2 to 6 inches. The maximum loads for these specimens are plotted against length in figure 2. They range from 6,650 pounds for the 2-inch specimen to 5,500 pounds for the 6-inch specimen.

Flat-end-column tests on two additional stringer specimens, 5 and 8 inches in length, were made at the National Bureau of Standards. These specimens were cast in Wood's metal to a depth of $3/8$ inch at each end as shown in figure 3A. Figure 3 also shows both specimens after failure. Figures 4 and 5 give the results of extreme fiber-strain measurements at the midlength of each stringer. The strains are practically identical nearly up to failure, thus showing that the stress distribution was very nearly

uniform over the section of the specimen and that failure must have occurred quite suddenly. Additional readings of twist on the short specimen showed that its failure was primarily one of torsional instability; this fact is also brought out by the final failure, which left the center line of the specimen practically straight. The failure of the 8-inch specimen, on the other hand, was principally due to column action; the center portion was severely bent after failure. The maximum loads are shown in figure 2 for comparison with value obtained at the model basin. They are a few percent higher; this discrepancy is probably due to the restraint of the ends by the Wood's metal.

TESTS

Loading

Figure 6 shows specimen 1 assembled for a compressive test in the horizontal hydraulic testing machine of 2,300,000 pounds capacity. The following procedure was used for mounting the specimen. Each end of the specimen was centered on the rigid steel block A in such a manner as to make the ends of the specimen equidistant from the ends of the block and to make the vertical axis through the centroid of the entire cross section of the specimen pass through the center of the face of block A, which was in contact with the specimen. Copper pins driven into holes in the contact faces of blocks A provided keys for holding Wood's metal. In order to hold the specimen in the centered position and to provide support against crinkling of the sheet, Wood's metal was poured around the ends of the specimen and the pins to a depth of $3/8$ inch. Later measurements showed that the centroid of the sheet-stringer section for specimen 1 lay 0.057 inch above the point halfway between the ends, which introduced a small bending moment due to eccentric application of load that had to be considered in analyzing the results of the test. Each steel block A was centered on the faceplate B of the loading head C with the help of a dowel fitting into a central hole in both A and B. The loading head C and the knife-edge support G were taken from a bell-crank fixture of 75,000 pounds capacity for testing wing beams under combined axial and transverse loads. The faceplate B was free to turn about a vertical axis by being placed in a cylindrical bearing cut in the loading head C. It was

also free to turn about the horizontal axis defined by the knife edge. This arrangement assured that the stress distribution over the end section of the specimen would be uniform at loads below those producing buckling of the sheet (except, in the case of specimen 1, the small bending moment due to the eccentricity already mentioned). The cylindrical bearings in the loading heads C were locked before the buckling load of the sheet was reached to hold the ends fixed against rotation about a vertical axis.

The edges of the sheet parallel to the load were supported by two pairs of bars D designed to approach as closely as practicable a condition of simple support (zero displacement normal to the plane of the sheet and zero bending moment). It is realized that these conditions of support did not exactly reproduce those at the stringers; however, the tests indicated that they were a satisfactory approximation. Figure 7 shows the construction of the edge-support bars. The bars were separated with spacers of thickness shown in figure 7. This allowed the sheet to slip in to the point of tangency with the two curved faces of the bars. The two pairs of bars D were then placed a constant distance apart with the help of the spreader bars E (fig. 6), allowing a small clearance between the spacers and the sheet in order to permit expansion of the sheet under the action of the compressive load. The whole framework D and E supporting the edges of the sheet was carried by a pair of rollers F resting on the end blocks A (fig. 6).

Measurement of Strain

Attachment of strain gages.— Several schemes were considered for attaching a large number of strain gages to the sheet without disturbing the strain distribution in the sheet by the method of attachment. Figures 8 and 9 illustrate the scheme that was finally adopted because of its relative simplicity and convenience. Each gage and its mate on the opposite side of the sheet were held directly against the sheet either by a wire or by a fork formed of aluminum-alloy sheet bearing and rocking on a roller, which in turn rested on the strain gage. The ends of the wire or of the fork, as the case might be, were held by stretched rubber bands whose sheet end was anchored to an aluminum-alloy hook attached to the sheet surface of the specimen. A particularly firm attachment of the anchoring

patch was obtained by first varnishing the specimen with a spar varnish, then placing on it a patch of Scotch tape, varnishing the edges of the Scotch tape down again to prevent peeling under sustained tension, and finally cementing the anchor piece of sheet metal to the patch with a drop of hot De Khotinsky cement. The intermediate patch of Scotch tape prevented spalling off of the anchoring patch even with severe buckles in the sheet.

Correction of readings for bowing of median fiber.-

A correction had to be applied to the average of the measured strains in order to give the actual median fiber strain in those cases in which the buckles were very severe. The average of the extreme fiber extensions or contractions does actually give the extension or contraction at the median fiber with great accuracy. Part of the contraction, however, is due to the bowing of the median fiber (fig. 10) and an amount equal to the shortening

$$\widehat{AA'} - \overline{AA'}$$

must be added to the average extensions to give the extensions due to strain only

$$\epsilon = \frac{\epsilon_1 + \epsilon_2}{2} + \frac{\widehat{AA'} - \overline{AA'}}{l} \quad (1)$$

where ϵ_1 and ϵ_2 are the measured extreme fiber extensions per unit length as given by the two strain gages attached to each side of the sheet. Assume that the radius of curvature r of the buckle remains constant over the gage length l . The shortening due to bowing is then, from figure 10,

$$\begin{aligned} \widehat{AA'} - \overline{AA'} &= r\varphi - 2r \sin \varphi/2 = r\varphi - 2r \left(\frac{\varphi}{2} - \frac{\varphi^3}{48} + \frac{1}{120} \frac{\varphi^5}{32} - \dots \right) \\ &= \frac{1}{24} r\varphi \left(\varphi^2 - \frac{\varphi^4}{80} + \dots \right) = \frac{l}{24} \left(\frac{l}{r} \right)^2 \left[1 - \frac{1}{80} \left(\frac{l}{r} \right)^2 + \dots \right] \quad (2) \end{aligned}$$

The radius of curvature r may be calculated from the difference in extreme fiber extensions per unit length by using

the well-known relation

$$\frac{1}{r} = \frac{\epsilon_1 - \epsilon_2}{h} \quad (3)$$

where h is the thickness of the sheet. Inserting this relation in equation (2) and the resulting expression in equation (1) gives the following relation between the median fiber strain ϵ and the measured extreme fiber extensions per unit length ϵ_1 and ϵ_2 :

$$\epsilon = \frac{\epsilon_1 + \epsilon_2}{2} + \left[\frac{1}{24} \left(\frac{l}{h} \right)^2 (\epsilon_1 - \epsilon_2)^2 \right] \left[1 - \frac{1}{80} \left(\frac{l}{h} \right)^2 (\epsilon_1 - \epsilon_2)^2 + \dots \right] \quad (4)$$

The correction that must be added to the average extension per unit length in order to give the strain at the median fiber is given by the second term on the right-hand side of equation (4). It may be calculated from the known gage length l , the sheet thickness h , and the measured extreme fiber extensions per unit length ϵ_1 and ϵ_2 .

Observed strain distributions.— The strain distribution in specimen 1 was measured at the locations shown in figure 9 with nine pairs of 1-inch Tuckerman optical strain gages attached to the sheet and three pairs of 2-inch Tuckerman optical strain gages attached to the stringers and the portion of the plate to which the stringers were rivoted. An attempt was made in a preliminary run to measure the axial strains at four stations between adjacent stringers, as shown in figure 6. It was found, however, that this procedure placed the gages so close to each other that several of them interfered with one another as soon as the plate began to buckle. All gages functioned properly with the distribution shown in figure 9 up to loads well beyond that required to buckle the sheet.

Figure 11 shows the distribution of axial median fiber strain along the transverse center line of specimen 1 at compressive loads ranging from 5,000 to 25,000 pounds. The median fiber strain was computed from the strains indicated by the two strain gages placed on opposite sides of the specimen, the correction for bowing (equation (4)) being made in those cases where the bowing was appreciable. The median fiber strains so obtained show a consistent behavior although the extreme fiber strains were in some cases very different from one another, owing to the bending produced

by the buckles. The amount and irregular nature of this bending for the 25,000-pound load can be seen from the plot of extreme fiber strains shown in figure 12. The extreme fiber strains are close to each other at the stringers only. The values of strain on the stringer side shown for these points were actually measured on the extreme fiber of the stringer; reducing to the extreme fiber of the sheet would bring the strains still closer together. Figure 12 emphasizes the necessity of measuring strains on opposite sides of the sheet in tests of this type. Figure 11 shows that the axial strain was approximately uniform up to loads of around 13,000 pounds. Beyond this load, the stringers took an increasing proportion of the load while the sheet was relieved of part of its share of the load by the formation of buckles.

The increase in strain on stringer A as compared to stringers B and C may be accounted for by the presence of the small moment $M_e = eP = 0.057 P$ inch-pound due to eccentric loading. This moment will produce a bending strain at a distance from the centroid (fig. 11) given approximately by $\Delta\epsilon_x = M_e x / EI$ for loads too low to produce buckling of the sheet. The resultant strain ϵ_x may be calculated by adding the bending strain to the axial strain:

$$\epsilon_x = \frac{P}{AE} \left(1 + ex \frac{A}{I} \right) \quad (5)$$

With the numerical values $A = 1.51$ sq. in., $E = 10.4 \times 10^6$ lb./sq. in., $I = 28.0$ in.⁴, and $e = 0.057$ in., this equation becomes

$$\epsilon_x = \frac{1}{15.7 \times 10^6} P(1 + 0.00307 x) \quad (6)$$

The corresponding straight lines are shown dotted in figure 11 for loads of 5,000, 9,000, and 13,000 pounds. The agreement between observed and calculated strains below the load producing buckles in the sheet is seen to be satisfactory. The simple beam formula (equation (6)) ceases to describe the strain distribution for loads equal to or greater than 17,000 pounds. Beginning with this load, the axial strain changes relatively slightly at a point midway between stringers while it increases rapidly near the stringers. The load carried by the sheet becomes

a decreasing proportion of the total load and the strain distribution takes on a characteristic wave pattern.

It would not be correct to conclude from the fairly regular wave pattern of the axial median fiber strains that the extreme fiber strains would be equally symmetrical. Figure 12, which shows both the axial extreme fiber strains and the median fiber strains along the transverse center line of specimen 1 for the 25,000-pound load, indicates almost no bending between stringers A and B, considerable bending between stringers B and C, and even more bending between stringer C and the outside edge of the specimen. A nodal line in the wave pattern between A and B was apparently associated with a crest between C and the edge; the buckle pattern in a given bay between two stringers seemed to be independent of the buckle pattern in adjacent bays up to a load of 25,000 pounds.

The beginning of buckling in the sheet was indicated by a sudden increase in the bending strain as measured by the difference in reading on strain gages on opposite sides of the sheet. This is clearly shown in figure 13 for the readings of the transverse strain gages. The bending strain increased ten times as the stringer stress increased 17 percent from 12,000 to 14,000 pounds per square inch.

All the strain gages were removed from the sheet at a load of 26,000 pounds and only the three pairs of gages shown in figure 14 were kept on to indicate stringer strains for loads above 26,000 pounds. The strain readings on the stringer gages are plotted against load in figure 15.

Figure 16 shows the axial strain distribution for specimen 6. Buckling of the sheet in the case of this specimen was observed at a load between 1,000 and 2,600 pounds corresponding to an average stress P/A between 1,260 and 3,300 pounds per square inch. With the progress of buckling, the average compressive strain at a section midway between the stringers decreased slowly until it actually turned into a small tensile strain for two of the bays.

The axial extreme fiber strains along the transverse center line of specimen 6 are shown for a load of 10,900 pounds in figure 17. As in the case of specimen 1, there seems to be no transfer of deformation due to buckles across the stringers; the buckle pattern in a given bay between two stringers seems to be unaffected by the buckle pattern of adjacent bays up to a load of 10,900 pounds.

The measurements of axial strain along the transverse center line of specimen 6 were followed by measurements of transverse and of axial strain in other portions of the specimen. In the course of these measurements, it appeared that the strain readings at a given load and a given location could be repeated within the observational error in successive tests. It was concluded that the measured strain distributions could be superposed on each other just as if they had all been determined simultaneously and that they could be applied in calculating stresses from strains.

The distribution of axial median fiber strains along the transverse center line was obtained from strain gages mounted on the specimen in the same locations as shown in figure 9 for specimen 1. Transverse strains were measured along three 1-inch gage lines on the transverse center line as shown in figures 18 and 19. The results of these measurements for bay 3 (between stringers S and R) are shown graphically in figure 20.

Figure 21 shows the distribution of both axial and transverse median fiber strain along an axial line midway between two stringers as obtained from strain gages mounted as shown in figures 19 and 22.

Three 2-inch strain gages were mounted on stringer R as shown in figure 22 to measure the variations of stringer strain along a buckle. The resulting average strains were found to be nearly constant; the gages apparently covered too large a portion of a buckle to indicate the variation of strain along the buckle.

All strain gages were removed from the sheet at a load of 12,500 pounds and only three pairs of gages were kept on the three stringers, as shown in figure 14 for specimen 1, to give values of the stringer strains for loads above 12,500 pounds. The strains in the individual stringers are shown in figure 23.

Shape of Buckle from Plaster Casts

The analysis of test results from the first specimen showed the importance of an experimental determination of the shape of the buckles in the sheet. It was decided, accordingly, to attempt plaster of paris casts of the contours after buckling of the sheet of specimen 6. Good plaster of paris casts of the sheet side of specimen 6 were obtained by the following method.

The specimen was very lightly greased with soft cup grease; a cover was placed between the sheet side of the specimen and the vertical suspension members E (fig. 14) to form a backboard for the plaster cast. A piece of paper was inserted between the backboard and the cast to prevent sticking of the plaster to the backboard. Scotch tape was used to seal the plaster container and to attach it to the specimen. The plaster was poured slowly into the container and was allowed to harden for 5 to 10 minutes; the cast was then removed from the specimen. Figure 24 shows sections of plaster casts obtained in this manner. Contours of the casts were measured as follows. The cast was fastened to the table of a milling machine so that the rivet lines were parallel to the longitudinal feed screw. A dial micrometer was attached to the spindle to measure the change in vertical distance between the surface of the cast and the spindle, from which the elevation of the measured point on the cast was computed. The position of the measured point in a horizontal plane was determined with the longitudinal and cross feed screws of the milling machine.

Some of the results of the contour measurements are shown in figures 25 to 28.

Figure 25 shows the deflection at a load of 6,800 pounds along lines parallel to the stringers extending the length of a complete buckle. The deflection is nearly sinusoidal except for lines close to the stringers. At the stringer, only the small buckles of the sheet between rivets remain.

Figure 26 shows the deflections at a load of 6,800 pounds along lines extending at right angles to the load from stringer to stringer. The deflection in the transverse direction is seen to deviate considerably from a sine curve. The slope of the curve decreases as the stringer is approached, owing to the restraining moment from the torsionally stiff stringer.

Figures 27 and 28 show deflections at loads of 6,800 and 10,900 pounds, respectively, along transverse and axial lines passing through the crest of a buckle. The approximately 60-percent increase in load produces an increase in deflection of about 30 percent without a noticeable change in the shape of the buckle.

Deformation of Stringers from Pointer Readings

It appeared desirable to follow the development of failure in the stringers and to obtain a qualitative picture of the type of failure.

The two strain gages placed on each stringer, one on the sheet side (fig. 14) and the other on the stringer side (fig. 9), will measure only the extreme fiber strains in the stringer; they will not indicate the amount of twist in the stringer, neither will they give a clear picture of the amount and the type of buckling.

In order to get a picture of the twisting and the buckling of the stringer up to failure, it was suggested by Dr. J. M. Frankland of the Bureau of Aeronautics that pairs of pointers should be attached to the outstanding flange of each Z-stringer. The displacements of these pointers would be a measure of the relative angular displacement of the sections to which they were fastened.

Two types of pointers were employed. The type used on specimen 1 is shown diagrammatically in figure 29. The pointers consisted of polished air rifle shot mounted on the ends of two wires, one normal to the sheet with coordinates b_1 , c_1 relative to the centroid of the stringer and the other parallel to the sheet with coordinates b_2 , c_2 . Figure 30 shows a photograph of the installation on specimen 1. The highlights on the balls served as reference points for measuring the distances from each ball to one of the horizontal and one of the vertical reference wires A-A, B-B connected to the heads of the machine. The photographs were made on glass plates with a highly corrected lens working at F32; measurements were made from the plate by means of a Zeiss traveling microscope. The least measurable relative displacement was of the order of 0.002 inch. A displacement of 0.002 inch corresponded to a twist of 0.0004 radian.

Since there are two pointers at each section, four displacements may be read: two displacements u_1 , u_2 in a horizontal direction (fig. 29) and two displacements v_1 , v_2 in a vertical direction. From these four displacements and the known axial strain ϵ_x in the stringer, the twists θ_x , θ_y , θ_z about three axes through the centroid may be computed for a stringer section at a dis-

tance x from the transverse center line by substituting in the following formulas:

$$\left. \begin{aligned} \epsilon_x &= \frac{v_2 - v_1}{c_1 - c_2} \\ \epsilon_y &= \frac{b_1 u_2 - b_2 u_1 + (b_2 - b_1)x\epsilon_x}{c_2 b_1 - c_1 b_2} \\ \epsilon_z &= \frac{c_1 u_2 - c_2 u_1 + (c_2 - c_1)x\epsilon_x}{c_2 b_1 - c_1 b_2} \end{aligned} \right\} \quad (7)$$

where the subscripts 1 and 2 refer to the pointers 1 and 2 in figure 29.

Substitution of the measured pointer displacements for stringer B in equation (7) gave the rotations ϵ_x , ϵ_y , ϵ_z , shown in figures 31 to 33 for loads from 23,000 to 36,500 pounds. Failure occurred by critical instability of the stringers at a load of 36,500 pounds.

The twist ϵ_x about the axis of the stringer is seen from figure 31 to alternate at low loads from positive to negative values corresponding roughly to the buckles, which are shown diagrammatically below the curves. As the load increases, a twist of the stringer as a whole is superposed on the alternating twist.

The twist ϵ_y about the axis normal to the stringer in plane of the sheet, which is shown in figure 32, approaches zero at the ends and the middle of the stringer. The stringer deforms like a column with clamped ends bending out of the plane of the sheet (see also sketch in fig. 32).

The twist ϵ_z of stringer B about an axis normal to the sheet is shown in figure 33. The twist about this axis is too small for accurate measurement; it shows oscillations that are probably due to the buckles in the adjacent sheet.

The curves $\epsilon_y(x)$ and $\epsilon_z(x)$ must have an average

value of zero to satisfy the condition of zero displacement v , w at the ends of the stringer; this requirement follows directly from the relations $\epsilon_y = dw/dx$ and $\epsilon_z = dv/dx$ connecting w and v with ϵ_y and ϵ_z , respectively. Actually, ϵ_y and ϵ_z were found to have average values definitely higher than zero. An examination of the data showed that this discrepancy could be ascribed to a small displacement to one side of the equidistant vertical wires B-B (fig. 30), the displacement increasing with the load. No attempt was made to correct the curves in figures 32 and 33 for this displacement, since the correction would only involve downward displacement of each curve as a whole.

The deformation of the stringers of specimen 6 was also measured with pointers. A different method was used which gave greater accuracy and was more convenient than the method applied to specimen 1. The twists ϵ_x , ϵ_y , and ϵ_z , were measured by the relative displacements $v_1 - v_3$, $u_1 - u_3$, and $u_2 - u_3$, of three black crosses that were marked on cardboard glued to sheet aluminum pointers attached to the web of the Z-section at the centroid as indicated in figures 34 and 35. The twists of the section about axes through the centroid are given by (see fig. 35):

$$\epsilon_x = \frac{v_1 - v_3}{c_{13}}, \quad \epsilon_y = \frac{u_1 - u_3}{c_{13}}, \quad \epsilon_z = \frac{u_2 - u_3}{b_{23}} \quad (8)$$

where c_{13} and b_{23} are the distances between the crosses indicated in figure 35 and where u_1 , u_2 , and u_3 denote displacements of the crosses 1, 2, and 3, parallel to the stringer, and v_1 and v_3 denote displacements of the crosses 1 and 3 normal to the stringer and parallel to the plane of the sheet. Attachment of the pointers to the web of the Z section rather than to the outstanding flanges prevented errors from local buckling of the flanges of the stringer. The use of the third cross 3 permitted the measurement of twists without having to measure displacements relative to a distant reference wire as in specimen 1 (fig. 30) and eliminated the errors from a displacement of the reference wires. The use of black crosses provided more accurate reference marks than the high lights on the rifle shot and permitted the measurement of twists ϵ_x and ϵ_y with a sensitivity of about ± 0.0002 radian.

Figures 36 to 38 show the rotations θ_x , θ_y , and θ_z for the central stringer R of specimen 6 for loads ranging from 1,400 to 18,000 pounds.

Figure 36 shows the twist θ_x about the axis of the stringer. Comparison with figure 31 shows a relative predominance of the over-all twist of the stringer as a rod twisted from the ends on which are superposed the alternating twists due probably to the buckles in the sheet.

Figure 37 shows the rotation θ_y of stringer R due to bending about an axis parallel to the plane of the sheet at right angles to the stringer. Comparison with figure 32 shows that this bending is different in distribution and is of much lower magnitude. The experimental error in reading θ_y is too large to establish the nature of the bending definitely; it is probably due in part to the action of the buckles in the sheet while, for specimen 1, the bending was due principally to column action of the stringer.

Figure 38 shows the rotation θ_z about an axis normal to the sheet. The measured rotations are very small and lie, in most cases, within the accidental scatter of points, which was found to be of the order of ± 0.002 radian for these measurements. This relatively large scatter can be ascribed to the replacement of the Zeiss traveling microscope by another microscope that could measure the relative displacement of two points as far apart as points 2 and 3 (fig. 35). The general slope of the points from right to left indicates a small amount of bending of the central stringer in the plane of the sheet.

Failure of specimen 6 occurred by critical instability of the stringers at a load of 18,400 pounds. The sheet side of specimen 6 after failure is shown in figure 39. Comparison with figure 14 shows that the 0.025-inch sheet of specimen 6 buckled between rivets in a number of places but that there was no buckling between rivets for the 0.07-inch sheet of specimen 1.

COMPARISON WITH MODEL BASIN RESULTS

A comparison of the test results from the two sheet-stringer specimens given herein with five specimens of the

same design and of various lengths tested at the Navy model basin are shown in figures 40 and 41 and in table III.

Figure 40 shows the average load per stringer element and per sheet element plotted as a function of the external load on the specimen for the three 0.07-inch Alclad panels tested at the model basin and for specimen 1 tested at the National Bureau of Standards. The stringer load for specimen 1 was calculated by multiplying the average stringer stress for the three stringers by the stringer area, the stringer stress being determined from the measured stringer strains (fig. 15) and the stress-strain curve of the stringer as given by the short-column test (fig. 4). The average plate load was then taken as one-fourth the difference between the total external load and the load on the three stringers. The points for the specimens tested at the model basin were taken from curves giving stringer loads and plate loads, which were obtained from the Bureau of Aeronautics of the Navy Department. The stringer loads for these curves were calculated by multiplying the measured average stringer strain at the center section by a Young's modulus of 10.5×10^6 pounds per square inch and by the stringer area of 0.13 square inch. The points in figure 40 were copied from these curves, except for a small correction for yielding made with the help of figure 4. The points for the four specimens scatter about a common curve beginning with a straight-line portion, in which the ratio of stringer load to plate load remains constant up to an external load of about 20,000 pounds. Beyond this load, the sheet ceased to carry its full share of the load because of buckling and the slope of the two curves changes to another pair of straight lines. The load at failure varied through a small range from 36,000 pounds to 37,000 pounds.

Figure 41 shows the corresponding set of curves for the three 0.025-inch specimens, two tested at the model basin and the third at the National Bureau of Standards (specimen 6). In this case, buckling of the sheet occurred at a much lower load and the two curves cease to be straight lines through the origin beginning at a load of about 2,000 pounds. The stringer loads for the specimens tested at the model basin were consistently lower than for specimen 6, the difference being as much as 8 percent for some of the points. There was also a considerable difference in the load at failure, which was 15,800 and 16,100 pounds for the specimens tested at the model basin and 18,400 pounds for the specimen tested at the National Bureau of Standards. The difference is believed to be due to the difference in

the end restraint of the panel for the two tests. The specimens at the model basin were tested with bare flat ends while the specimen at the National Bureau of Standards was tested with flat ends cast in Wood's metal. The casting-in of the ends probably served to give greater end restraint to the stringers and to prevent local crinkling and subsequent failure of the thin sheet at the ends.

The sheet-load curves in figures 40 and 41 were used to compute the effective width of the sheet by applying the definition of effective width as the width of sheet that, subjected to a uniform stress equal to the stringer stress, will support a load equal to the sheet load. The ratio of the effective width w to the initial width w_0 of the sheet between adjacent stringers is then equal to the ratio of the average sheet stress P_s/A_s to the average stringer stress P_{st}/A_{st} , which leads to the formula

$$w = \frac{P_s/A_s}{P_{st}/A_{st}} w_0 \quad (9)$$

where P_s and P_{st} are the measured sheet loads and stringer loads, $w_0 = 4$ inches is the initial sheet width, and A_s and A_{st} are the cross-sectional areas of a sheet element and of a stringer element, respectively. The effective widths for the specimens with the 0.070-inch sheet in figure 42 group about a common curve for stringer stresses above the buckling stress. Figure 43 shows that the effective widths of the thin-sheet specimens 4 and 5 tested at the model basin were generally greater than those for specimen 6 up to loads approaching failure; near the ultimate, the effective widths of all three specimens had approximately the same value.

Table III summarizes the loads per sheet element and stringer element, together with the average stringer stresses and effective widths at failure for the five specimens tested at the model basin and the two specimens tested at the National Bureau of Standards.

The total loads at failure for the four specimens of 0.070-inch 24ST Alclad were found to be nearly independent of the length of specimen and the location of test, the values ranging from 36,000 pounds to 37,000 pounds. In the case of the three specimens of 0.025-inch 24ST sheet mate-

rial, the total load at failure of 18,400 pounds for the specimen tested at the National Bureau of Standards is about 15 percent higher than the loads of 15,800 and 16,100 pounds for the two specimens tested at the model basin. The difference is due principally to the increase of about 21 percent in the average load carried by the stringer element for specimen 6 as compared to that carried by the stringer element of the specimens tested at the model basin.

The sheet load at failure was very nearly constant for a given thickness of sheet, ranging from 5,500 to 5,650 pounds for the 0.070-inch 24ST Alclad sheet and ranging from 900 to 1,100 pounds for the 0.025-inch 24ST sheet.

The average stringer stress at failure was equal to 36,200 pounds per square inch for each one of the two specimens tested at the National Bureau of Standards. It ranged from 30,200 to 38,400 pounds per square inch for the specimens tested at the model basin, the stringer stress at failure being about 10 to 20 percent lower in two 19-inch specimens tested at the model basin compared with the two 19-inch specimens tested herein. Good agreement was obtained between the stringer stress at failure for the shorter specimens 2A and 2B and the two specimens tested at the National Bureau of Standards. The relative loss in buckling strength of the stringers for specimens 4 and 5 tested at the model basin is probably due to the difference in end condition, the bare, flat-end condition providing less restraint than the casting of the ends in Wood's metal used in the present tests.

COMPARISON WITH THEORETICAL RESULTS

Deformation of Sheet

Timoshenko's theory.— The deformation of the buckled sheet between the stringers may be theoretically approximated by Timoshenko's theory (reference 19, pp. 370, 390, etc.), which considers each buckle to be deformed as a rectangular plate or sheet buckling under edge compression. Figure 44 shows the coordinates that were used in applying Timoshenko's theory as well as the other theories considered later in this paper. Timoshenko assumes the displacement w normal to the plane of the sheet to be a sinusoidal buckle:

$$w = f \cos \frac{\pi x}{2a} \cos \frac{\pi y}{2b} \quad (10)$$

He approximates the displacement u in the plane of the sheet and in the direction of the load by

$$u = C_1 \sin \frac{\pi x}{a} \cos \frac{\pi y}{2b} - ex \quad (11)$$

The mean displacement in the direction of the load therefore corresponds to a compressive strain e . The displacement v in the plane of the sheet normal to the load is taken as

$$v = C_2 \sin \frac{\pi y}{b} \cos \frac{\pi x}{2a} + \alpha y \quad (12)$$

The constants f , C_1 , and C_2 are determined by making the strain energy corresponding to a given compression e a minimum. The constant α is taken as zero for the case in which the edges $y = \pm b$ of the plate are assumed to be fixed against a displacement v in the y direction. It is calculated for the case of edges $y = \pm b$ free to expand in the y direction by so determining α that the sum of the normal stresses along the vertical edges of the plate is equal to zero.

In applying expressions (10) to (12) to describe the deformation in a buckled sheet, the edge conditions of zero curvature and constant displacement along the nodal lines $x = \pm a$ of the buckle are satisfied. The restraint along the stringer edges $y = \pm b$ is far more complicated. It will be affected by the torsional and flexural rigidity of the stringer as well as by the method of attachment of the sheet to the stringer. The assumptions (10) to (12) correspond to edge conditions of zero bending moment and zero normal displacement at the stringer. Such edge conditions cannot be satisfied by a stringer of practical design since these stringers would necessarily have zero torsional rigidity coupled with infinite flexural rigidity about one principal axis. It will be assumed, nevertheless, for the purpose of comparison, that the sheet deforms as described by equations (10) to (12), α in equation (12) being chosen for the case of free expansion in the y direction along the stringer edges. The order of agreement between observed and calculated deformations will then be taken as a measure of the adequacy of Timoshenko's approximate theory as applied to the present problem of the deformation of the buckled sheet in sheet-stringer panels.

The median-surface strains may be calculated according to Timoshenko from the assumed displacements u , v , and w by substituting them in the equations

$$\left. \begin{aligned} \epsilon_x &= \frac{\partial u}{\partial x} + \frac{1}{2} \left(\frac{\partial w}{\partial x} \right)^2 \\ \epsilon_y &= \frac{\partial v}{\partial y} + \frac{1}{2} \left(\frac{\partial w}{\partial y} \right)^2 \\ \gamma_{xy} &= \frac{\partial v}{\partial x} + \frac{\partial u}{\partial y} + \frac{\partial w}{\partial x} \frac{\partial w}{\partial y} \end{aligned} \right\} \quad (13)$$

Equations (13) will contain the unknown constants C_1 , C_2 , and f . The values of these constants are determined by making the total strain energy stored in the plate a minimum. The procedure of calculation is outlined in detail in reference 19 (p. 391). Timoshenko carries the calculations to a numerical conclusion only for the case of a square sheet ($b/a = 1$). If the calculations are carried out for the more general case of a rectangular sheet, the following expressions result for the constants f , C_1 , and C_2 with an assumed value of Poisson's ratio $\nu = 1/3$:

$$\left. \begin{aligned} f &= 1.07 t \frac{(b/a)^2 + 1}{2R(b/a)^2} \sqrt{n - 1} \\ C_1 &= 0.139 \frac{f^2 R_1}{a} \\ C_2 &= 0.139 \frac{f^2 R_2}{a} \end{aligned} \right\} \quad (14)$$

where t is the thickness.

$n = e/e_{cr}$, ratio of sheet strain at stringer
 $y = ab$ to the critical strain e_{cr} at
 which buckling occurs.

R , R_1 , and R_2 , functions of b/a given by figure 45 (R^2 rather than R was plotted because it occurs more frequently in subsequent equations).

The critical strain for buckling of the sheet is given by the equation

$$\epsilon_{cr} = 0.927 \frac{t^2}{a^2} \left[\frac{(b/a)^2 + 1}{2(b/a)^2} \right]^2 \quad (15)$$

The functions R , R_1 , and R_2 were adjusted to be equal to unity for the case of the square sheet ($b/a = 1$). For this special case, the formulas (14) and (15) will reduce to the corresponding expressions given by Timoshenko except for minor differences that may be ascribed to Timoshenko's choice of Poisson's ratio as $\nu = 0.3$ compared to the present choice of $\nu = 1/3$. The value of $1/3$ was chosen herein since it led to cancellation of several terms with the factor $1 - 3\nu$.

Substitution of equation (14) in equation (13) gives the following expressions for the axial and transverse median-surface strains:

$$\left. \begin{aligned} \epsilon_x &= \frac{t^2}{a^2} \left[\frac{(b/a)^2 + 1}{2(b/a)^2} \right]^2 \left[-0.927n + (n-1) \left(0.499 \frac{R_1}{R^2} \cos \frac{\pi x}{a} \cos \frac{\pi y}{2b} \right) \right. \\ &\quad \left. + (n-1) \left(\frac{1.415}{R^2} \sin^2 \frac{\pi x}{2a} \cos^2 \frac{\pi y}{2b} \right) \right] \\ \epsilon_y &= \frac{t^2}{a^2} \left[\frac{(b/a)^2 + 1}{2(b/a)^2} \right]^2 \left[0.309n + (n-1) \left(\frac{0.317R_2}{(b/a)R^2} - \frac{0.704}{(b/a)^2 R^2} \right) \right. \\ &\quad \left. + \frac{0.498R_2}{(b/a)R^2} (n-1) \cos \frac{\pi x}{2a} \cos \frac{\pi y}{b} + \frac{1.408}{(b/a)^2 R^2} (n-1) \sin^2 \frac{\pi y}{2b} \cos^2 \frac{\pi x}{2a} \right] \end{aligned} \right\} \quad (16)$$

The stresses may be calculated from the strains by using the familiar relations

$$\left. \begin{aligned} \sigma_x &= \frac{E}{1 - \nu^2} (\epsilon_x + \nu \epsilon_y) \\ \sigma_y &= \frac{E}{1 - \nu^2} (\epsilon_y + \nu \epsilon_x) \end{aligned} \right\} \quad (17)$$

where ν is the value of Poisson's ratio for the sheet material. The load P_s carried by the sheet must be equal to the resultant of the axial stresses across the edge $x = \text{constant}$. Making use of equations (16) and (17), P_s becomes

$$\begin{aligned}
 P_s &= t \int_{-b}^{+b} \sigma_x dy \\
 &= \frac{bEt^3}{a^2} \left[\frac{(b/a)^2 + 1}{2(b/a)^2} \right]^2 \left[\frac{1.591(n-1)}{R^2} \sin^2 \left(\frac{\pi x}{2a} \right) + \right. \\
 &\quad \left. + \frac{0.528(n-1)}{(b/a)^2 R^2} \cos^2 \left(\frac{\pi x}{2a} \right) + \frac{0.715(n-1)R}{R^2} \cos \left(\frac{\pi x}{a} \right) - \right. \\
 &\quad \left. - 1.852n + (n-1) \frac{0.238 R_2}{(b/a)R^2} - \frac{0.529}{(b/a)^2 R^2} \right] \quad (18)
 \end{aligned}$$

It follows from equation (18) that the compressive (negative) load carried by the sheet is least at the crest of a buckle ($x = 0$) and greatest at the nodes ($x = \pm a$). The total load must be independent of x ; therefore, the load taken by the stringers must vary in such a way as to compensate for the variations in sheet load.

The expressions (16) to (18) may be applied directly to predict the behavior of the sheet in a sheet-stringer specimen provided that the ratio b/a of buckle width to buckle length is known. The length $2a$ of the buckle will depend on the condition of restraint of the sheet at the stringer edges; in addition, there must be an integral number of buckles along the length of the stringer. A rough calculation of a (reference 19, p. 329, and reference 32, p. 245) for sheet-stringer specimen 1 having a free length

$$l = 19 \text{ in.}$$

and a stringer spacing

$$2b = 4 \text{ in.}$$

gave five buckles or

$$2a = 3.8 \text{ in.}$$

for the extreme case of simply supported edges and seven buckles or

$$2a = 2.7 \text{ in.}$$

for the case of rigid clamping at the stringer edges $y = \pm b$ and simple support at the loaded edges. Direct measurement of the buckle length for the 0.070-inch specimen (specimen 1) gave on the average

$$2a = 2.7 \text{ in.}$$

or approximately seven buckles; that is, $2a$ agrees closely with the theoretical value for rigid clamping. Assuming seven buckles and neglecting the effect of the Wood's metal end supports gives the following values for the parameters b/a , R^2 , R_1 , and R_2 found in equations (15) to (18):

$$b/a = 1.473, \quad R^2 = 0.737, \quad R_1 = 1.112, \quad R_2 = 0.526 \quad (19)$$

Substituting further

$$E = 10.5 \times 10^6 \text{ lb./sq. in.}, \quad \nu = 1/3, \quad b = 2 \text{ in.}$$

$$t = 0.07 \text{ in.}, \quad a = 1.358 \text{ in.} \quad (20)$$

gives, for specimen 1, the following value for the critical strain:

$$e_{cr} = 13.1 \times 10^{-4} \quad (21)$$

This strain corresponds to a critical load of

$$P_{cr} = E e_{cr} A = 20800 \text{ lb.} \quad (22)$$

and a critical stress of 13,800 pounds per square inch, which is in good agreement with the observed stress of around 13,000 pounds per square inch (fig. 42) at which buckling started. The sheet load per element is, from equation (18),

$$P_s = 2150 - 1717n + 344(n-1)\cos \frac{\pi x}{a} \text{ lb.}, \text{ for } P > P_{cr} \quad (23)$$

where

$$n = e/e_{cr} = e/13.1 \times 10^{-4} \quad (24)$$

In order to compare this sheet load with the observed sheet load plotted in figure 40, it was necessary to determine the theoretical total load P on the sheet-stringer panel. This total load consisted of the load carried by four sheet elements and by three stringer elements. The load carried by the four sheet elements will be approximately equal to four times the average sheet load given by equation (23) if the cosine term is neglected since the buckle pattern on the four sheet elements will be, in general, out of phase with each other by a random amount. The total load carried by the stringers was estimated by multiplying the average stringer strain e by $E = 10.5 \times 10^6$ pounds per square inch and the resulting stress by the total stringer area. Figure 40 shows as curves a the sheet load against the total load on the specimen estimated by the foregoing procedure for the extreme cases of a section through a crest $x = 0$, where the sheet load is a minimum, and a section through a node $x = \frac{1}{2}a$, where it is a maximum. The corresponding maximum and minimum possible loads per stringer element were calculated from these curves by subtracting the minimum and maximum possible sheet loads from the theoretical total load just defined and dividing by 3:

$$P_{st} = \frac{P - 4P_s}{3} = -1782n + 459 \text{ lb.}, \text{ for } P > P_{cr} \quad (25)$$

The corresponding two curves are also shown in figure 40. The measured loads per stringer element and per sheet element are seen to lie between the extreme values. They scatter through a much smaller range than that corresponding to the difference between the extremes. This fact in itself does not necessarily indicate a weakness in Timoshenko's theory. One would expect the spread in the observed sheet loads to be reduced by the method of measuring stringer loads over a gage length of 2 inches, which is comparable to the length of 2.7 inches of a buckle; the measured sheet load would be an average value over a 2-inch length. It will furthermore be noticed that the measured sheet loads represent averages of four sheet elements. The average values could only reach the extremes if the

buckle patterns in the four sheet elements were either in phase or 180° out of phase; figures 12 and 17 indicate that the buckles in both specimens were distributed more nearly at random. The difference between observed and theoretical loads at high stresses is also probably due in part to the plastic behavior of the material. At failure, the average observed sheet load was about 7 percent below the average calculated load and the stringer load was the same percentage above it.

The theoretical values of sheet load P_s determined from equation (23) were used to calculate the effective width (b) of the sheet as a function of the stringer stress (10.5×10^6 e). The resulting curves for effective width at the buckle crest and the buckle node are shown as curves a in figure 42 for comparison with the measured values, which lie between the two curves within the observational error.

In order to compute the axial median fiber strain ϵ_x along the transverse center line through bay 3 (fig. 11), the phase x/a of the buckle at this section must be known. The phase of the buckle was not accurately known, but it was roughly the same as for the center line through bay 3 of specimen 6, for which it was $x/a = 0.696$. Substituting this value of x/a and the values of the constants given in equations (19) in equations (16) gave the following strain distribution along the transverse center line through bay 3:

$$\epsilon_x = 10^{-4} \left[-13.1 n + (n-1) \left(-6.16 \cos\left(\frac{\pi y}{2b}\right) + 21.5 \cos^2\left(\frac{\pi y}{2b}\right) \right) \right] \quad (26)$$

Figure 46 shows a comparison of the strain calculated from this expression, curve (a), with the measured strains at a total external load of 25,000 pounds. The observed values scatter uniformly about the theoretical curve.

Figures 47 to 52 give the results of a comparison of Timoshenko's theory, shown as curves (a), with the test results on specimen 6. In this case, a more complete comparison was possible than for specimen 1 because contours and transverse strains were measured in addition to axial strains. At the same time the sheet material did not have an Alclad coating, so that the possibility of premature yielding of the coating did not enter as a complicating factor.

In the determination of the length of the buckles in this case, the same values, that is, $2a = 2.7$ inches, seven buckles, for clamped edges $y = \pm b$, and $2a = 3.8$ inches, five buckles, for simply supported edges, are obtained from the theory. The measured value of the buckle length was found to be

$$2a = 2.35 \text{ in.}$$

(see figs. 27 and 28) as against 2.7 inches for specimen 1; this corresponds to eight buckles. Inspection of the other two bays showed seven instead of eight buckles.

Assuming seven buckles as for specimen 1 gives the following values for the parameters entering equations (15) to (18):

$$b/a = 1.473, \quad R^2 = 0.737, \quad R_1 = 1.112, \quad R_2 = 0.526 \quad (27)$$

Substituting further

$$E = 10.5 \times 10^6 \text{ lb./sq. in.}, \quad \nu = 1/3, \quad b = 2 \text{ in.},$$

$$a = 1.358 \text{ in.}, \quad t = 0.025 \text{ in.} \quad (28)$$

for specimen 6 gives the following values for the critical strain and the critical load:

$$e_{cr} = 1.67 \times 10^{-4} \quad (29)$$

$$P_{cr} = 1390 \text{ lb.} \quad (30)$$

The measured buckling load was more nearly 2,000 pounds (fig. 52). The sheet load is, from equation (18),

$$P_s = -97.7 - 78.0 n + 15.63 (n-1) \cos \frac{n\pi}{a} \text{ lb.} \quad (31)$$

The maximum and minimum loads per stringer element are by the same procedure as that used for calculating equation (25),

$$P_{st} = -228 n \pm 20.8 (n-1) \text{ lb.} \quad \text{for } P > P_{cr} \quad (32)$$

where

$$n = e/e_{cr} = e/1.67 \times 10^{-4} \quad (33)$$

The sheet load and the stringer load were calculated as a

function of total load as for specimen 1 to give the set of curves (a) shown in figure 41. The measured values lie between the limiting theoretical curves up to loads within 12 percent of the ultimate load. At this load, there may have been a drop in effective width due to buckling of the sheet between rivets (see next paragraph).

The effective width corresponding to the crest and node of the buckle was calculated from the theoretical values of sheet load and was plotted against the stringer stress in figure 43 for comparison with the measured values. The measured effective width lies within the wide band defined by the two theoretical curves up to a compressive stress of about 30,000 pounds per square inch. The observed effective width values fall below Timoshenko's curves at this stress, owing to a sudden drop in effective width at a stress of about 28,000 pounds per square inch. This sudden drop is probably due to the buckling of the sheet between rivets (see fig. 39), since it was found that the stress of 28,000 pounds per square inch corresponded almost exactly to the buckling stress of the sheet between rivets as calculated upon Howland's assumption (reference 33) that the sheet between rivets will buckle like an Euler column of rectangular section with clamped ends having a thickness t equal to that of the sheet and a length L equal to the rivet spacing. This assumption leads to the expression:

$$\sigma_{cr} = \frac{\pi^2 E t^3}{3 L^3} = \frac{\pi^2 \times 10.5 \times 10^6 \times 0.025^3}{3 \times 10.875^3} = 28,300 \text{ lb./sq. in.}$$

The theoretical shape of the buckle for specimen 6 is, from equations (10) and (14):

$$w = 0.0228 \sqrt{n-1} \cos \frac{\pi y}{2b} \cos \frac{\pi x}{2a} \text{ in.} \quad (34)$$

The normal displacement w was calculated from equation (34) for sections $x = 0$ and $y = 0$ through the crest of a buckle and for total loads of 3,800 pounds and 10,900 pounds. The resulting values are shown in figures 27 and 28 as dotted curves for comparison with the measured values. Timoshenko's assumed contour is seen to agree approximately with the observed contour except near the stringer, which exerts a restraining moment on the sheet not considered in Timoshenko's theory.

Measurements of the buckle contours from plaster casts

indicated that the transverse center line on bay 3 between stringers R and S, on which axial and transverse strain distributions were measured occurred at a section

$\frac{x}{a} = 0.696$ relative to the crest of a buckle. Substituting this value of $\frac{x}{a}$ as well as equations (27) in equations (16) gave the following theoretical relations for the longitudinal and transverse strain:

$$\left. \begin{aligned} \epsilon_x &= 10^{-4} \left[-1.68 n + (n-1) x \right. \\ &\quad \times \left(-0.786 \cos \frac{\pi y}{2b} + 2.74 \cos^2 \frac{\pi y}{2b} \right) \\ \epsilon_y &= 10^{-4} \left[0.519 + 0.041 n + (n-1) x \right. \\ &\quad \times \left(0.201 \cos \frac{\pi y}{b} + 0.337 \sin^2 \frac{\pi y}{2b} \right) \end{aligned} \right\} \quad (35)$$

Figures 47 and 48 show as curves (a) the axial strains ϵ_x calculated from equations (35) for loads of $P = 6,800$ and $10,900$ pounds for comparison with the measured strains, which are shown as points. The measured values are found to scatter about the calculated curves.

The transverse strain for the $10,900$ -pound load is shown as curve (a) in figure 49, together with the measured values of strain over a 1-inch gage length as recorded in figure 20. The theoretical curve does not describe the measured strain at all; even the sign of the strain is opposite to that measured at the center of the bay. The discrepancy may be traced principally to the use by Timoshenko of an arbitrary though mathematically convenient assumption for the transverse displacement v (equation 12).

The distribution of axial stress across the sheet was calculated for the transverse center line by substituting the strains given by equations (35) in the plane stress equations (17). Figure 50 shows the resulting values for a load of $6,800$ pounds as curves (a), together with corresponding values for the stress distribution along a transverse section through the crest of a buckle and through the node of a buckle. The stresses calculated from the observed strains are shown as open points for comparison. The points represent single measurements of stress except

for the stresses at the axial center line, which were averages of readings over a 1-inch gage length on three buckles. A similar set of stress-distribution curves for a load of 10,900 pounds is shown in figure 51.

The observed points scatter about the theoretical curves. They do not confirm the large variation in stress distribution in going from buckle node to buckle crest that follows from Timoshenko's theory. The points are too few in number to give a satisfactory check of the theory. It is hard to believe, however, that the actual stress-distribution curve would fall off as rapidly as curve (a) for a section through a buckle crest and that it would rise to a maximum away from the stringer edge for a section through a buckle node.

The axial and transverse stresses at the crest of a buckle were calculated to be

$$\left. \begin{aligned} \sigma_x(0,0) &= -1580 - 186n \text{ lb./sq. in.;} \\ \sigma_y(0,0) &= 440(n-1) \text{ lb./sq. in.} \end{aligned} \right\} \quad (36)$$

These stresses are plotted as curves (a) in figure 52 with measured values of the stresses shown for comparison. It is interesting to note that the measured transverse tensile stress is greater in magnitude than the axial compressive stress for total loads greater than 8,400 pounds. Curves (a) deviate increasingly from the measured stresses for loads greater than 4,000 pounds. The calculated axial stress increases with increasing load, while the observed axial stress decreases and actually becomes zero at a load of 12,000 pounds. The measured transverse stress tends toward a constant value at high loads while it increases linearly according to the theory.

J. M. Frankland's theory.—An approximate theoretical solution for the stress distribution in the buckled sheet of a sheet-stringer panel under end compression has been worked out by J. M. Frankland of the Bureau of Aeronautics. Frankland's solution differs from Timoshenko's in assuming initially only a normal displacement w , which is approximated by the series

$$w = t \sum_{mn} A_{mn} \cos \frac{n\pi x}{2a} \cos \frac{m\pi y}{2b} \quad (37)$$

without making any assumptions relative to the other two displacements u and v . The contour defined by equation (37) satisfies the assumed end conditions of zero bending moment and zero normal displacement at the edges $x = \pm a$, $y = \pm b$ of the buckle. The median fiber stresses are determined from equation (37) to give the required force resultants in the plane of the plate and to maintain the originally rectangular portion of plate $2a$ by $2b$ rectangular after buckling by making use of von Kármán's differential equations linking the bending stresses due to buckling with the median surface stresses (reference 32, p. 349). The coefficients A_{mn} entering in the resulting expressions are finally determined by the principle of least work.

Carrying out this calculation for a buckle shape with four unknown coefficients A_{11} , A_{13} , A_{31} , A_{33} showed an appreciable variation between the plate load at the crest and that at a node. Such a condition would necessitate shears between the plate and the stringer that had not been considered in the expression for the strain energy.

In order to include these shears in the expression for the total energy stored in the panel, a further analysis was made by J. M. Frankland. This analysis was carried to a numerical conclusion for the special case of a square sinusoidal buckle pattern described by

$$w = A \cos \frac{\pi x}{2a} \cos \frac{\pi y}{2a} \quad (38)$$

with the following results for the stress distribution:

$$\left. \begin{aligned} \sigma_x &= \sigma_c \left[\lambda - \frac{\lambda - 1}{1 + r} (r + \cos 2 \alpha y) + 0.341 f'' \cos 2 \alpha x \right] \\ \sigma_y &= -\sigma_c \left(\frac{\lambda - 1}{1 + r} + 0.341 f' \right) \cos 2 \alpha x \\ \tau &= \sigma_c (0.341 f' \sin 2 \alpha x) \end{aligned} \right\} \quad (39)$$

where

$$\sigma_c = \frac{-\pi^2 E t^3}{12 b^3 (1 - \nu^2)} \quad \text{is the critical stress for buckling of sheet into rectangular lobes} \quad (40)$$

λ , load parameter ($\lambda = 1$, $\sigma = \sigma_c$)

$$r = \frac{A_{st}/2 bt}{1 + (A_{st}/2 bt)}, \quad \text{relative reinforcement by stringer}$$

$$\frac{A_{st}}{2 bt} = \frac{\text{stringer area}}{\text{plate area}}$$

$$\alpha = \frac{\pi}{2 a} = \frac{\pi}{\text{buckle length}}$$

$$a = b$$

The coefficients f , f' , f'' in equation (39) are given by

$$\left. \begin{aligned} 0.341f &= k \frac{\lambda - 1}{1 + r} \left[2.603 \frac{\cosh 2\alpha y}{e^{\pi/2}} - 2\alpha y \frac{\sinh 2\alpha y}{e^{\pi/2}} \right] \\ 0.341f' &= k \frac{\lambda - 1}{1 + r} \left[1.603 \frac{\sinh 2\alpha y}{e^{\pi/2}} - 2\alpha y \frac{\cosh 2\alpha y}{e^{\pi/2}} \right] \\ 0.341f'' &= k \frac{\lambda - 1}{1 + r} \left[0.603 \frac{\cosh 2\alpha y}{e^{\pi/2}} - 2\alpha y \frac{\sinh 2\alpha y}{e^{\pi/2}} \right] \end{aligned} \right\} \quad (41)$$

where

$$k = \frac{\nu A_{st}/(2bt)}{\frac{2}{1 + \nu} + \pi(3 - \nu) \frac{A_{st}}{2bt}} \quad (42)$$

and ν is Poisson's ratio.

Frankland derived the following expressions for the stringer load and the sheet load in his second analysis:

$$\left. \begin{aligned} P_{st} &= A_{st} \sigma_c \left[\lambda + \frac{1-r}{1+r} (\lambda - 1) \left(1 + 0.490 \frac{k}{r} \cos 2\alpha x \right) \right] \\ P_s &= 2 b t \sigma_c \left[\lambda - \frac{r}{1+r} (\lambda - 1) \left(1 + 0.490 \frac{k}{r} \cos 2\alpha x \right) \right] \end{aligned} \right\} (43)$$

Equations (43) were applied to calculate the plate loads and stringer loads for specimens 1 and 6 by substituting (20) and (28) in equations (43). The results for sections through the crest and the node of a buckle ($x = 0$, $x = a$) are shown as curves (b) in figures 40 and 41 for comparison with the observed results and the results of Timoshenko's approximate theory. Satisfactory agreement with the observed values for specimen 1 was obtained up to loads within 20 percent of the load at failure. The observed sheet loads for specimen 6 were about 10 percent below the theoretical loads. There was much less variation in the theoretical stringer load along a buckle than for Timoshenko's theory.

The effective width of the sheet for both specimens was calculated from equations (43) as a function of stringer stress using the same procedure as already outlined for a similar comparison with Timoshenko's theory. The resulting values, which are shown as curves (b) in figures 42 and 43 are seen to give an approximate description of the effective width for the specimens with the 0.070-inch sheet (fig. 42), whereas they give high values for the effective width of the other specimens (fig. 43) for stringer stresses in excess of 15,000 pounds per square inch.

A direct comparison with the measured strain distribution was obtained by converting the first two equations (39) into strain equations with the help of Hooke's law for plane stress:

$$\left. \begin{aligned} \epsilon_x &= \frac{\sigma_x - \nu \sigma_y}{E} \\ \epsilon_y &= \frac{\sigma_y - \nu \sigma_x}{E} \end{aligned} \right\} (44)$$

and then substituting the numerical values

(20) and (28) for the two specimens. The resulting strain distributions are compared in figures 46 to 49 with the observed values and with those given by Timoshenko's theory. The calculated axial strain distribution agrees as well with the observed values as Timoshenko's theory and it has the added advantage of not leading to a maximum strain away from the stringer edge. The transverse strain (fig. 49) agrees very much better with the observed values than for Timoshenko's theory, probably because no arbitrary assumption has been made for the transverse displacement v .

Stress distributions across the sheet according to Frankland's theory were calculated from equations (39) and were plotted as curves (b) in figures 50 and 51. The curves agree with the measured points somewhat better than do Timoshenko's curves (a). The stress distribution changes only slightly in going from node to crest and there is no stress-maximum away from the stringer edge, as for Timoshenko's theory.

The axial and transverse stresses at the crest of a buckle were calculated as a function of total load and were plotted as curves (b) in figure 52 for comparison with the observed values. The agreement with the measured axial stresses is better than for Timoshenko's theory, especially at high values of the load, but that for the transverse stresses is not so good.

The following value was obtained by Frankland for the amplitude A_t of the buckle:

$$A_t = 1.7lt \sqrt{\frac{\lambda - 1}{1 + r}} \quad (45)$$

The sine curve of this amplitude is compared in figures 27 and 28 with the deflection curves observed on specimen 6 and with the curve calculated from Timoshenko's theory. The curves given by Timoshenko's theory are seen to come considerably closer to the observed deflections than those given by Frankland's theory.

K. Marguerre's theory.— K. Marguerre has recently published the results of a number of different attacks on the problem of determining the stress distribution and effective width for a long sheet with supported edges that has buckled into a series of square buckles (reference 23).

He first considers the stress distribution for the

square sinusoidal buckle also considered by Frankland and proceeds to a solution in a manner quite analogous to that used by Frankland in his first solution, which neglects the shears between the sheet and the stringer.

In a second attack on the problem (see also reference 24), Marguerre assumes a somewhat more complicated shape for the square buckle than the sinusoidal shape assumed by both Timoshenko and Frankland in their numerical examples, namely:

$$w = \left(f_1 \cos \frac{\pi Y}{2a} - f_3 \cos \frac{3\pi Y}{2a} \right) \cos \frac{\pi X}{2a} \quad (46)$$

He calculates f_1 and f_3 by the energy method combined with the assumption that the shearing stresses along the lateral edges of the sheet are zero. The results of this calculation give only a slight correction to the results of the same calculation for the sinusoidal square buckle ($f_3 = 0$).

Marguerre's third attack proceeds from the observation that neither equation (38) nor (46) is a good description for the contour of a severely buckled sheet. In a severely buckled sheet, most of the load will be carried by the sheet close to the edges and this portion of the sheet will develop local buckles that are superposed on the main square buckles having a half wave length equal to the stringer spacing.

A contour that would describe a state of buckling with small buckles having one-third the wave length of the main buckles would be

$$w = f_1 \cos \frac{\pi X}{2a} \cos \frac{\pi Y}{2a} + f_3 \cos \frac{3\pi X}{2a} \left(\cos \frac{\pi Y}{2a} - \eta \cos \frac{3\pi Y}{2a} \right) \quad (47)$$

The ratio f_3/f_1 will then measure the relative intensity of the small buckles near the edge. The parameter η measures the increase in amplitude of the small buckles in passing from the center of the sheet to the edge. For $\eta = 0$, the small buckles have a maximum amplitude at the center of the sheet and, for $\eta = 1$, they have zero amplitude at the center of the sheet and maximum amplitude near the edge. Marguerre assumes $\eta = 1/2$ in his numerical work in order to reduce the number of unknown parameters from three to two. A further simplification is obtained by Marguerre

in his numerical example by taking Poisson's ratio $\nu = 0$. This somewhat arbitrary assumption, together with the assumptions of zero shear stress and zero resultant transverse force along the lateral edges of the sheet, leads to the following relation for the average axial stress $\bar{\sigma}$ carried by the sheet:

$$\frac{\bar{\sigma} - \sigma_{cr}}{e - e_{cr}} = \frac{E}{2} \left(\frac{4 - 6\xi + 8\xi^2}{4 - 3\xi + 26.5\xi^2} \right) \quad (48)$$

where

σ_{cr} is the axial stress for buckling of the sheet

e_{cr} , axial strain for buckling of the sheet

e , axial strain (stringer strain)

E , Young's modulus

$$\xi = f_3 / f_1$$

The ratio ξ may be eliminated by a second relation:

$$\frac{e - e_{cr}}{e_1 - 4.02e_{cr}} = 11.25 \left(\frac{4 - 3\xi + 26.5\xi^2}{26.5 - \frac{1}{\xi} + 350\xi^2} \right) \quad (49)$$

In addition to his approximate calculation, Marguerre carried out a more "exact" calculation proceeding by his first method of attack (similar to that used by Frankland) and assuming the contour given by equation (47) with $\eta = 1/2$. Unfortunately, he gives only the result for the expressions replacing equations (48) and (49), which were found to be independent of the value of ν and equal to

$$\left. \begin{aligned} \frac{\bar{\sigma} - \sigma_{cr}}{e - e_{cr}} &= \frac{E}{2} \left(\frac{4 - 6\xi + 18.6\xi^2}{4 - 3\xi + 31.8\xi^2} \right) \\ \frac{e - e_{cr}}{e_1 - 4.02e_{cr}} &= 11.25 \left(\frac{4 - 3\xi + 31.8\xi^2}{31.8 - 1/\xi + 350\xi^2} \right) \end{aligned} \right\} \quad (50)$$

It will be noticed that equations (48) and (49) agree with equation (50) for small values of the relative amplitude f_3/f_1 of the local buckle.

The sheet load may be calculated from the preceding formulas by multiplying the average longitudinal stress $\bar{\sigma}$ by the sheet area 2 at:

$$P_s = 2 \text{ at } \bar{\sigma} \quad (51)$$

The amplitude f_1 in equation (47) may be calculated by substituting the value of ξ calculated for a given compressive strain e from equations (48) and (49) in Marguerre's expression

$$e - e_{cr} = \frac{\pi^2 f_1^2}{64a^2} (4 - 3\xi + 26.5\xi^2) \quad (52)$$

Knowing f_1 , ξ , and η , one can calculate the buckle shape from equation (47) and the axial and transverse stresses from Marguerre's approximate expressions

$$\begin{aligned} \sigma_x = \frac{E\pi^2 f_1^2}{32a^2} & \left[-\frac{32a^2 e}{\pi^2 f_1^2} + 1 + \cos\left(\frac{\pi y}{a}\right) + \right. \\ & \left. + 9\xi^2 \left(1.25 - \cos\frac{2\pi y}{a} + 0.25 \cos\frac{3\pi y}{a} \right) \right] \quad (53) \end{aligned}$$

and

$$\begin{aligned} \sigma_y = \frac{E\pi^2 f_1^2}{32a^2} & \left[\cos\frac{\pi x}{a} - 2\xi \left(\cos\frac{\pi x}{a} + \cos\frac{2\pi x}{a} \right) + \right. \\ & \left. + \xi^2 \left(3.25 \cos\frac{3\pi x}{a} \right) \right] \quad (54) \end{aligned}$$

The axial stresses are independent of the coordinates x along the buckle (fig. 44), because of the assumption $v = 0$. It follows that the sheet load and the effective

width do not vary along the buckle as they do according to the theories of Timoshenko and of Frankland with $\nu = 1/3$.

Equations (48) to (50) were applied to calculate the sheet and stringer loads for specimens 1 and 6 by substituting values of E , $a = b$, and t from (20) and (28). The quantity E_{cr} was taken as the critical stress σ_c used in Frankland's theory (equation 40) with $\nu = 1/3$. The results for both the approximate relations (48) and (49) and the more "exact" relation (50) came very close to each other for specimen 1 (fig. 40, curves (c), (d)). There was a small difference between the two curves for specimen 6 (fig. 41, curves (c) and (d)). The calculated loads given by curves (c) and (d) are seen to agree with the measured values practically up to failure.

The effective width of the sheet of specimens 1 and 6 was calculated from these curves using the procedure already outlined. The resulting curves are shown as curves (c) and (d) in figure 42 and 43. The agreement with the measured effective width is good up to a stringer stress of about 30,000 pounds per square inch. It is better than that for the other two theories, curves (a) and (b), in the case of specimen 6. Marguerre's "exact" theory (curve (d)) describes the observations more closely in this case than the approximate theory, curve (c).

The theoretical distribution of strain across the sheet of specimen 1 and specimen 6 was calculated by dividing Marguerre's approximate expression (53) and (54) for the stress by Young's modulus $E = 10.5 \times 10^6$, which gave the curves (c) shown in figures 46 to 49. The calculated distributions of axial and transverse strains agree less satisfactorily with the observed values than the curves calculated from either Timoshenko's or Frankland's theory. The transverse strain distribution along the center line of specimen 6 at a load of 10,900 pounds (curve (c), fig. 49) differs radically from the observed strain distribution. This discrepancy may be explained by the difference between the buckle shape (47) assumed by Marguerre and the measured buckle shape.

Curve (c) in figures 27 and 28 shows sections through Marguerre's buckle for loads of 6,800 and 10,900 pounds

for comparison with the observed values and the results of the other two theories. The axial section of the buckle comes somewhat closer to the observed values than the buckle according to Frankland's theory but is not nearly so close as that according to Timoshenko's theory. The transverse section of the assumed buckle differs more radically from the observed buckle shape than either Frankland's or Timoshenko's theory, particularly for the higher load of 10,900 pounds. Marguerre's choice of contour (equation (47)) is apparently not suited to describing the buckles in the sheet between stringers. It takes no account of the torsional rigidity of the stringers and actually increases the slope of the deflection curve near the stringer instead of lessening it. The amplitude of the short wave-length buckles is also too large, especially at the higher load.

The axial stress distributions for specimen 6 at a load of 6,800 pounds and at a load of 10,900 pounds are shown as curves (c) in figures 50 and 51. At the 6,800-pound load, the curves (c) agree with curves (a) and (b) taken from Timoshenko's theory and from Frankland's theory, at least within the scatter of the measured points. At the 10,900-pound load, Marguerre's theory gives a more nearly constant stress in the center of the sheet than either the points or the other two theories.

Curves (c) in figure 52 compare the theoretical axial and transverse stresses at a buckle crest of specimen 6 with observed values and values taken from Timoshenko's and from Frankland's theory. Marguerre's theory gives results approaching those of Frankland's theory up to a load of about 4,000 pounds. Above 8,000 pounds, Marguerre's curve for axial stress deviates increasingly from the observed values while that for transverse stress approaches the measured stresses.

Formulas for effective width.— The load carried by the sheet of a sheet-stringer panel under end compression may be computed by considering the width of the sheet between stringers to be reduced by buckling to an effective width carrying a uniform stress equal to the stress at the stringer edge of the sheet. The effective width will then depend on the stress in the sheet, the dimensions of the sheet, the condition of restraint at the stringer edges, and the stress-strain curve of the material. The effective width, w , is upon this definition given by the simple relation

$$w = \frac{P_s}{t\sigma} \quad (55)$$

where P_s is the sheet load
 t , the thickness of the sheet
 and σ , the compressive stress at the edges of the sheet

It will be noted that this definition of effective width coincides with the definition given by equation (9) only for the special case that the stringer stress and the stress at the stringer edge of the sheet are identical. It appears, fortunately, from a comparison of figures 42 and 43, derived by the use of equation (9) with figure 55, which was derived from equation (55), that the two definitions of effective width led to practically the same result in the present sheet-stringer panels. It seemed preferable for a general discussion of effective width to adhere to equation (55) because of its independence of the stringers.

The ultimate sheet load P_{ult} for a sheet with simply supported edges would correspond to an edge stress σ equal to the yield strength in compression $\sigma_{y.p.}$.

Von Kármán (reference 5) has proposed the following formula for this load:

$$P_{ult} = Ct^2 \sqrt{E \sigma_{y.p.}}$$

which gives for the effective width corresponding to the ultimate sheet load

$$w_{y.p.} = Ct \sqrt{E/\sigma_{y.p.}} \quad (56)$$

The value of the constant C will depend on the condition of restraint of the sheet at the stringer edges. Von Kármán has derived the limiting values $C = 1.24$ and 1.90 for a sheet with supported edges of material having $\nu = 0.3$. Sechler has empirically obtained a relation between C and the ratio

$$\lambda = \frac{t}{2a} \sqrt{E/\sigma_{y.p.}} \quad (57)$$

where $2a$ is the width of the sheet, according to which C drops from about 2 for $\lambda = 0.05$ to about 0.7 for $\lambda = 1.0$ (reference 9). A value of $C = 1.7$ is widely used for sheet-stringer panels of typical designs and falls between von Kármán's limiting values of 1.24 and 1.90.

Although von Kármán's equation and Sechler's empirical curve were derived specifically for determining the ultimate load of the sheet in sheet-stringer combinations, they have been used by designers to estimate the load carried by the sheet for edge stresses σ less than the yield strength of the material. The variation of effective width with edge stress would then be given by

$$w = Ct \sqrt{E/\sigma} \quad (58)$$

It is convenient for purposes of comparison to reduce equation (58) to a dimensionless form as follows. Let σ_{cr} be the stringer stress at which buckling of the sheet begins. Up to this stress, the effective width will be equal to the full width $2a$ of the sheet:

$$2a = Ct \sqrt{E/\sigma_{cr}} \quad (59)$$

Solving for C and substituting in equation (58) gives for the relative effective width the simple relation

$$\frac{w}{2a} = \sqrt{\frac{\sigma_{cr}}{\sigma}} \quad (60)$$

The relative effective width given by this equation depends only on the ratio of the stringer stress to the critical stress.

Instead of using σ/σ_{cr} as independent variable, one may use the strain ratio e/e_{cr} as long as the stresses are within the range of validity of Hooke's law. Beyond

this range, the edge stress can be computed approximately from the known edge strain, which is equal to the stringer strain, provided that the compression stress-strain curve of the sheet material is known. In the present instance it was not possible, unfortunately, to obtain undeformed coupons for determining the compressive properties of the sheet of specimens 1 and 6. Compression stress-strain curves had, however, been obtained at the National Bureau of Standards by the pack method on specimens of 0.064-inch 24ST Alclad sheet loaded in the direction of rolling (figure 53) and on 0.032-inch 24ST sheet loaded in the direction of rolling (fig. 54). It seemed permissible to describe the compressive properties of the sheet material by these stress-strain curves at least for an approximate analysis. It should be noted in this connection that the direction of rolling coincided with the direction of the load in specimens 1 and 6.

Figure 55 shows as curve (a) a plot of $\frac{w}{2a}$ from equation (60) against ratio σ/σ_{cr} . The individual points shown in figure 55 were calculated from the test results on specimens 1 and 6 as plotted in figures 42 and 43. The stress-strain curve (fig. 4) of the stringer material and the stress-strain curves (figs. 53 and 54) of sheet material similar to the sheet material in the specimens were used to calculate the edge stress in the sheet from the stringer stress and from the assumption that stringer strain and edge strain were identical.

The critical edge stress σ_{cr} was calculated upon two assumptions. The circular points were plotted by choosing σ_{cr} as equal to the value for a long, rectangular plate with supported edges:

$$\sigma_{cr} = \frac{\pi^2 E}{3(1 - \nu^2)} \left(\frac{t}{2a} \right)^2 \quad (61)$$

which gives, with $E = 10.5 \times 10^6$ lb./sq. in., $\nu = 1/3$, and $2a = 4$ in., the following values for specimen 1 ($t = 0.070$ in.)

$$\sigma_{cr} = 11,900 \text{ lb./sq. in.}$$

and for specimen 6 ($t = 0.025$ in.)

$$\sigma_{cr} = 1,520 \text{ lb./sq. in.}$$

The crosses in figure 55 were calculated by choosing for σ_{cr} the observed critical stresses

$$\sigma_{cr} = 13,000 \text{ lb./sq. in.}$$

for specimen 1 (fig. 42) and

$$\sigma_{cr} = 2,500 \text{ lb./sq. in.}$$

for specimen 6 (fig. 52).

In the case of the specimen with the heavy sheet, the buckling stress was about 9 percent greater than for supported edges; while, in the case of the thin-sheet specimen, it was about 64 percent greater. Replacement of the approximate critical stress calculated from equation (31) (circular points) by the observed critical stress (crossed points) throws the points for both specimens about a common curve excepting those points where the yielding of the sheet is appreciable.

Von Kármán's formula is seen to be on the conservative side by as much as 25 to 35 percent in the case of the thin-sheet specimen. It agrees satisfactorily with the observed values for specimen 1.

A somewhat better agreement with the observed results is to be expected if von Kármán's constant C is varied in accordance with Sechler's curve. In order to verify this assumption, it is necessary to convert Sechler's curve of $C = f(\lambda)$ to the variables shown in figure 55 by redefining λ as

$$\lambda = \frac{t}{2a} \sqrt{\frac{E}{\sigma}} \quad (62)$$

where σ is the edge stress, which may be below the yield strength of the material. The two definitions of λ (equations (57) and (62)) coincide for $\sigma = \sigma_{y.p.}$ Taking σ_{cr} as equal to the value given by equation (61) for a long rectangular sheet with supported edges gives

$$\lambda = 0.520 \sqrt{\frac{\sigma_{cr}}{\sigma}} \quad (63)$$

Substituting this value of λ in equation (59), which, with equation (62), may be written as

$$\frac{w}{2a} = \lambda C(\lambda) \quad (64)$$

gives curve (b) in figure 55. The effective width, according to this formula, is even less than for Von Kármán's formula. It is on the conservative side by as much as 35 to 50 percent for specimen 6.

Recently Sechler has proposed the following formula for the effective width of the sheet in a sheet-stringer panel (reference 30).

$$\frac{w}{2a} = 0.50 + 1.81 \lambda^2 \quad (65)$$

Substituting equation (63), equation (65) becomes

$$\frac{w}{2a} = 0.50 + 0.50 \frac{\sigma_{cr}}{\sigma} \quad (66)$$

A plot of equation (66) is shown as curve (c) in figure 55. It is seen to err on the unconservative side for high ratios σ/σ_{cr} by as much as 35 to 40 percent in the case of specimen 6.

H. L. Cox (reference 7) obtained an approximation to the effective width of sheet under edge compression by considering the sheet as made up of a set of column strips whose axes were parallel to the load and calculating the load distribution over these columns for a given value of the compression at the ends and an assumed buckle contour. Choosing the buckle contour to give simple support at the stringer edges gave a curve that could be approximated by

$$\frac{w}{2a} = 0.09 + 0.80 \sqrt{\frac{\sigma_{cr}}{\sigma}} \quad \left(\text{for } \frac{\epsilon_{cr}}{\epsilon} = \frac{\sigma_{cr}}{\sigma} \right) \quad (67)$$

and choosing it for clamping at the stringer edges gave a curve that could be approximated by

$$\frac{w}{2a} = 0.14 + 0.85 \sqrt{\frac{\sigma_{cr}}{\sigma}} \quad \text{for} \quad \frac{\epsilon_{cr}}{\epsilon} = \frac{\sigma_{cr}}{\sigma} \quad (68)$$

The corresponding curves are shown as (h) and (i) in figure 55. The curve (i) for clamped edges agrees satisfactorily with the crossed points which are based on the observed critical stress. Both curves (h) and (i) are generally on the conservative side of the circular points based on the critical stress for supported edges.

A better fit to the circular points for specimen 6 is obtained by the following modification of Cox's formula used by Marguerre (reference 23):

$$\frac{w}{2a} = 0.19 + 0.81 \sqrt{\frac{\sigma_{cr}}{\sigma}} \quad (69)$$

Equation (69) is shown as curve (d) in figure 55.

An independent calculation of the effective width of buckled sheet has been made by Marguerre (see previous section), who arrived at curves (e) and (g) on the basis of the relations (48) to (50) given in the previous section. Marguerre noticed that the curve (e) could be closely approximated by the simple relation

$$\frac{w}{2a} = \sqrt[3]{\frac{\sigma_{cr}}{\sigma}} \quad (70)$$

which is shown as curve (f) in figure 55. Curve (e) is seen to approximate the circular points for specimen 6 more closely than any of the other curves. Marguerre's "exact" formula (curve (e)) holds for the circular points of both specimens up to values of $\sigma = 30,000$ pounds per square inch ($\sigma/\sigma_{cr} = 2.5$ for specimen 1, $\sigma/\sigma_{cr} = 19.7$ for specimen 6) at which yielding becomes appreciable for the 0.070-inch Alclad sheet of specimen 1 and at which the 0.025-inch sheet of specimen 6 has probably buckled between rivets. Equation (70) describes the measured effective width for both specimens up to an edge stress of about 30,000 pounds per square inch within 10 percent provided that σ_{cr} is taken from equation (31) as the buckling stress for supported edges. Upon this basis, equation (70) may be written in the form

$$w = 1.54 t \sqrt{\frac{E}{\sigma} \frac{2a}{t}} \quad (70a)$$

Equation (70a) describes the effective width up to failure of specimens 1 and 6 within 12 percent while von Kármán's well-known formula (curve (a)), which is upon the same basis

$$w = 1.92 t \sqrt{\frac{E}{\sigma}} \quad (70b)$$

is about 35 percent low for specimen 6 near failure.

The best description of the observed effective widths based on the actual critical stress is that of curve (i), corresponding to Cox's formula for sheet with clamped edges.

Deformation of Stringers

In the computation of the actual strength of a sheet-stringer panel, it is not sufficient to know the load carried by the sheet as a function of the stringer stress and then to let the ultimate load of the panel be that for which the stringer stress attains the yield strength of the stringer material. This assumption would lead to results on the unconservative side in all those cases in which the sheet-stringer combination fails by instability of the stringers. It is not possible with the present development of the theory to compute the buckling load of a sheet-stringer panel, even within the elastic range. The buckling load will be an exceedingly complicated function of the dimensions and elastic properties of the sheet and the method of attachment of the sheet to the stringers.

Timoshenko (reference 19, p. 371) has considered the buckling load of a sheet-stringer panel, where the failure of both sheet and stringer is simultaneous and where the stringers fail by bending without twisting. In the present panels, the sheet buckles long before the ultimate load of the panel has been reached. Also, the displacements of pointers attached to the stringers (figs. 31 and 36) indicated a rapidly increasing twist of the stringers with increasing stringer loads. It was concluded that Timoshenko's theory could not be expected to give an adequate description of the strength of the sheet-stringer panels tested.

A method of attack that takes account of the twisting of the stringer by the sheet is outlined by Lundquist and Fligg (reference 35, p. 12). Lundquist and Fligg confined themselves to stringers with a symmetrical section. They carried their calculations through for a numerical example in which it was required to find the strength of a sheet-stringer panel consisting of I-type stringers fastened to 0.025-inch sheet. The Z-type stringers used in the present specimens are not symmetrical and their buckling strength could not be computed by this theory. The torsional instability of asymmetrical stringers has been investigated by Robert Kappus in a recent article (reference 36). Kappus did not consider the effect of sheet on the stability of his stringers. No attempt was made to extend his theory so as to include this effect.

The theories for the buckling strength of sheet-stringer panels become of increasingly doubtful application as the stresses in the stringer and in the sheet cease to be proportional to the strains. This will be the case in practically all well-designed sheet-stringer panels in which the strength of the material is utilized to carry the load appreciably beyond the elastic range.

Several relations have been proposed for reducing the elastic modulus to take care of the beginning of yielding of the material (reference 19, p. 384; reference 35, p. 15). Unfortunately, too little is known of the yielding of material under combined stress to make any of these relations acceptable without the support of an extensive series of tests. The present tests on only two specimens would not suffice to give a useful comparison with any of the theoretical extrapolations into the plastic range.

APPLICATION OF SOUTHWELL'S METHOD TO STRINGER DEFORMATION

In the absence of an adequate theory for the buckling failure of a stringer in a sheet-stringer combination, the analysis of the measured deformations of the stringers was confined to an application of Southwell's method of determining the elastic buckling load of a column from deflection readings at low loads (reference 37). Southwell noticed that a straight line should be obtained by plotting observed deflections δ of an initially slightly bent column against δ/P when the observed loads P were not high enough to

produce stresses beyond the elastic limit. The line would have the equation

$$P_{cr} \frac{\delta}{P} - \delta - a = 0 \quad (71)$$

Its slope would equal the critical buckling load P_{cr} , and the intercept on the axis of δ would be the initial deflection a . H. R. Fisher has shown (reference 38) that Southwell's method of plotting will give nearly correct values of the critical load for members of constant section subjected to certain combinations of axial and transverse loads.

H. J. Gough and H. L. Cox (reference 39) have applied Southwell's method of plotting to determine the critical buckling load of sheet stressed by shearing forces S acting in the plane of the sheet. In place of plotting δ/P against δ , they plotted w/S against w , where w was the measured amplitude of the wrinkles and S was the shear stress. They obtained agreement within a few percent with the theoretical buckling shear S_{cr} although, in this case at least, there was no proof given that Southwell's method of plotting would result in the correct buckling load. In view of this success, it seemed of interest to apply the method to the analysis of the measured deformation of the stringers of specimens 1 and 6.

Two types of reading were available for the deformation of the stringer as a bent column, that is, the strains read with Tuckerman optical strain gages mounted on the stringer flange (figs. 12 and 17) and the readings of pointer displacement indicating rotation about the y axis (figs. 32 and 37). Twisting deformation of the stringer about the x axis was measured by means of pointers only (figs. 31 and 36).

If a zero error exists in the observed deflections, or deformations, a plot of δ against δ/P will not lie on a straight line. If a straight line is to be obtained, the deflection δ must be due to the load alone. In general, a zero correction δ_0 must be applied to the indicated deformation δ_1 , so that

$$\delta = \delta_1 - \delta_0 \quad (72)$$

actually represents the deformations leading to the final

failure. The zero correction was determined in the present case to give an optimum fit to Southwell's relation (71) by successive substitutions of equation (72) in equation (71).

A much more direct method of freeing Southwell's method from errors due to the unknown zero correction has been suggested by Lundquist (reference 40). Lundquist noticed that equation (71) could be written in the form

$$\delta - \delta' = \frac{\delta - \delta'}{P - P'} (P_{cr} - P') - (\delta' + a) \quad (73)$$

where δ is the deformation corresponding to a load P and δ' is the deformation corresponding to an initial load P' . Hence a straight line results if the difference in deformation is plotted against the ratio of difference in deformation to difference in load. The slope of the straight line will give the difference between the desired elastic buckling load P_{cr} and the initial load P' ; the intercept gives the sum of the unknown deformation δ' at the initial load and the initial deflection a . By taking the initial load P' sufficiently high, one avoids the disturbing effects of initial alignments, buckling of thin sheet, etc. Lundquist's method will lead to the same answer as the method of successive approximation used in the computations given in this report. It is also more convenient to use and would have been used for the present paper if it had been discovered earlier.

A large number of curves of deformation against deformation over load were plotted from the observed strain readings and the observed pointer displacements using the method of successive approximations. It was found from the plots that for large deformations, the points showed an irregular behavior and also a large scatter in some cases although in most cases the points tended to scatter about a straight line. Some of the irregularities were probably due to the initial adjustments of the structure to the load, and others to buckling at low loads of the sheet; most of the scatter could be ascribed to inaccuracies in the reading of the deformations.

A few of the plots showed a small scatter and therefore led to an accurate value of the slope. These curves are shown in figures 56 to 59.

Figure 60 shows a similar plot for the twisting defor-

mation of the 5-inch stringer specimen tested as a short column (fig. 3). The twist was determined by using a Tuckerman autocollimator to measure the angular displacement of a stellite mirror glued to the Z bar.

The solid points shown in figures 58 to 60 were taken from deformation readings at loads within 10 percent of the ultimate load. These points seem to follow Southwell's relation as well as the open points, which correspond to loads less than 90 percent of the ultimate load. It seems advisable to read deformations up to loads within nearly 10 percent of the ultimate load to obtain a sufficient number of points for a Southwell plot.

The Southwell method could not be applied to the buckling of the sheet between stringers, as measured by the bending strain in the sheet, because of the lack of observations below the buckling load.

The elastic buckling loads calculated from figures 56 to 60 are compared with the observed buckling loads in table IV. The comparison shows a close agreement between the observed ultimate load for specimen 1 and the elastic buckling loads for both column failure and for torsional instability as calculated from the pointer readings. The pointer readings indicate that the actual failure was one where bending and twist were combined in the deformation leading to failure.

Figure 56 shows a Southwell plot of bending strain as measured by Tuckerman strain gages in addition to the plots of pointer readings. It was impossible to bring all the strain readings to scatter about a common straight line. The curve includes two approximately straight line portions, however, one for relatively low loads indicating an elastic buckling load of 48,800 pounds and another close to failure indicating the correct buckling load of 36,500 pounds. A Southwell plot that would have included only readings on the first straight-line range would obviously have led to the wrong answer. The Southwell method must, therefore, be used with caution; a sufficiently large number of observed deformations must be plotted to establish the existence of a linear relation between δ and δ/P over a large range of deformations.

In the case of specimen 6, the observed ultimate load agrees well with the calculated critical load for bending

failure but is about 8 percent less than the calculated load for twisting failure. This difference is too small to indicate that buckling failure must have occurred in preference to twisting failure. It is likely that the final failure of specimens 1 and 6 both was due to a deformation in which the stringers were simultaneously bent and twisted.

In the case of the 5-inch, short-column specimen, a good, straight line was obtained only for the twist, with a slope of 6,400 pounds, which was in close agreement with the observed ultimate load of 8,300 pounds.

The last column of table IV lists the stringer stress corresponding to the elastic buckling load, which was obtained by extrapolating the experimental curves of stringer load in figures 40 and 41 to an external load equal to the elastic buckling load. Comparison with figure 4 shows that the stringer stress for elastic buckling lies well beyond the elastic portion of the stress-strain curve in most cases. In the case of the 5-inch Z bar, which failed by twisting, it is actually 20 percent above the compressive yield strength of the material; it may be concluded that the section retained its torsional rigidity under stresses producing plastic yielding in compression.

CONCLUSIONS

The deformation of two sheet-stringer panels subjected to end compression under carefully controlled end conditions (ends cast in Wood's metal, sides simply supported) was measured at a number of points and at a number of loads, most of them above the load at which the sheet had begun to buckle. The two panels were identical except for the sheet, which was 0.070-inch 24ST Alclad for the first panel, designated as specimen 1, and 0.025-inch 24ST aluminum alloy for the second panel, designated as specimen 6.

A technique was developed for attaching Tuckerman optical strain gages to the sheet without disturbing the strain distribution in the sheet by the method of attachment. By means of this technique, extreme fiber strains were measured in an axial as well as in a transverse direction at a sufficient number of points on specimen 6 to give a fairly complete picture of the strain distribution in the buckled sheet.

The shape of the buckles in the sheet of specimen 6 was recorded at two loads by means of plaster of paris casts.

The twisting and the bending of the stringers were measured by means of pointers attached to the stringers at a large number of sections. Pointer positions were recorded photographically up to the ultimate load, at which the stringers failed by buckling.

The sheet loads at failure and the stringer loads at failure were compared with the corresponding loads for a set of five similar panels tested at the Navy model basin. The sheet load at failure was found to be nearly constant for a given size of sheet, ranging from 5,500 to 5,650 pounds for the 0.070-inch 24ST Alclad and from 900 to 1,100 pounds for the 0.025-inch 24ST sheet. The average stringer stress at failure was equal to 36,200 pounds per square inch for each one of the two specimens tested at the National Bureau of Standards. It ranged from 30,200 to 38,400 pounds per square inch for the specimens tested at the model basin. The loss in buckling strength of the stringers in some of the panels tested at the model basin was probably due to a difference in end restraint, the flat-end condition used at the model basin tests providing less restraint than the casting of the ends in Wood's metal used at the National Bureau of Standards.

A detailed comparison was made between the measured deformation of the buckled sheet and the deformation calculated from approximate theories for the deformation in a square sheet with freely supported edges buckling under end compression which have been advanced by Timoshenko, Frankland, and Marguerre. Frankland's theory is the only one of the three considering the effect of the stringer. Timoshenko's solution was extended to cover the case of rectangular buckles that were not square. The buckles in the sheet-stringer panels had a ratio of 0.6 to 0.7 of length to width so that this extension seemed desirable. Frankland's theory and Marguerre's theory were used without going beyond the relatively simple special case of the square sheet. The comparison led to the following results.

The sheet load and the effective width of the sheet was most accurately described by Marguerre's approximate theory; a relatively "exact" formula due to Marguerre gave still better agreement with the observed sheet load. Frankland's theory described the effective width for spec-

imen 1 but gave values that were too high for specimen 6. Timoshenko's theory resulted in a variation (up to 25 percent) in effective width in passing from the node of a buckle to its crest, which was larger than that observed but which covered the observed values within its range.

The distribution of median fiber strain across the sheet was fairly well described by all three theories, with Timoshenko's and Frankland's theories somewhat better than Marguerre's. Timoshenko's theory predicted, in particular, the somewhat paradoxical setting up of median fiber tensile strain in the center of the sheet under sufficiently high end compression.

The distribution of transverse strain was found to be described satisfactorily by Frankland's theory only. The distribution given by Timoshenko's and Marguerre's theories differed from the observed values not only quantitatively but even in sign.

The measured distribution of axial stress across the sheet of specimen 6 was described most satisfactorily by Frankland's theory. Timoshenko's theory indicated a change in stress distribution in passing from a buckle node to a buckle crest which was greater than the observed change and which differed from it in character. Marguerre's approximate theory showed no change in stress distribution in an axial direction; the shape of the stress-distribution curve differed considerably from the observed curve especially at high loads. The variation with load of the axial stress at the buckle crest for specimen 6 was best described by Frankland's theory while that of the transverse stress at the buckle crest was best described by Marguerre's theory. The shape of the buckle was best described by Timoshenko's theory. A corresponding agreement could not be expected from Marguerre's and Frankland's theories, which had not been extended to the case of rectangular buckles different from a square. Marguerre's buckle had a transverse section which was not sinusoidal as for the other two theories but which had a third-order harmonic to describe the presence of local buckles near the edge of the sheet. The third-order component increased rapidly as the buckles in the sheet became deeper and led to an increased difference between the calculated and the measured buckle contour.

It is probable that both Frankland's and Marguerre's theories would describe the deformation of the buckled sheet better than Timoshenko's theory if the numerical

solutions were extended to rectangular buckles that are not square. An improvement in all three theories as applied to the buckling of the sheet between stringers is to be expected from the assumption of a buckle contour whose transverse section more nearly corresponded to that of the measured buckles; the transverse sections of the measured buckles showed a lessening in the slope near the stringer edge due to the restraint from the stringers to which the sheet is attached, while the slope of the theoretical buckles was a maximum at the stringer edge.

The measured effective width for specimens 1 and 6 was compared with the effective width given by nine different relations for effective width as a function of the edge stress σ divided by the buckling stress σ_{cr} of the sheet, which were found in the literature. The value of σ_{cr} will, in general, depend on the method of attachment of the sheet to the stringer and also on the rigidity of the stringer. Taking it equal to the measured critical stress brought the points for both specimens to scatter about a common curve excepting those points where yielding of the plate was appreciable. The most satisfactory description of this curve was given by Cox's formula

$w/2a = 0.14 + 0.85 \sqrt{\sigma_{cr}/\sigma}$ in which $w/2a$ is the ratio of the effective width w of the sheet to its initial width $2a$. Approximating σ_{cr} by its value for a long rectangular sheet with supported edges gave values that were about 8 percent low for specimen 1 and about 40 percent low for specimen 6. Applying this convenient though inaccurate approximation gave the best results with

Marguerre's formula $w = 2a \sqrt[3]{\sigma_{cr}/\sigma} = 1.54 t \sqrt[3]{\frac{E}{\sigma} \frac{2a}{t}}$ where

t is the sheet thickness; this formula was found to describe the observed effective width of both specimens up to failure within 12 percent. Von Kármán's well-known formula, which is upon the same basis $w = 2a \sqrt{\sigma_{cr}/\sigma} = 1.92 t \sqrt{E/\sigma}$, was found to lead to effective widths up to 35 percent below those observed for specimen 6.

The analysis of the measured stringer deformation was confined to an application of Southwell's method of plotting deformation against deformation over load. If the stringer approaches instability in accordance with Southwell's relation, the deformation will be a linear function of the deformation divided by the load and the

slope of the straight line obtained will be equal to the elastic buckling load. Care must be taken to plot the deformation due to the load, which necessitates a small zero correction to the measured deformation in many cases. Applying this correction to the twisting deformation of one of the stringers of specimen 1, as measured by the displacement of pointers attached to the stringer, gave excellent straight lines with a slope in remarkable agreement with the observed ultimate load of the panel. A very good check with the observed ultimate load was also obtained from a plot of the bending deformation as indicated by the pointer readings. A plot of bending deformation of the stringer as indicated by the difference in extreme fiber strains measured by Tuckerman optical strain gages gave a number of points which could not be brought to scatter about a common straight line but which had two approximately straight-line portions, one with a slope 34 percent greater than the ultimate load and the other with a slope equal to the ultimate load. A Southwell plot that would have included only readings in the first straight-line range would, obviously, have led to the wrong answer. In the case of specimen 6, buckling loads for twisting deformation and for bending deformation were not in as striking agreement with the observed buckling load, but the agreement was still sufficient to indicate that the stringer failure in both specimens was due to an instability in which the stringer was simultaneously twisted and bent as a column. The conclusion that the failure of the stringers of both specimens was due to a combination of twisting instability and column instability was also drawn from the plots of observed twists about three mutually perpendicular axes, which were obtained from the displacements of the pointers attached to the stringers.

Application of Southwell's method to the twisting failure of a 5-inch stringer specimen tested as a short column led to a buckling load that was in close agreement with the observed buckling load, although the axial compressive stress at failure was well above the yield strength of the material.

It must not be concluded from the success of Southwell's method in all those cases in which the existence of a straight-line relation between deformation and deformation over load was established over a large range of deformations that Southwell's method is applicable to the whole range of primary instabilities that may be encountered in monocoque construction. Proofs for the

validity of the method have been found in the literature for only two cases: the slightly bent elastic column, and the elastic member of constant section under certain combinations of axial and transverse loads. Except for these special cases, the validity of the method rests on rather meager experimental evidence such as the work of Gough and Cox on the buckling of plates subjected to edge shears and the work presented in this paper. Much more empirical evidence and much more theoretical knowledge are needed on the change of deformation with load of structures approaching instability to establish the scope of the method and to clear up cases of straight-line plots over a limited range of deformation which may lead to erroneous conclusions.*

National Bureau of Standards,
Washington, D. C., September 21, 1938.

*A theoretical explanation for the greater generality of Southwell's method has been advanced by L. B. Tuckerman since the preparation of this note. Tuckerman showed in a paper entitled "Heterostatic Loading and Critical Astatic Loads" (Jour. Res., Natl. Bur. Stand., vol. 22 (1939) pp. 1-18, RP 1163) that Southwell's relation will apply to any one of the great family of instabilities included in Westergaard's general theory for the buckling of elastic structures.

REFERENCES

1. Schnadel, G.: Über Knickung von Platten. Werft Reederei Hafen, 9, 1928, pp. 500-502.
2. Schnadel, G.: Die Überschreitung der Knickgrenze bei dünnen Platten. Verh. d. dritten Inter. Kong. f. Tech. Mech. (Stockholm), III, 1931, pp. 73-81.
3. Sezawa, Katsutada: On the Buckling under Edge Thrusts of a Rectangular Plate Clamped at Four Edges. Report 69 (vol. VI, no. 3), Aero. Res. Inst., Tokyo Imperial Univ., April 1931.
4. Donnell, L. H., Sechler, E. E., and von Kármán, Theodor: Survey of Problems of Thin Walled Structures. Guggenheim Aeron. Lab., Cal. Inst. Tech. Pub. 16 (1932).
5. Von Kármán, Theodor, Sechler, Ernest E., and Donnell, L. H.: The Strength of Thin Plates in Compression. A.S.M.E. Trans., APM-54-5, Jan. 30, 1932, pp. 53-57.
6. Sezawa, Katsutada: Das Ausknicken von allseitig befestigten und gedrückten rechteckigen Platten. Z.f.a.M.M., Bd. 12, 1932, S. 227-229.
7. Cox, H. L.: The Buckling of Thin Plates in Compression. R. & M. No. 1554, Brit. A.R.C., 1933.
8. Von Kármán, Theodor: Survey of Problems of Thin Walled Structures. Part III - Analysis of Some Typical Structures. A.S.M.E. Trans., AER-55-19c, Oct.-Dec. 1933, pp. 155-158.
9. Sechler, E. E.: The Ultimate Strength of Thin Flat Sheets in Compression. Guggenheim Aeron. Lab., Calif. Inst. Tech. Pub. 27 (1933).
10. Taylor, G. I.: The Buckling Load for a Rectangular Plate with Four Clamped Edges. Z.f.a.M.M., Bd. 13, 1933, S. 147-152.
11. Leggett, D. M. A.: On the Elastic Stability of a Rectangular Plate when Subjected to a Variable Edge Thrust. Proc. Cambridge Phil. Soc. 31, pp. 368-381 (1935).

12. Sattler, K.: Beitrag zur Knicktheorie dünner Platten. Mitt. Forsch. Anst. GHW-Konzern 3, (1935) S. 257-279.
13. Schmieden, C.: Das Ausknicken eines Plattenstreifens unter Schub- und Druckkräften. Z.f.a.M.M., Bd. 15, Heft 5, Oct. 1935, S. 278-285.
14. Trefftz, E.: Die Bestimmung der Knicklast gedrückter, rechteckiger Platten. Z.f.a.M.M., Bd. 15, Heft 6, Dec. 1935, S. 339-344.
15. Yamamoto, Mineo, and Kondo, Kazuo: Buckling and Failure of Thin Rectangular Plates in Compression. Aero. Res. Inst., Tokyo Imp. Univ. Report No. 119, (vol. 10, no. 1), April 1935.
16. Kaufmann, W.: Über unelastisches Knicken rechteckiger Platten. Ingenieur-Archiv 7, (1936), S. 153-165.
17. Miles, Aaron J.: Stability of Rectangular Plates Elastically Supported at the Edges. A.S.M.E. Trans., vol. 3, no. 2, June 1936, pp. A47-A52.
18. Iguchi, S.: Allgemeine Lösung der Knickungsaufgabe für rechteckige Platten. Ingenieur-Archiv 7, (1936), S. 207-215.
19. Timoshenko, S.: Theory of Elastic Stability. McGraw-Hill Book Co., Inc. (1936).
20. Barbré, R.: Stabilität gleichmäßig gedrückter Rechteckplatten mit Längs- oder Querstreifen. Ingenieur-Archiv ~~2~~, (1937), S. 117-150. ³³²⁻³⁴⁸
21. Burchard, W.: Beulspannungen der quadratischen Platte mit Schrägsteife unter Druck bzw. Schub. Ingenieur-Archiv 8, (1937), S. 332-348.
22. Grzedzielski, A., and Billewicz, W.: Sur la rigidité de la tôle flambée. Sprawozdanie I.B.T.L., No. 1 (21) 1937, pp. 5-22.
23. Marguerre, Karl: Die mittragende Breite der gedrückten Platte. Luftfahrtforschung, Bd. 14, Lfg. 3, March 20, 1937, S. 121-128.
24. Marguerre, K., and Trefftz, E.: Über die Tragfähigkeit eines längsbelasteten Plattenstreifens nach Überschreiten der Beullast. Z.f.a.M.M., Bd. 17, Heft 2, April 1937, S. 85-100.

25. Schuman, Louis, and Back, Goldie: Strength of Rectangular Flat Plates under Edge Compression. T.R. No. 356, N.A.C.A., 1930.
26. Schwartz, E. H.: An Investigation of the Compressive Strength Properties of Stainless Steel Sheet-Stringer Combinations, Part II. Air Corps Tech. Rep. 4096. (1936)
27. Matulaitis, J., and Schwartz, E. H.: An Investigation of the Compressive Strength Properties of Stainless Steel Sheet-Stringer Combinations. Part IV. Air Corps Tech. Rep. 4271 (1936).
28. Lahde, R., and Wagner, H.: Experimental Studies of the Effective Width of Buckled Sheets. T.M. No. 814, N.A.C.A., 1936.
29. Newell, J. S., and Harrington, J. H.: Progress Report on Methods of Analysis Applicable to Monocoque Aircraft Structures. (Coordinated by P. H. Kemmer) Air Corps Tech. Rep. 4313 (1937).
30. Sechler, E. E.: Stress Distribution in Stiffened Panels under Compression. Jour. Aero. Sci., vol. 4, no. 8, June 1937, pp. 320-333.
31. Army-Navy-Commerce Committee on Aircraft Requirements: Strength of Aircraft Elements. ANC-5, Jan. 1938.
32. Nadai, A.: Elastische Platten. Julius Springer (Berlin), 1925.
33. Howland, W. L.: Effect of Rivet Spacing on Stiffened Thin Sheet under Compression. Jour. Aero. Sci., vol. 3. (1936) pp. 434-39.
34. Von Kármán, Th.: Festigkeitsprobleme in Maschinenbau. Encyk. der Math. Wissen. 4, 1910, S. 311-385.
35. Lundquist, Eugene E., and Fligg, Claude M.: A Theory for Primary Failure of Straight Centrally Loaded Columns. T.R. No. 582, N.A.C.A., 1937.
36. Kappus, Robert: Twisting Failure of Centrally Loaded Open-Section Columns in the Elastic Range. T.M. No. 851, N.A.C.A., 1938.

37. Southwell, R. V.: On the Analysis of Experimental Observations in Problems of Elastic Stability. Proc. Roy. Soc. (London), ser. A, vol. 135, 1932, pp. 601-616.
38. Fisher, H. R.: An Extension of Southwell's Method of Analyzing Experimental Observations in Problems of Elastic Stability. Proc. Roy. Soc. (London), ser. A, vol. 144, 1934, pp. 609-630.
39. Gough, H. J., and Cox, H. L.: Some Tests on the Stability of Thin Strip under Shearing Forces in the Plane of the Strip. Proc. Roy. Soc. (London), ser. A, vol. 137, 1932, pp. 145-157.
40. Lundquist, Eugene E.: Generalized Analysis of Experimental Observations in Problems of Elastic Stability. T.N. No. 358, N.A.C.A., 1938.

TABLE I - DESCRIPTION OF SHEET-STRINGER SPECIMENS
[See also fig. 1]

Specimen	Material		Length (in.)	Width (in.)	Sheet thick- ness (in.)	Total stringer area $3A_{st}$ (sq.in.)	Total sheet area $4A_s$ (sq. in.)	Ratio of stringer area to total area $\frac{3A_{st}}{4A_s + 3A_{st}}$
	Stringers	Sheet						
1	24ST Extruded	24ST Alclad	19	16	0.070	0.39	1.12	0.26
6	24ST Extruded	24ST	19	16	.025	.39	.40	.49

TABLE II - TENSILE PROPERTIES OF SHEET AND Z STRINGERS
AS OBTAINED BY NAVY DEPARTMENT

	Young's modulus (kips per sq. in.)	Tensile yield strength (kips per sq. in.)	Tensile strength (kips per sq. in.)
Specimen 1: 24ST Alclad sheet Stringer	9,700	49.7	62.8
A	10,800	47.9	-
B	10,500	52.8	64.0
C	10,400	50.1	63.6
Specimen 6: 24ST sheet Stringer	10,500	47.3	65.5
Q	10,500	51.8	63.3
R	10,500	51.9	63.6
S	10,400	51.6	65.0

TABLE III - RESULTS OF END COMPRESSION TESTS OF SHEET-STRINGER PANELS

Specimen	Sheet		Length	Loads at failure			Stringer stress at failure (average)	Effective width of plate at failure
	Material	Thickness		Total	Average			
					Sheet element	Stringer element		
		(in.)	(in.)	(lb.)	(lb.)	(lb.)	(lb./sq. in.)	(in.)
1 National Bureau of Standards	24ST Alclad	0.070	19.00	38,500	5,600	4,700	36,200	2.35
2A Navy model basin	24ST Alclad	.070	7.28	38,800	5,650	4,750	38,400	2.59
2B Navy model basin	24ST Alclad	.070	11.82	37,000	5,600	4,870	37,400	2.35
3 Navy model basin	24ST Alclad	.070	19	36,000	5,500	5,000	38,400	2.55
4 Navy model basin								
Top section	24ST	.025	19	15,800	900	4,070	31,300	1.12
Middle section	24ST	.025	19	15,800	1,000	3,930	30,300	1.25
5 Navy model basin	24ST	.025	19	16,100	1,050	3,970	30,400	1.35
6 National Bureau of Standards	24ST	.025	19	18,400	1,100	4,700	36,200	1.27

¹Extrapolated to load at failure

TABLE IV - RESULTS OF SOUTHWELL PLOTS OF STRINGER DEFORMATION
(Confined to plots with a scatter of points about a common straight line)

Specimen	Type of deformation	Measured by	Estimate of elastic buckling load by Southwell's method (lb.)	Observed load at failure (lb.)	¹ Stringer stress for elastic buckling (lb./sq. in.)
1	Bending as a column	Rotation of pointer 8, stringer A	36,000	36,500	33,800
	Bending as a column	Rotation of pointer 9, stringer A	38,000	36,500	33,800
	Twisting	Rotation of pointer 5, stringer A	36,500	36,500	35,800
	Twisting	Rotation of pointer 6, stringer A	36,500	36,500	35,800
	Twisting	Rotation of pointer 7, stringer A	38,500	38,500	35,600
	Twisting	Rotation of pointer 9, stringer A	36,500	36,500	35,600
6	Bending as a column	Difference in strain at center, stringer R	19,100	18,400	37,100
	Bending as a column	Pointer 3, stringer R	19,100	18,400	37,100
	Bending as a column	Pointer 4, stringer R	19,100	18,400	37,100
	Twisting	Pointer 6, stringer R	20,000	18,400	39,200
	Twisting	Pointer 7, stringer R	20,000	18,400	39,200
	Twisting	Pointer 8, stringer R	20,000	18,400	39,200
5-inch 2 bar	Twisting	Rotation of section	6,400	6,300	49,200

¹Stringer stress calculated by extrapolation from figures 40 and 41.

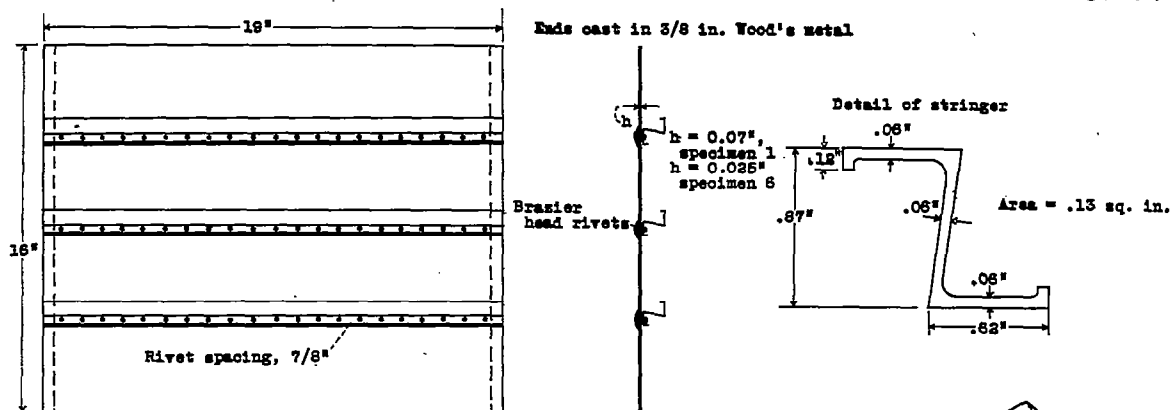


Figure 1.- Sheet-stringer specimens 1 and 6.

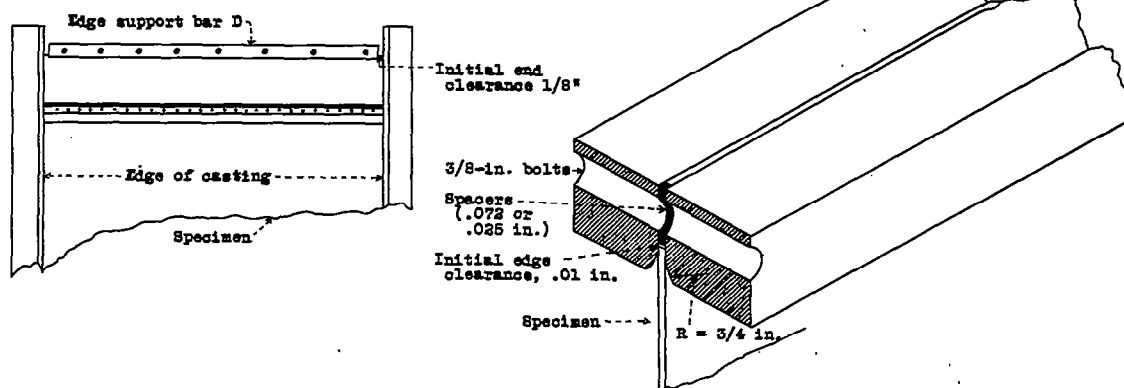


Figure 7.- Edge support bar.

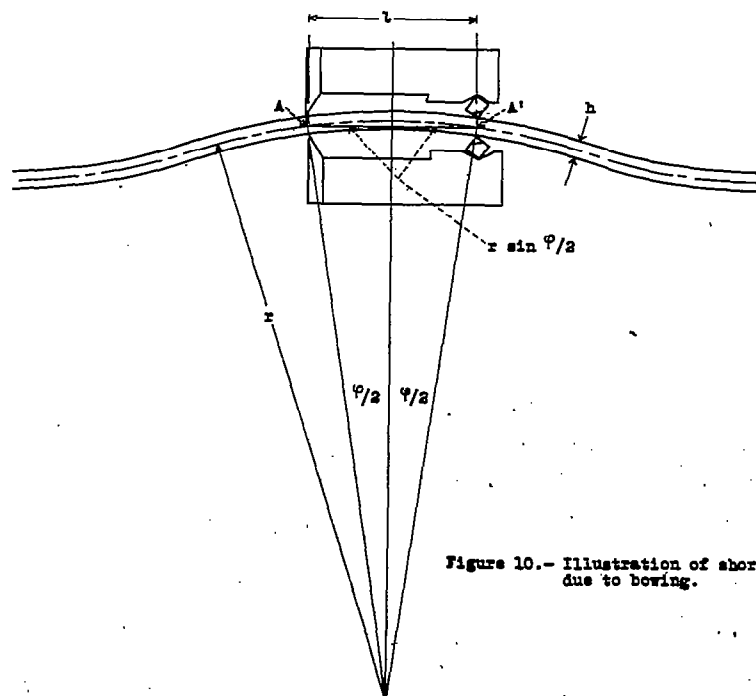


Figure 10.- Illustration of shortening due to bowing.

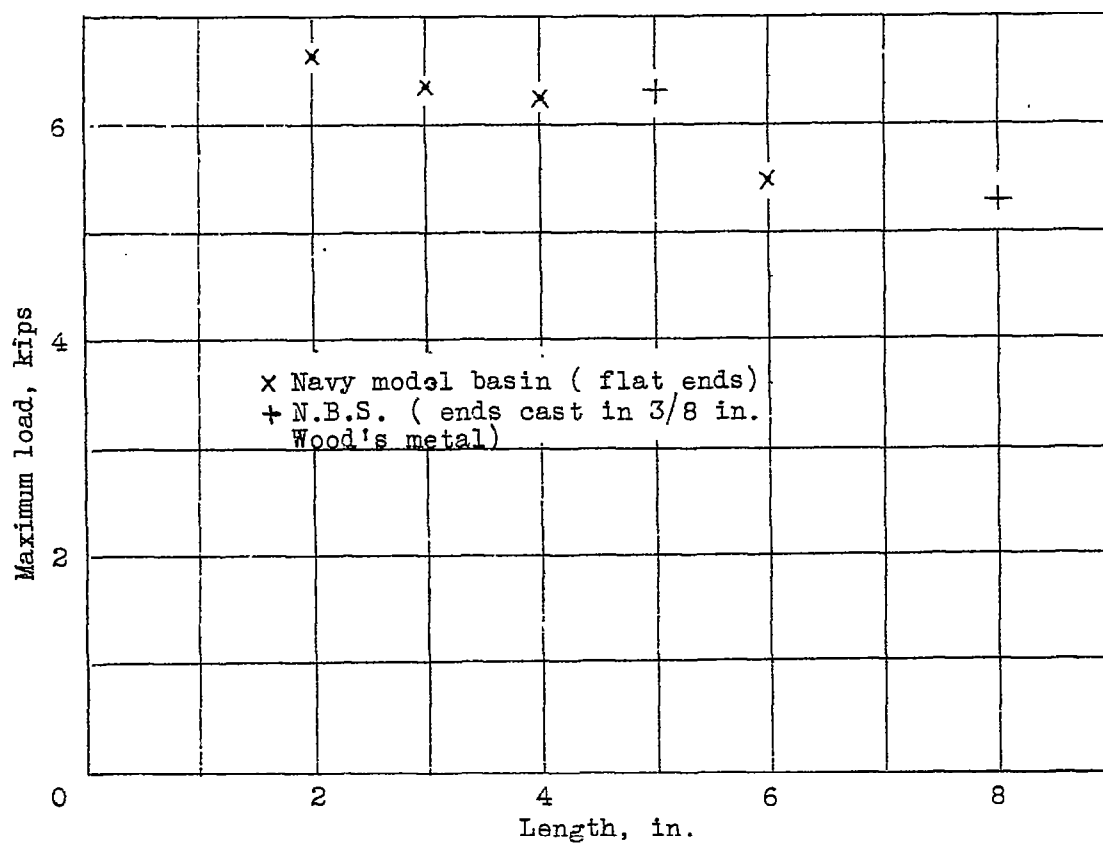


Figure 2.- Column strength of Z stringers.

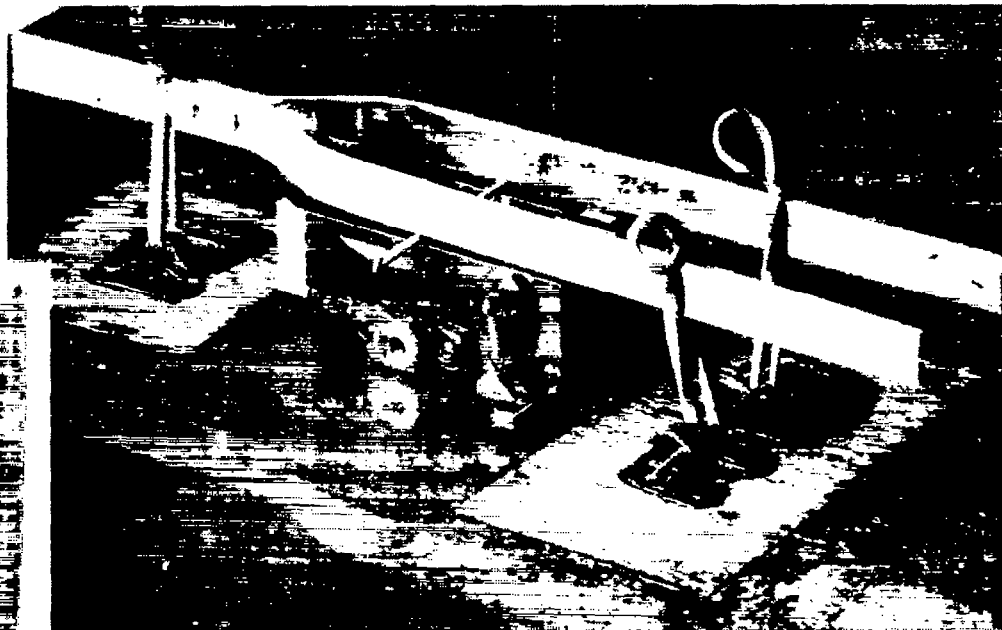


Figure 8.- Method of holding strain gage on sheet.

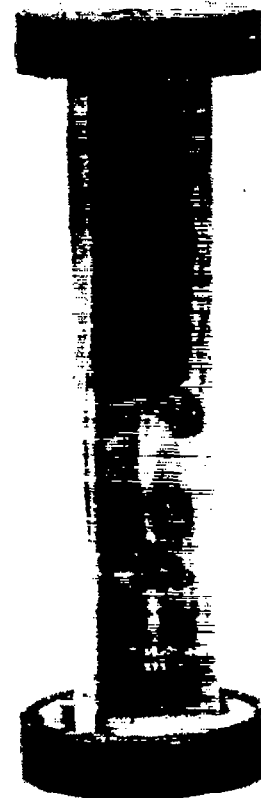
B

A

A 5-inch short column specimen after failure, showing method of casting ends in Wood's metal.

B 8-inch short column specimen after failure.

Figure 3.- Flat - end-column specimens.



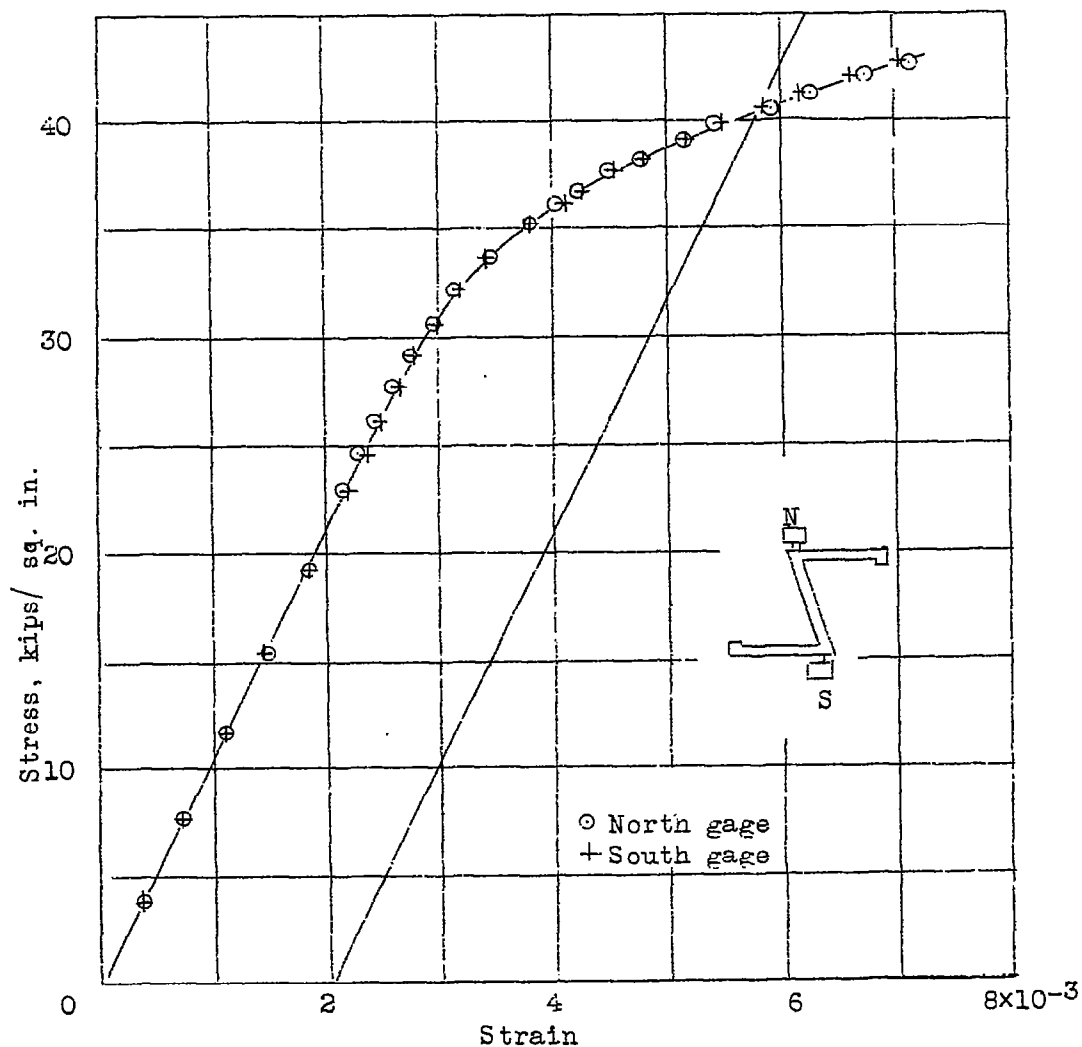


Figure 4.- Column test of 5 inch Z bar specimen. (ends cast in Wood's metal). Yield strength, 40.5 kips /sq. in., Column strength, 48.3 kips/sq. in. . maximum load, 6.3 kips, area= 0.1304 sq. in.. $1/r = 14.3$.

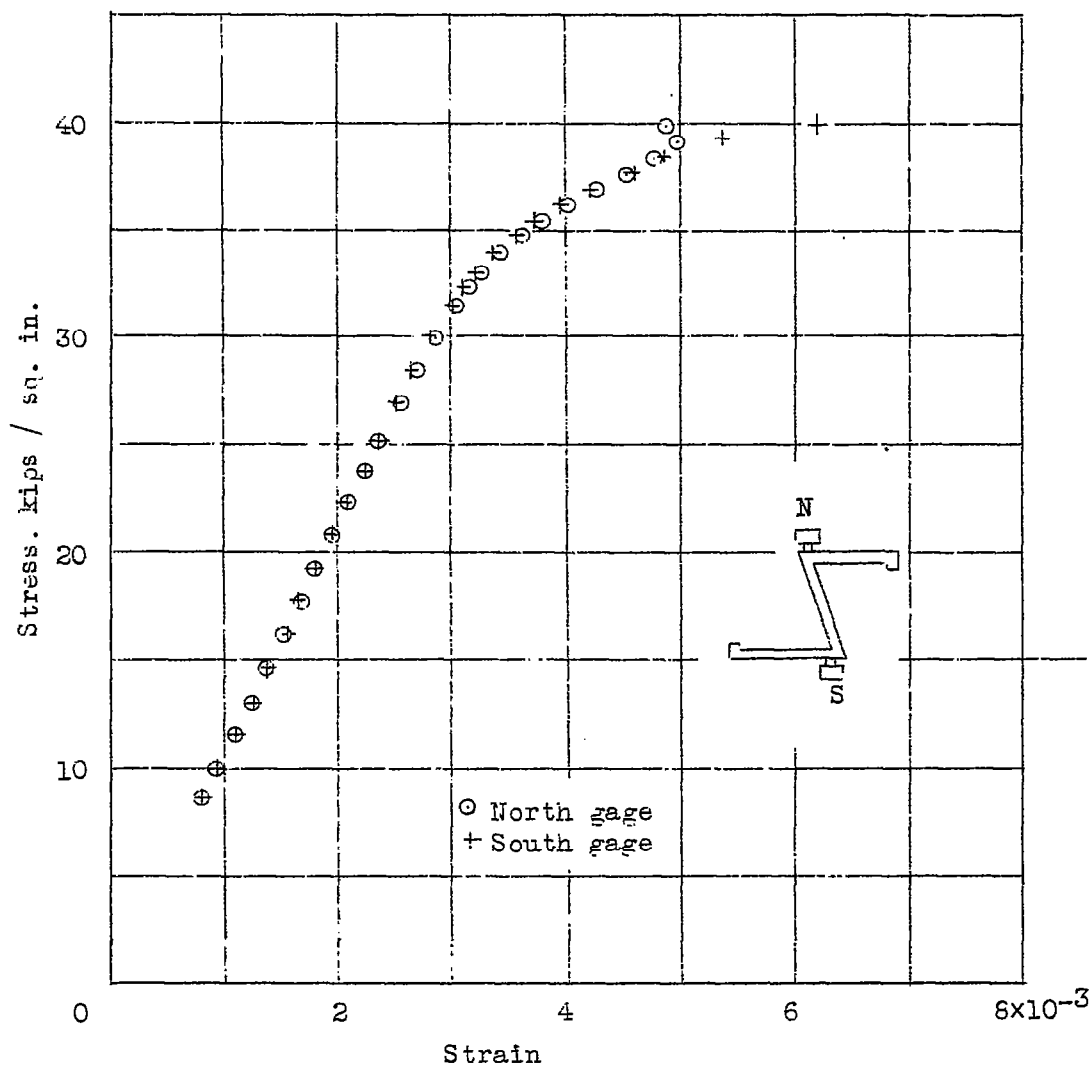


Figure 5.- Column test of 8 inch Z bar specimen. (ends cast in Wood's metal) Column strength, 40.65 kips/sq. in.; maximum load, 5.3 kips.; area, 0.1304 sq. in.; $1/r = 22.9$.

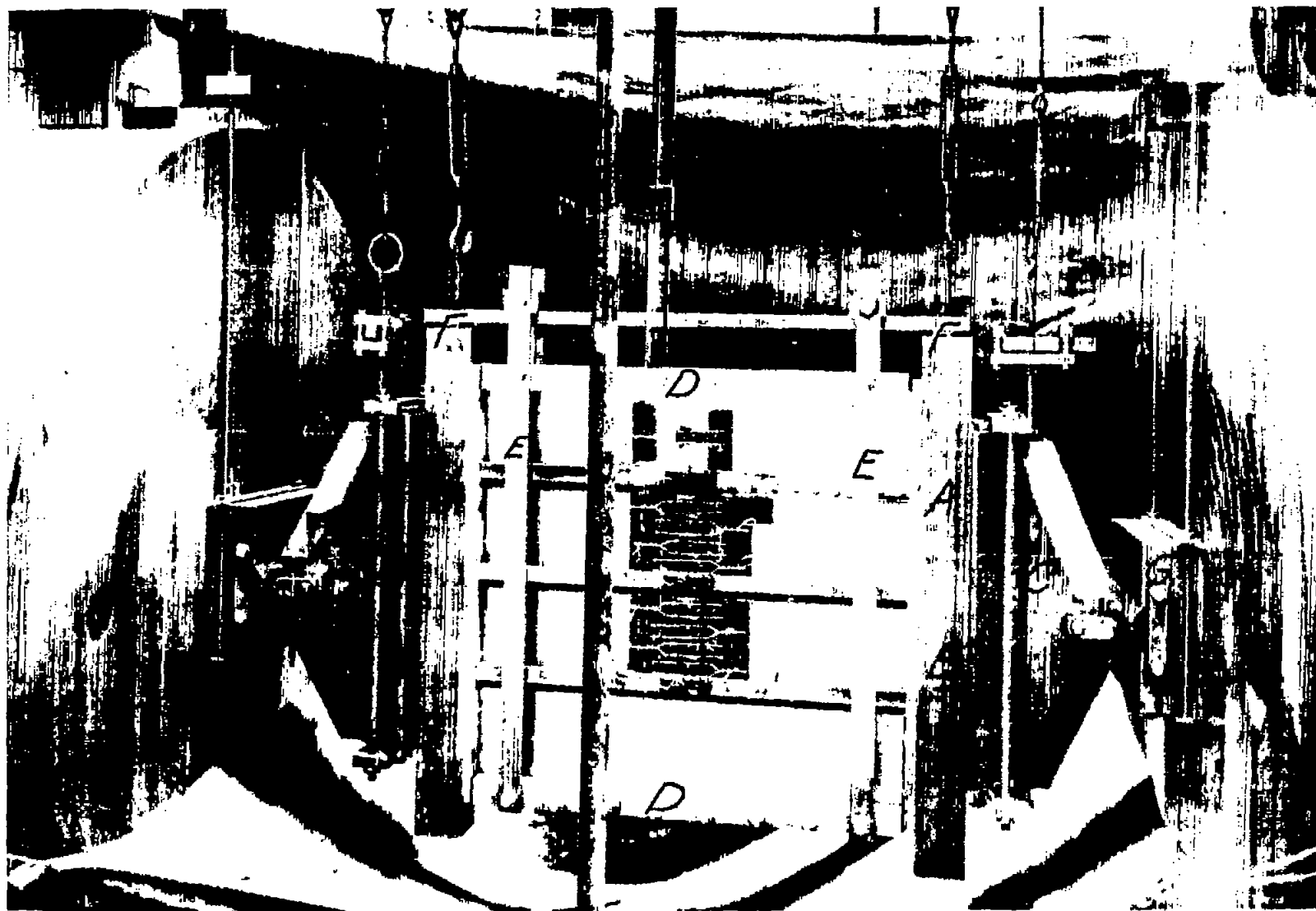


Figure 6.- Specimen 1 with four pairs of strain gages to measure axial strain between adjacent stringers.

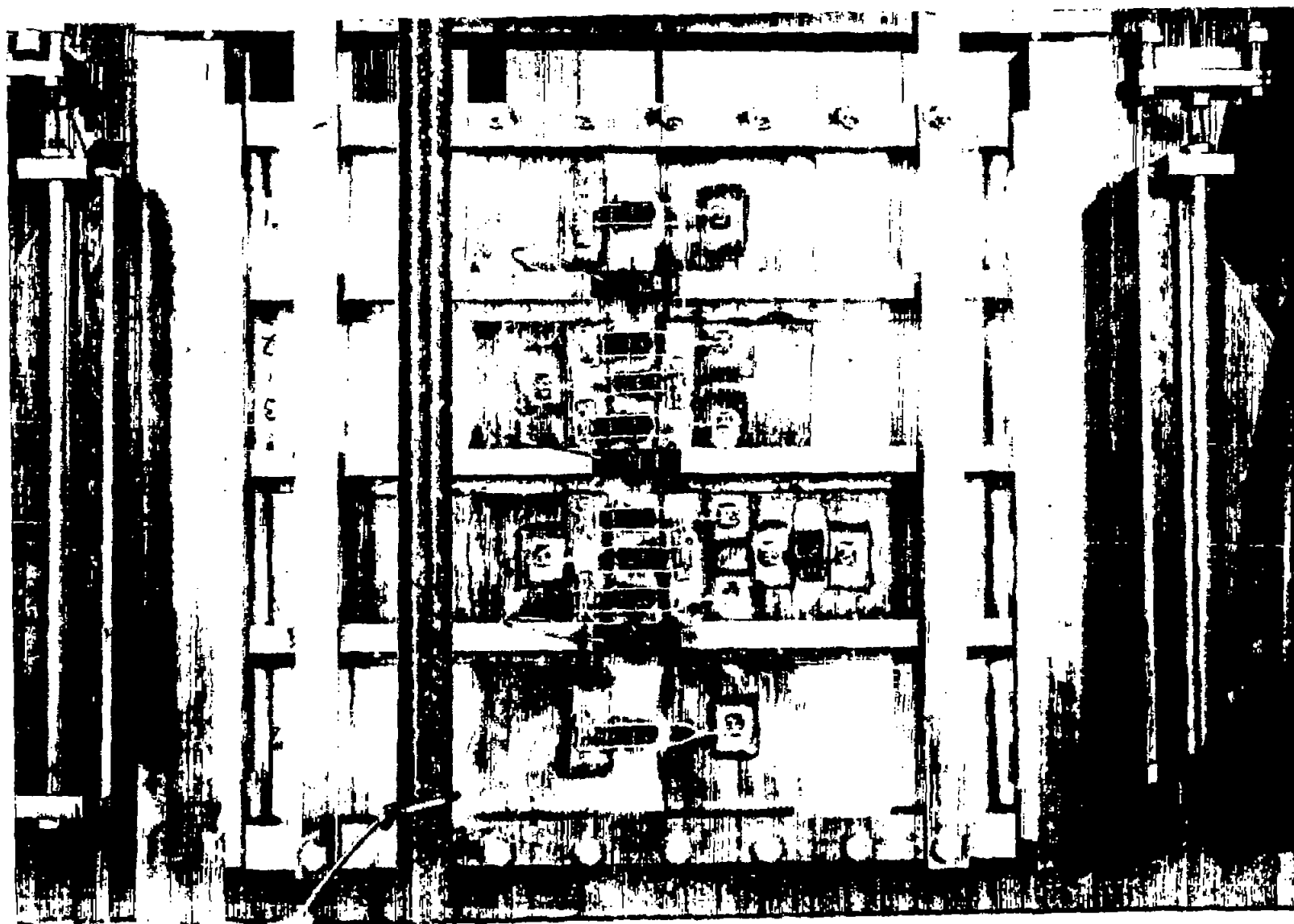


Figure 9.- Specimen 1 with three pairs of strain gages to measure strain between adjacent stringers.

Load kips

Strain
 20×10^{-4}

Load kips

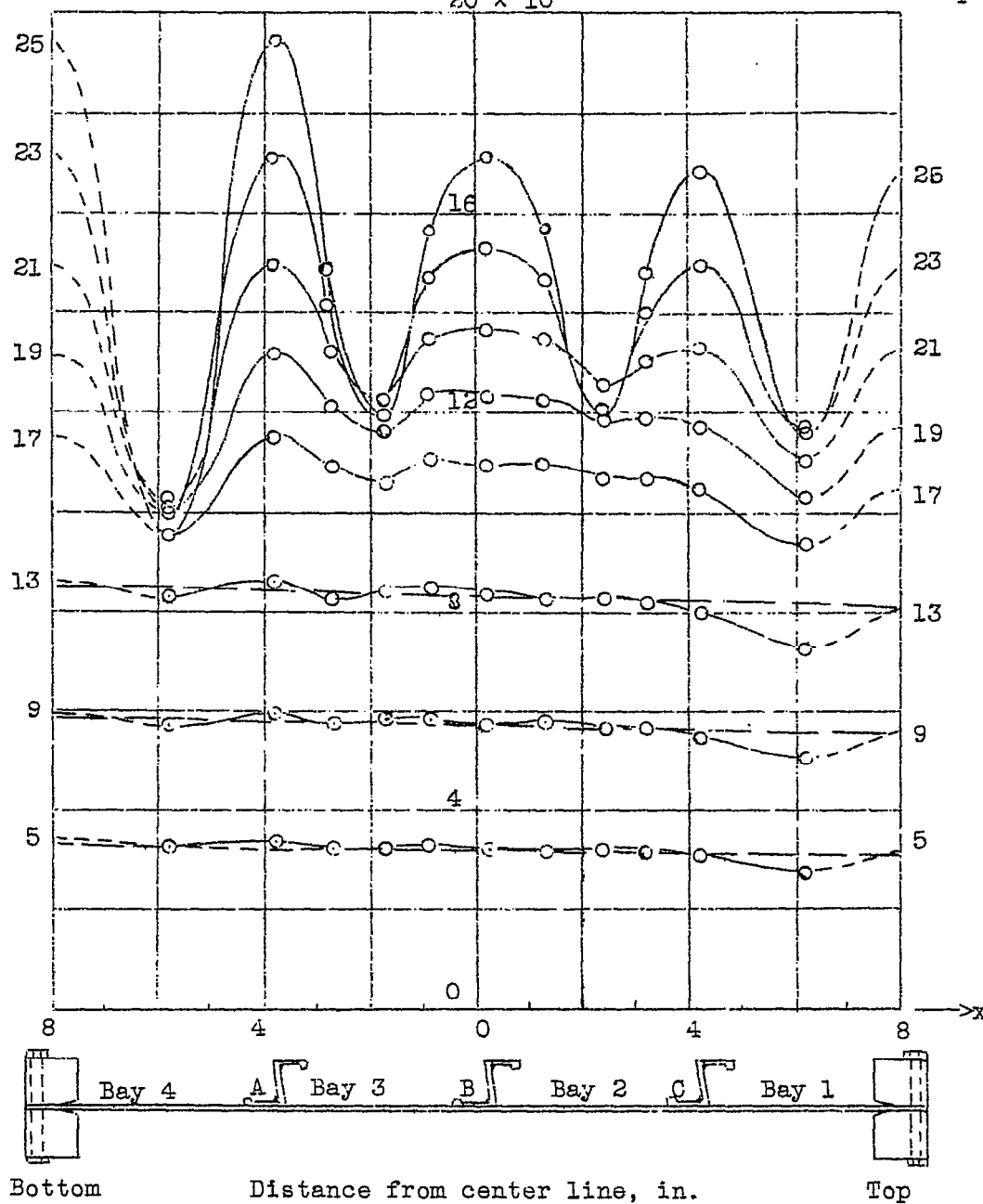


Figure 11.- Distribution of axial strain at median fiber along transverse center line, Specimen 1.

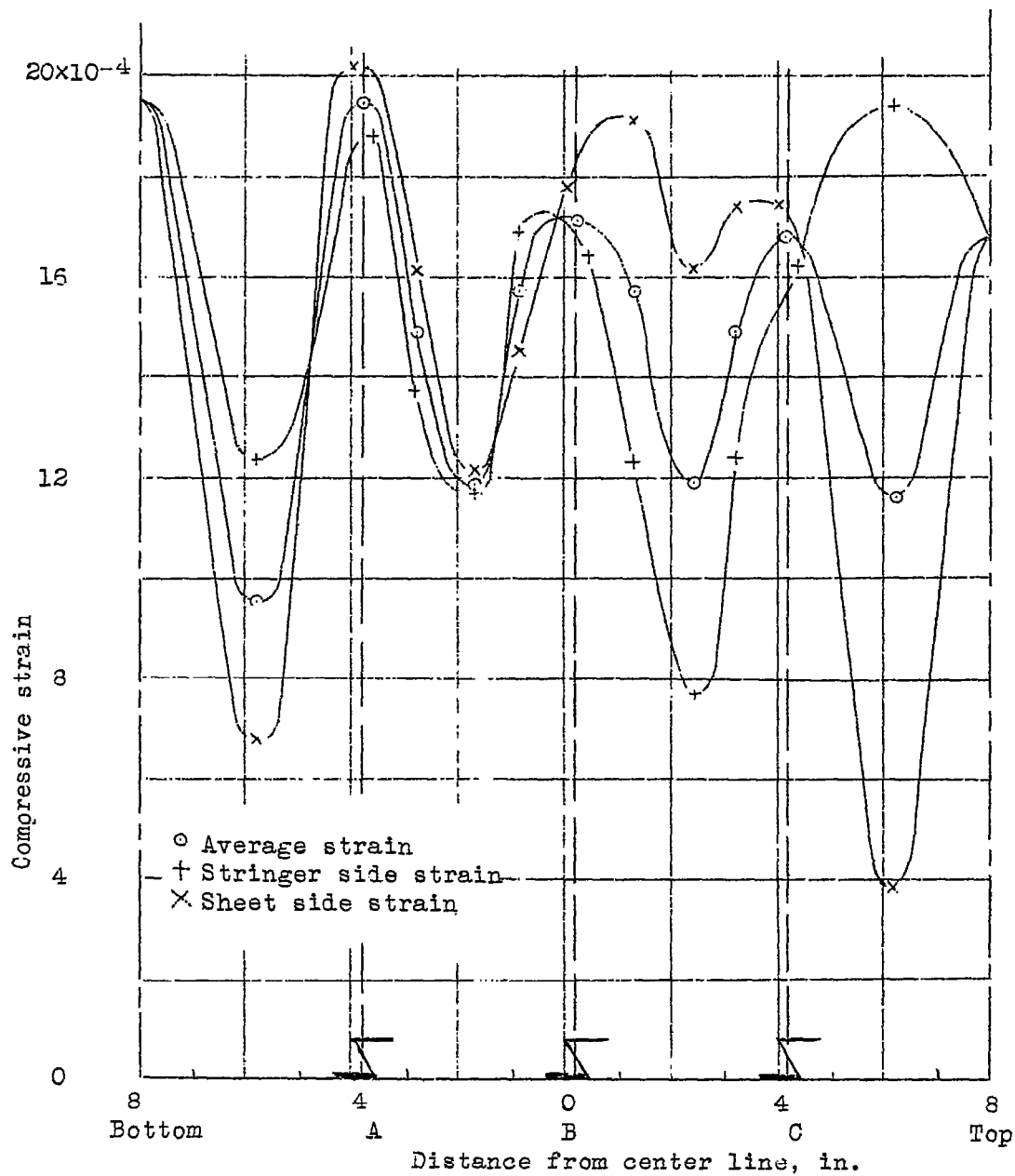


Figure 12.- Distribution of extreme fiber strains along transverse center line. Specimen 1, load, 25,000 lb.

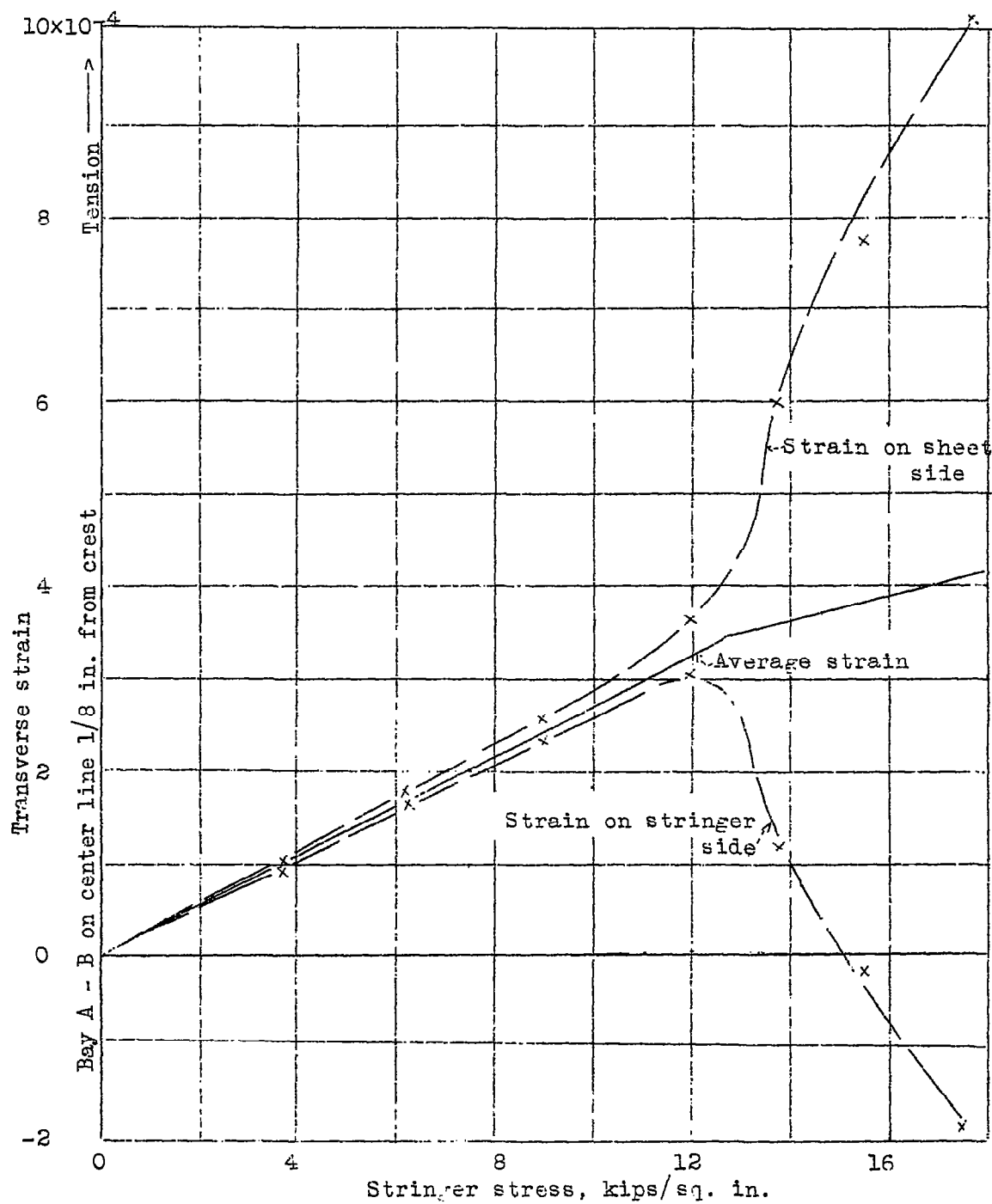


Figure 13.- Buckling indicated by spread of extreme fiber strains.
Specimen 1.

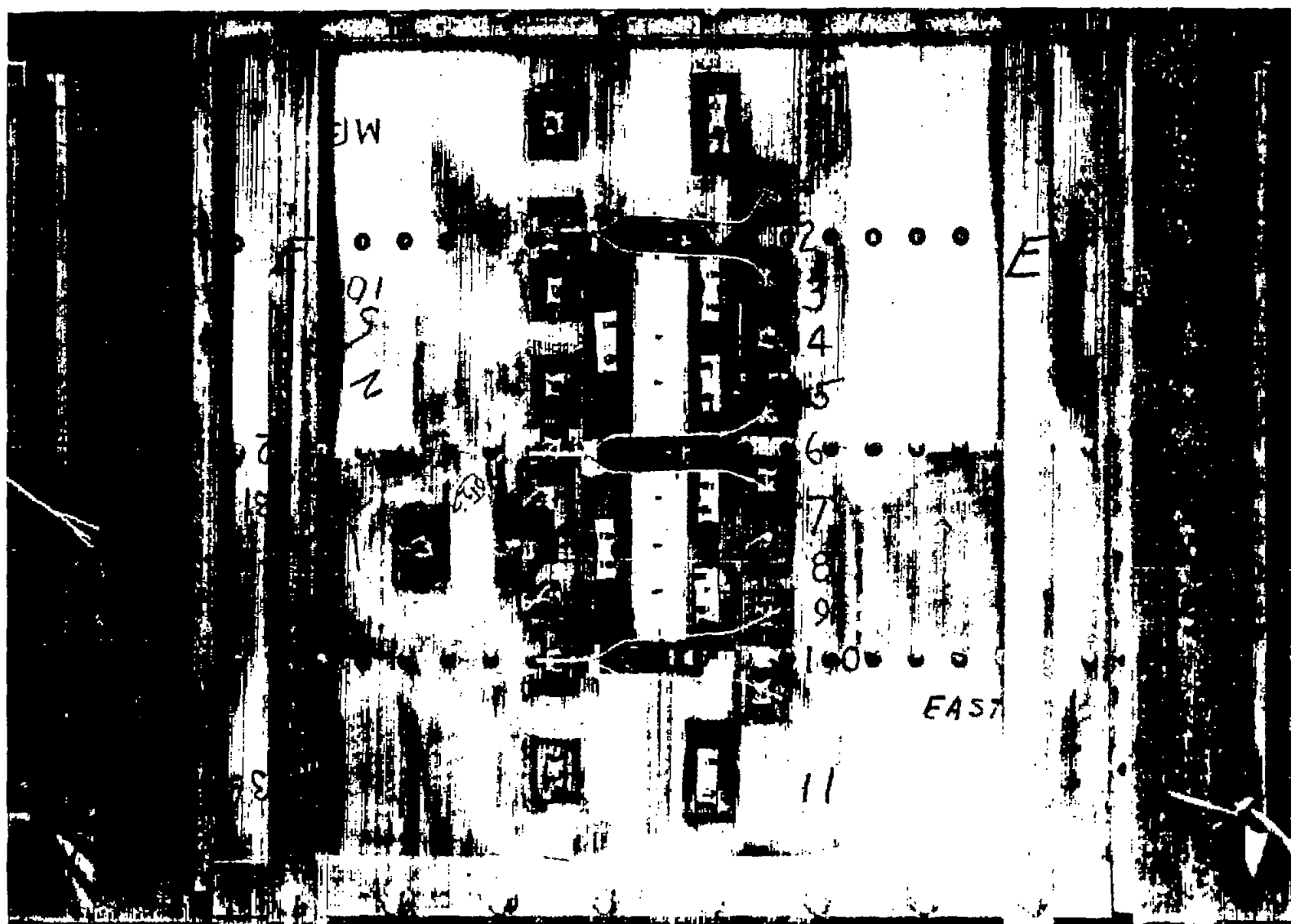


Fig. 14

Figure 14.- Sheet side of specimen 1 after failure.

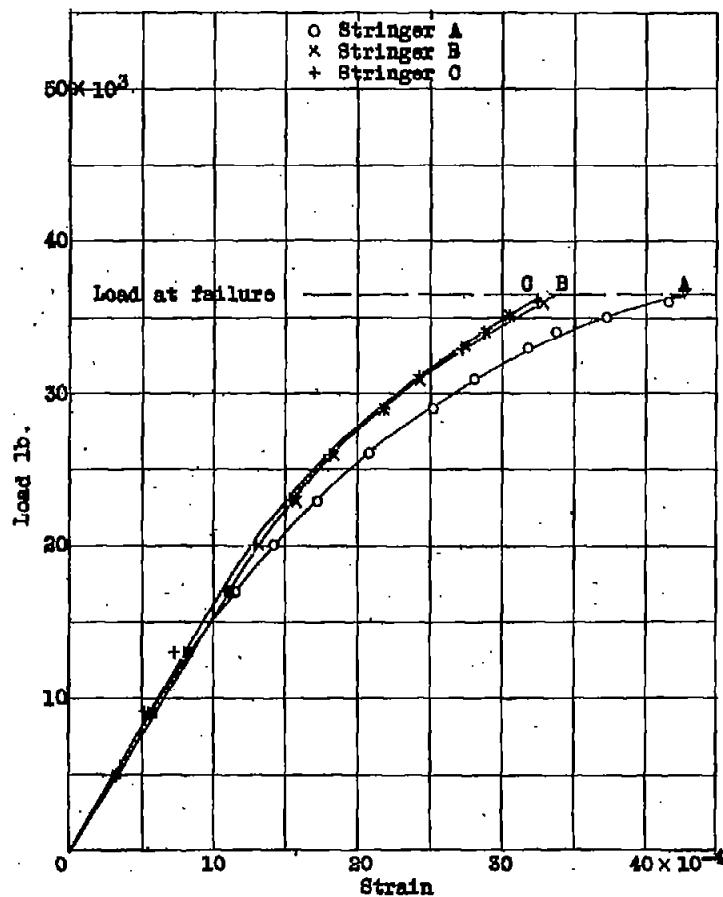


Figure 15.- Stringer strain against total load.
Specimen 1.

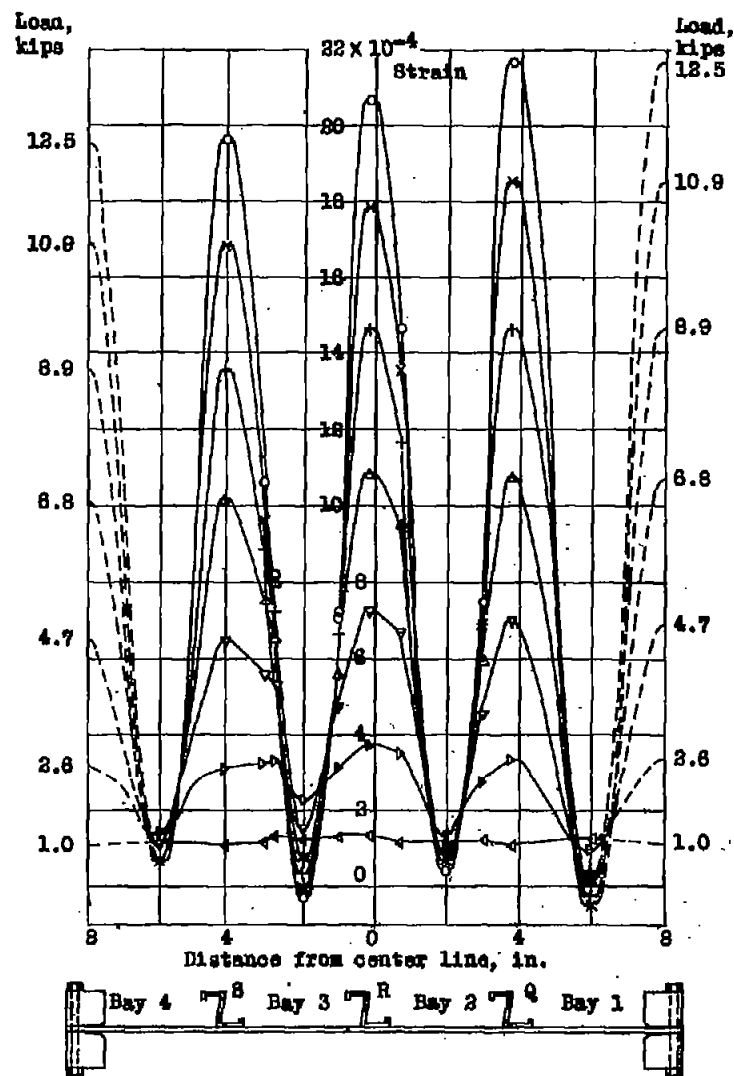


Figure 16.- Distribution of axial strain at median
fiber along transverse center line.
Specimen 8.

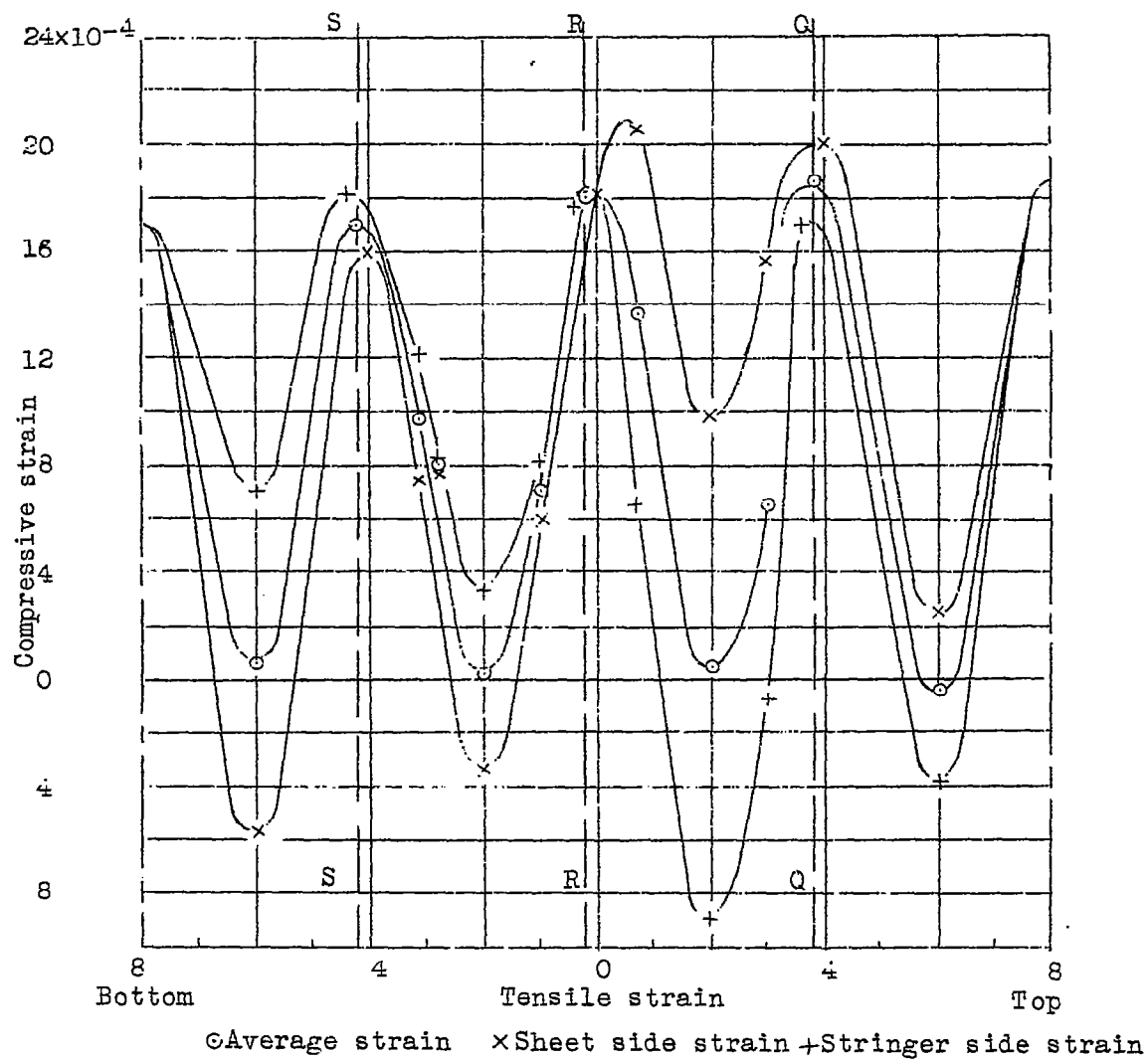


Figure 17.- Distribution of extreme fiber strains along transverse center line. Specimen 6; Load, 10,900 lb.

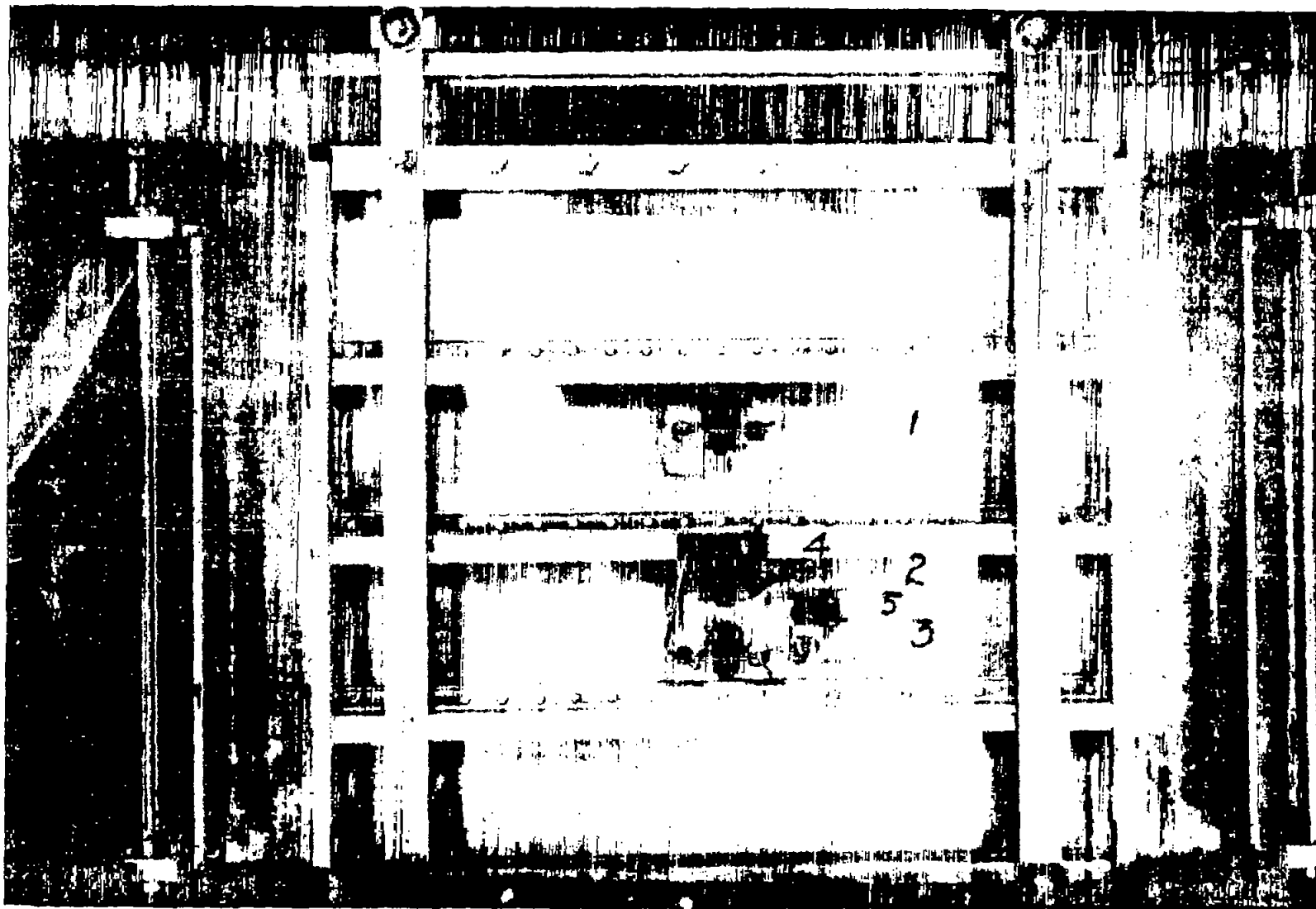


FIG. 18

Figure 18.- Strain gages set up to measure variation of transverse strain in transverse direction.
Specimen 6.

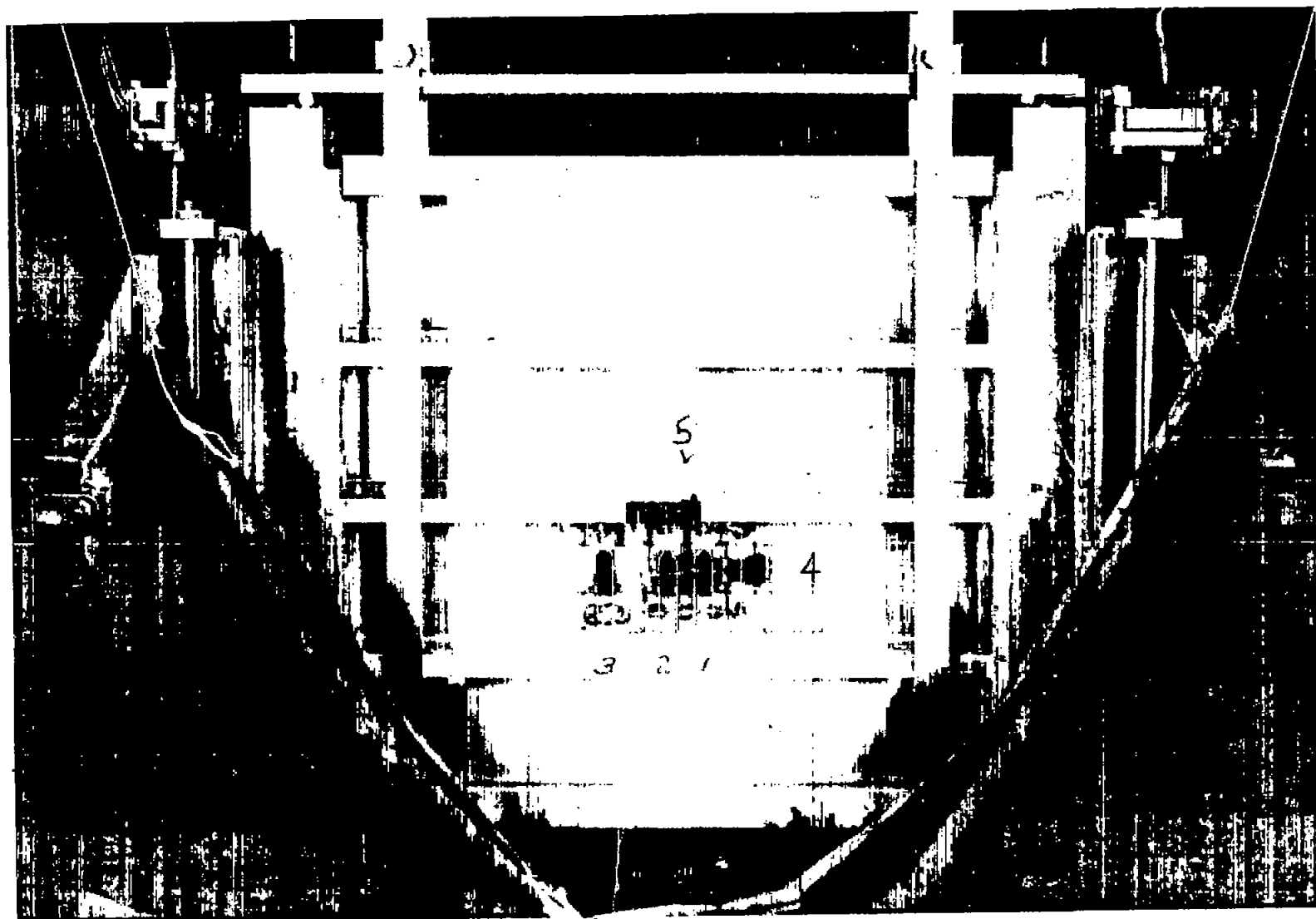
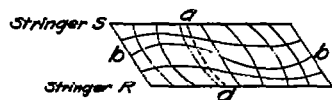


FIG. 19

Figure 19.- Strain gages set up to measure variation of transverse strain in axial direction. Specimen 6.

Average over 2 in. gage length at stringer.
Average over 1 in. gage length in sheet.



—●— Strain parallel to stringers
—○— Strain perpendicular to stringers
- - - - - Extrapolated

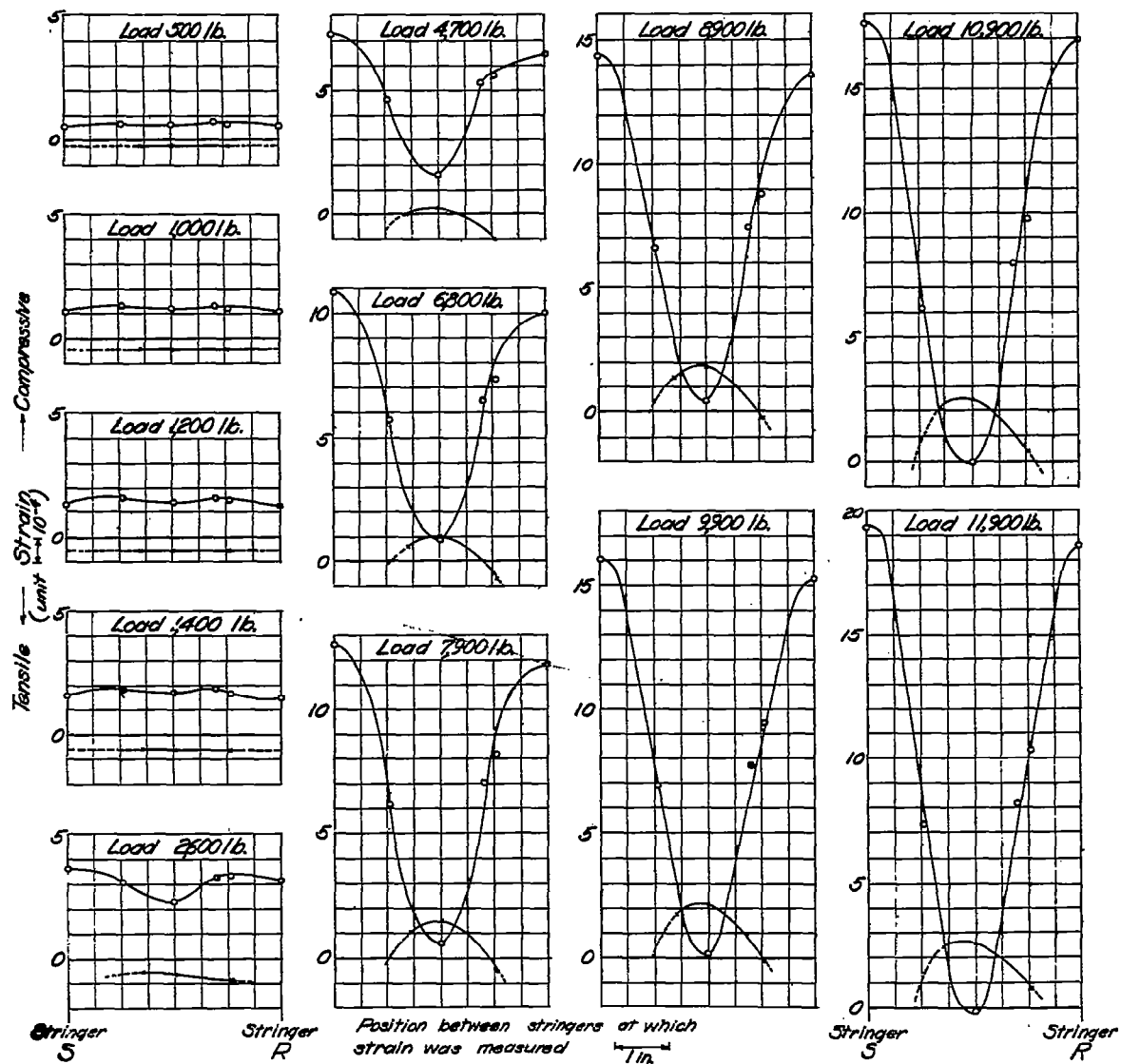


Figure 20.- Median fiber strain distribution along transverse center line.
Bay 3, specimen 6, 0.025 in. sheet.

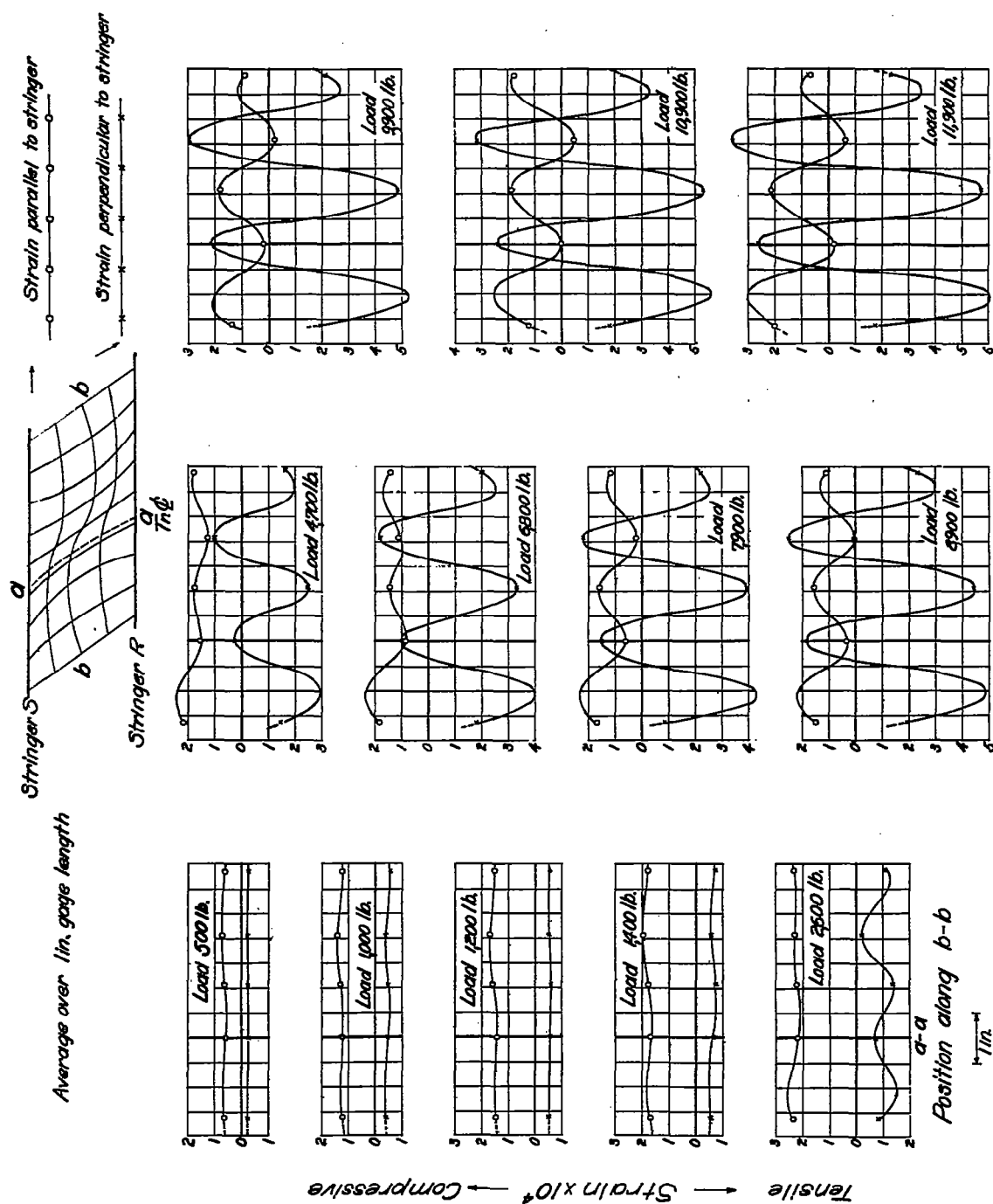


Figure 21.- Median fiber strain distribution along axial center line *b-b*. Bay 3, specimen 6.

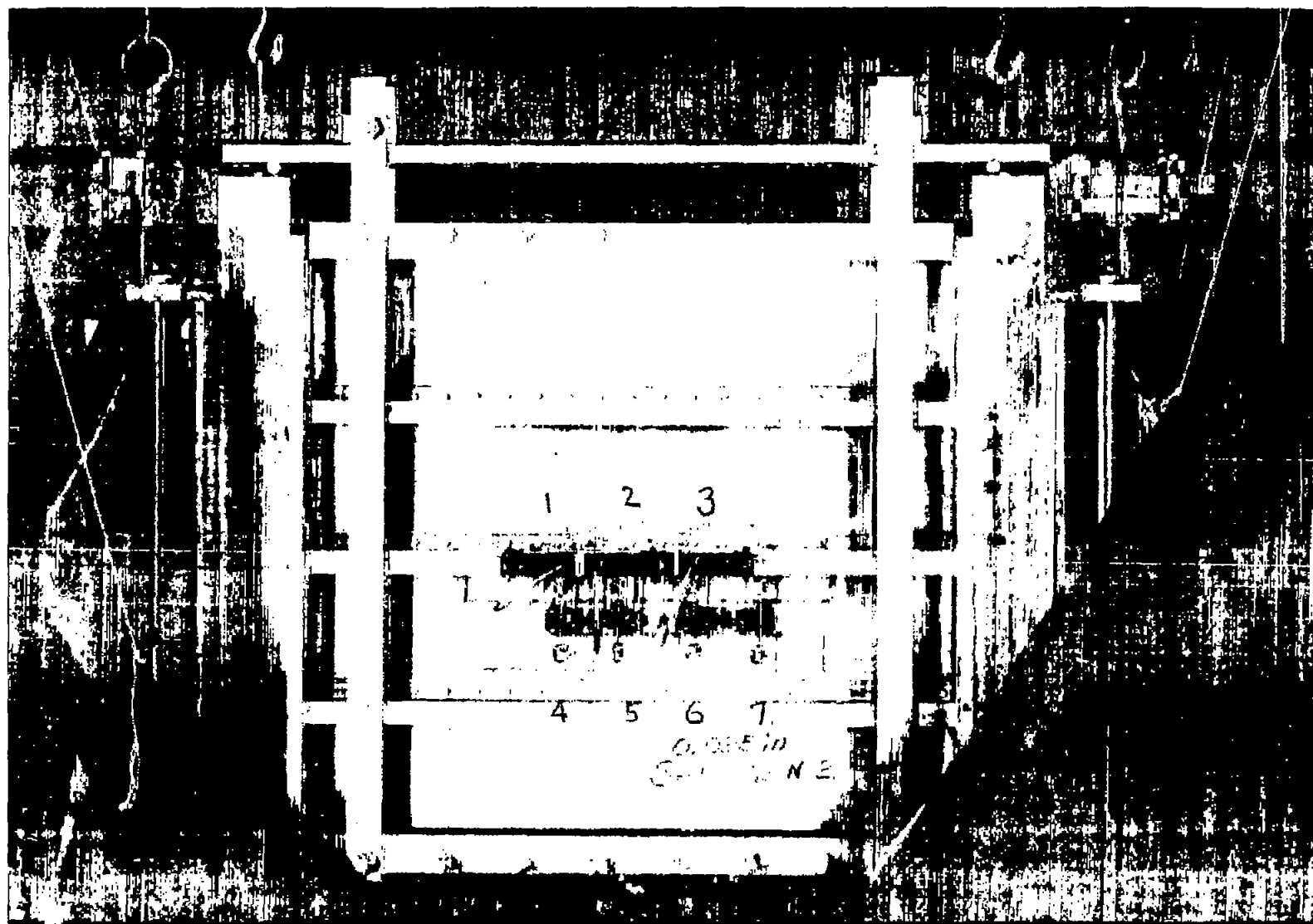


Figure 22.- Strain gages set up to measure variation of axial strain in axial direction. Specimen 6.

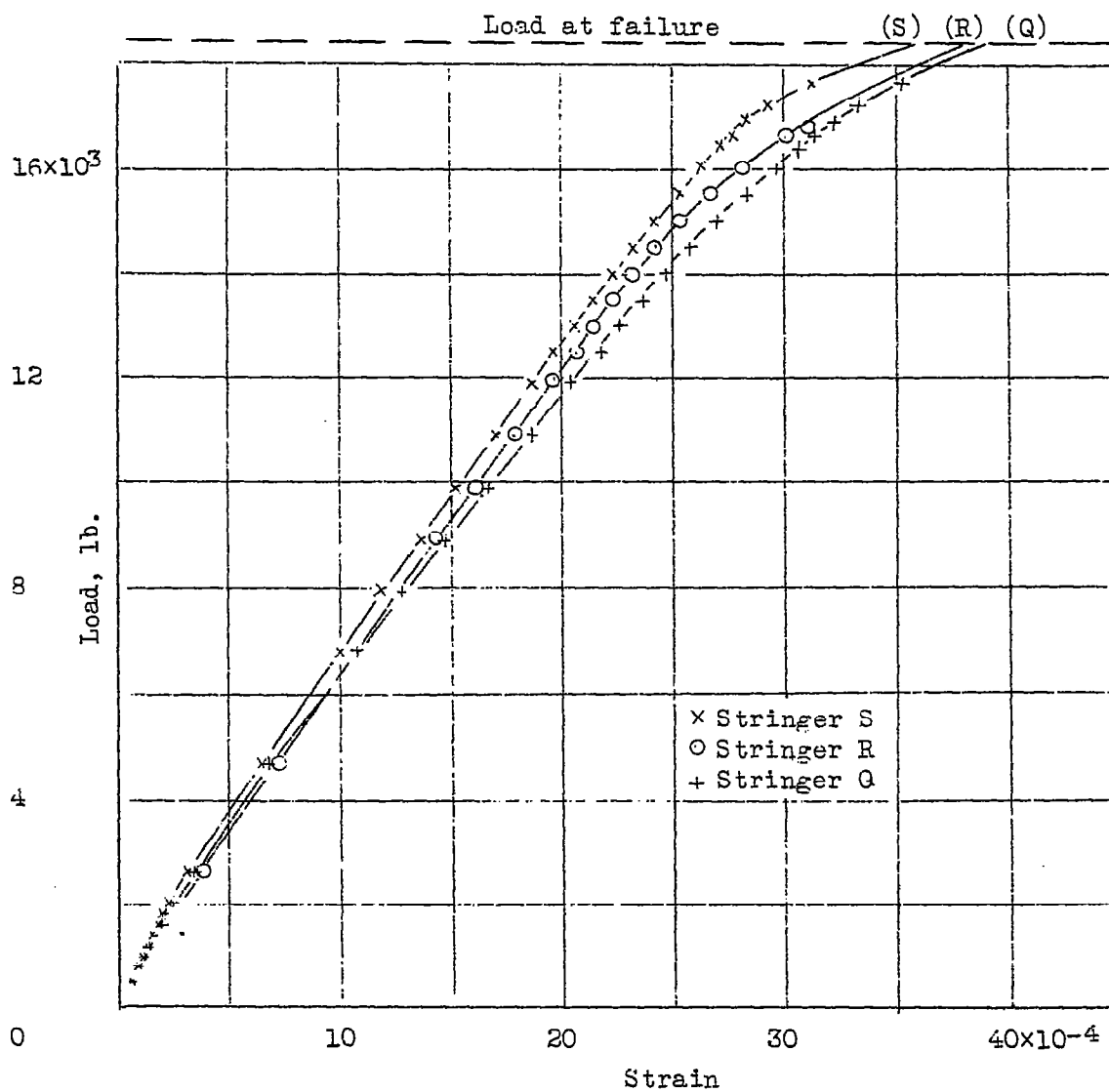
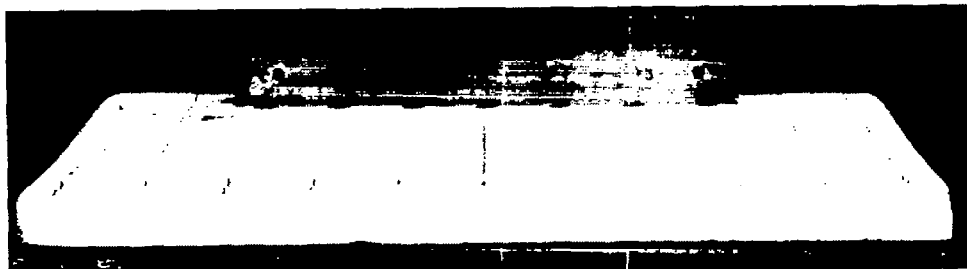
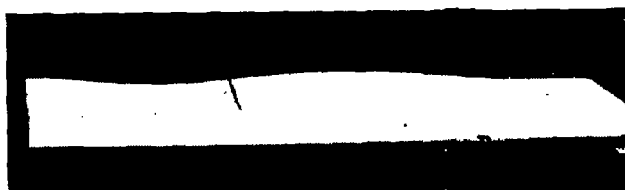


Figure 23.- Stringer strain against load. Specimen 6, (0.025 in. sheet)



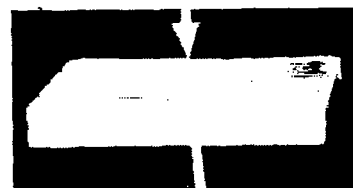
Complete cast. Straight edge along rivet line.



Cast split along horizontal center line and rivet line

Along node

Cast split transversely.



Along crest

Figure 24.-- Plaster cast of bay 3, specimen 6. (load, 10,900 lb.)

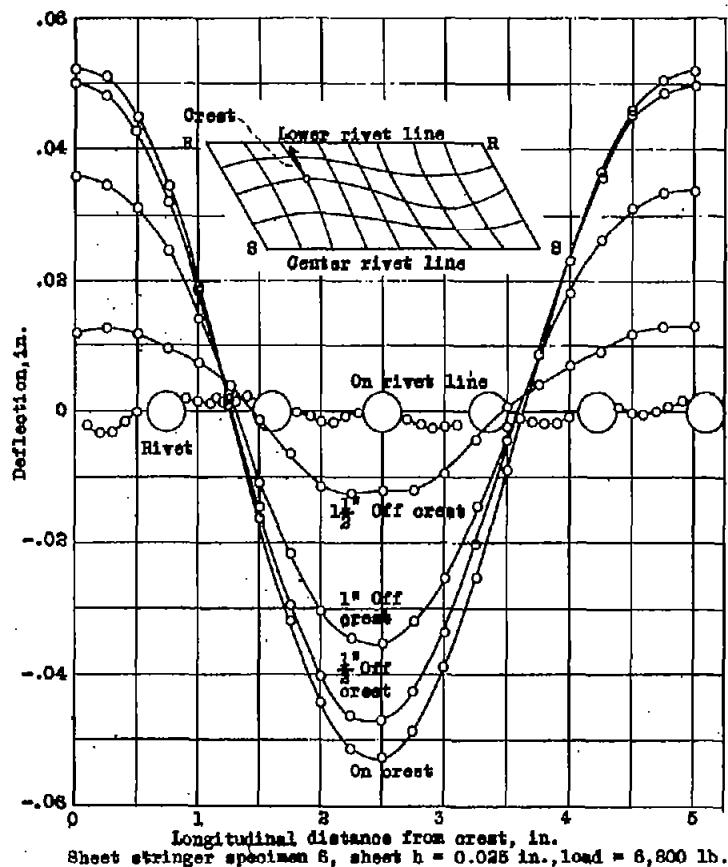


Figure 25.- Deflection due to buckling.

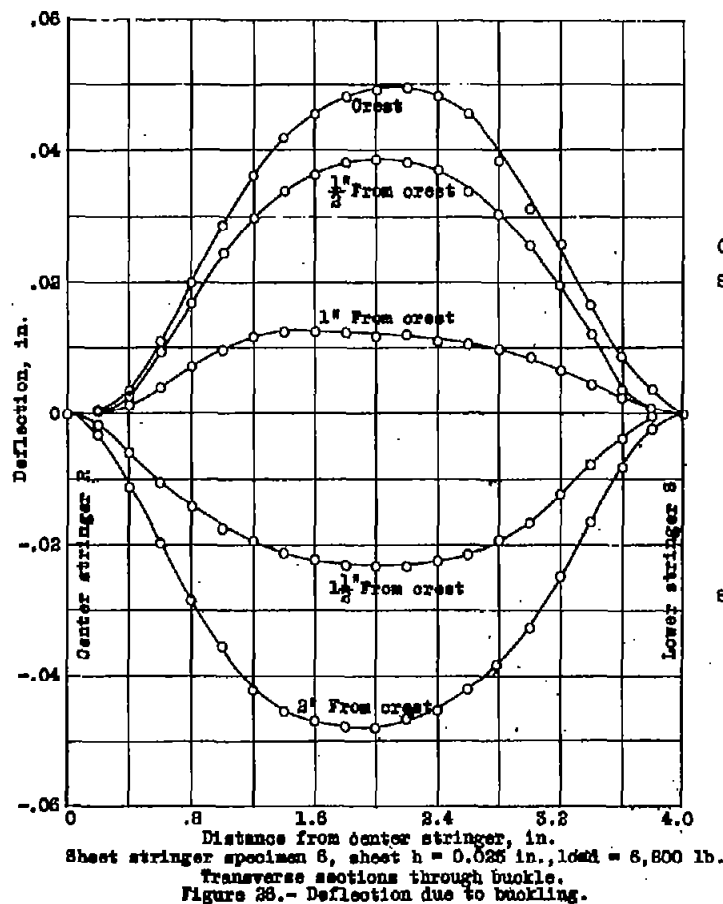
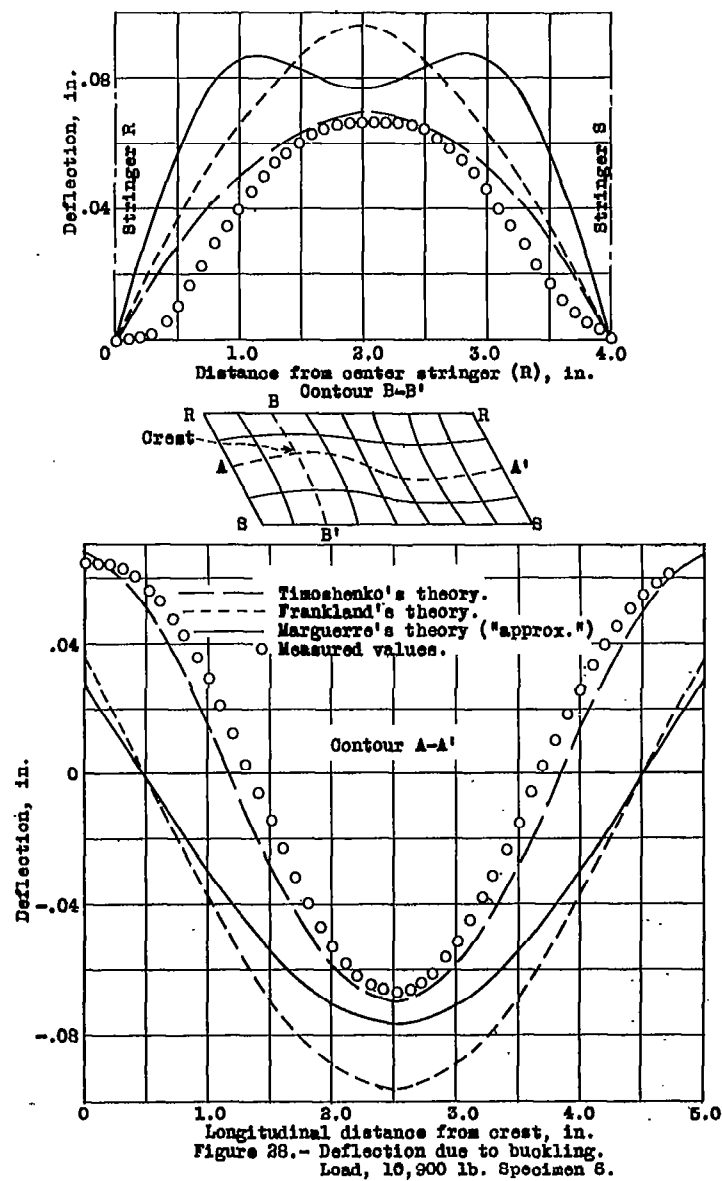
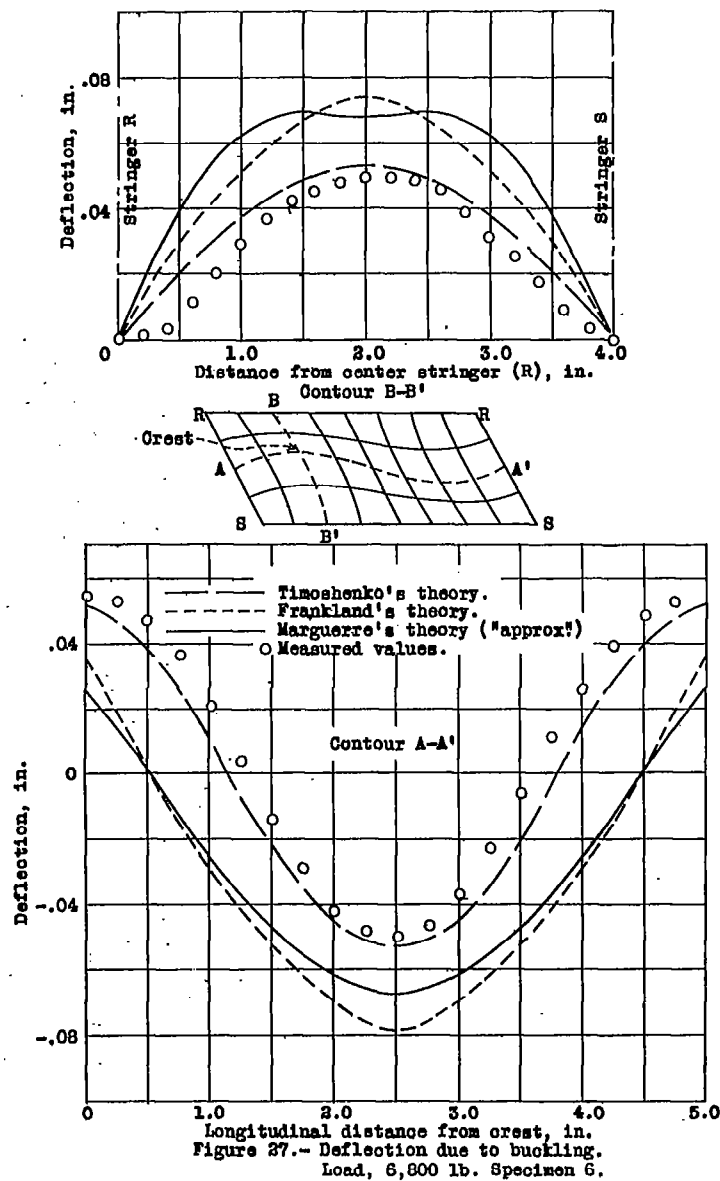


Figure 26.- Deflection due to buckling.



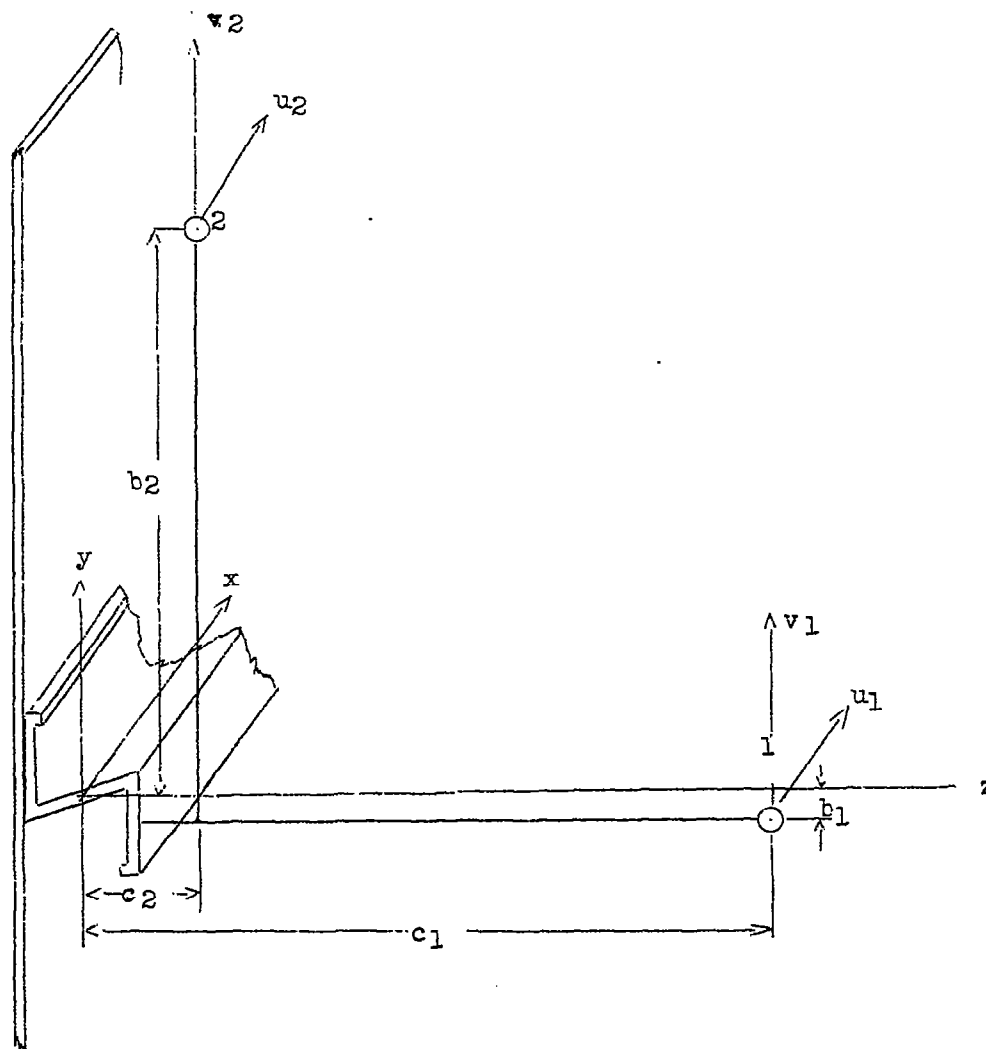


Figure 29.- Diagram of pointers attached to stringers of specimen 1.

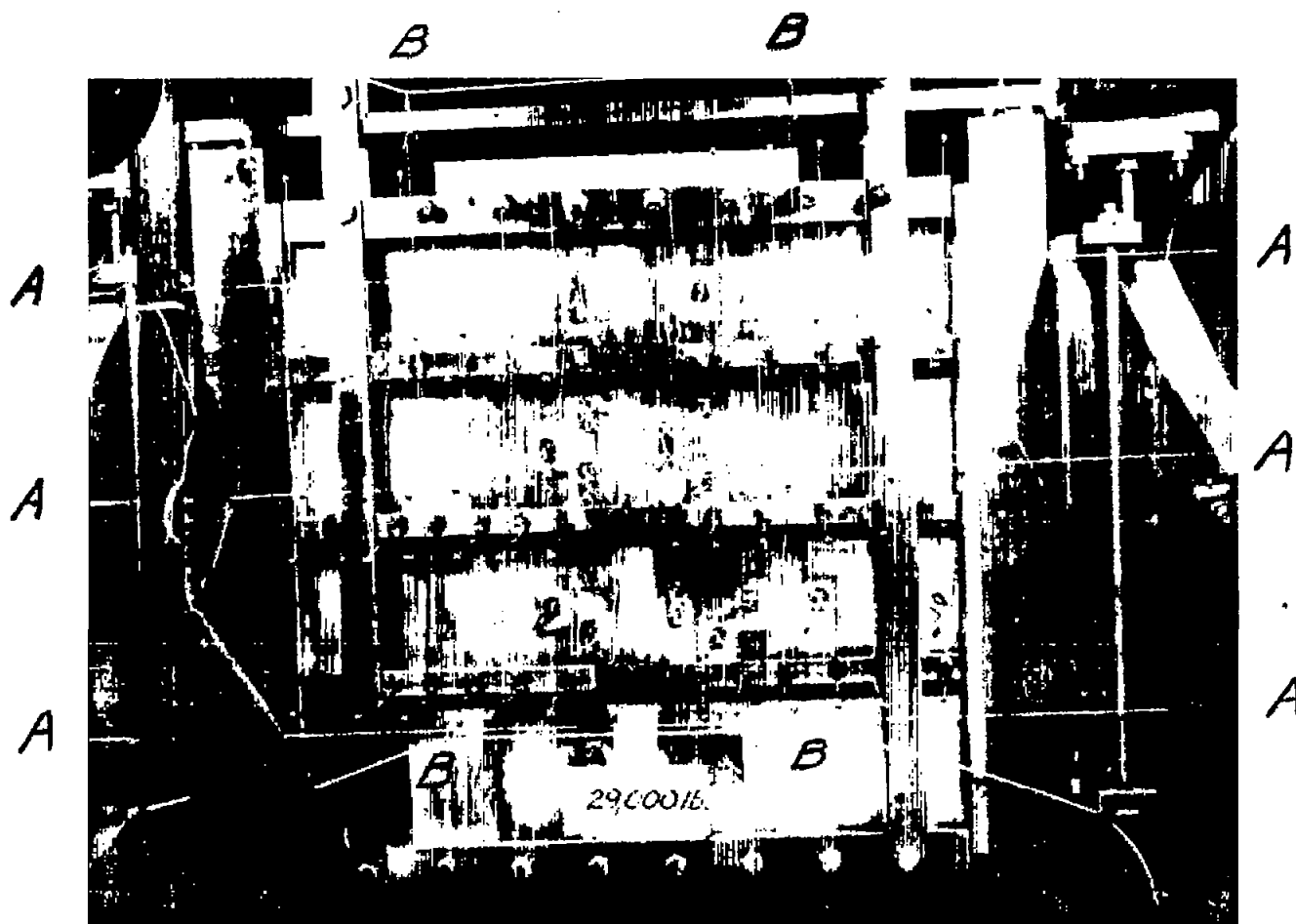


Figure 30.- Specimen 1 with pointers attached to measure stringer deformation. Load, 29,000 lb.

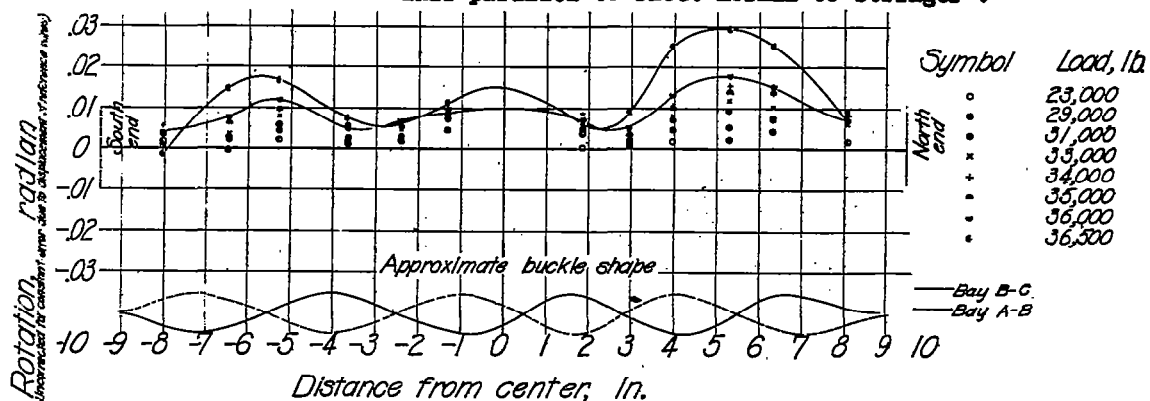
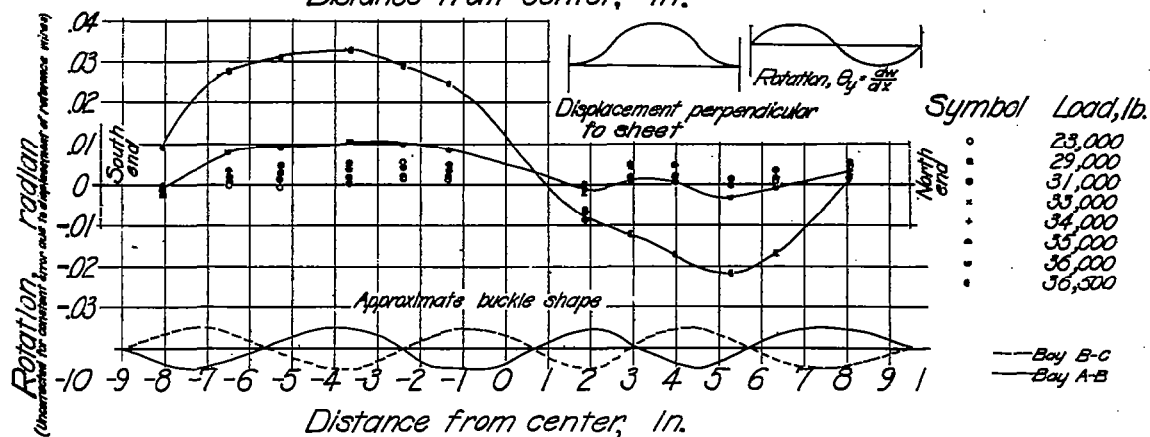
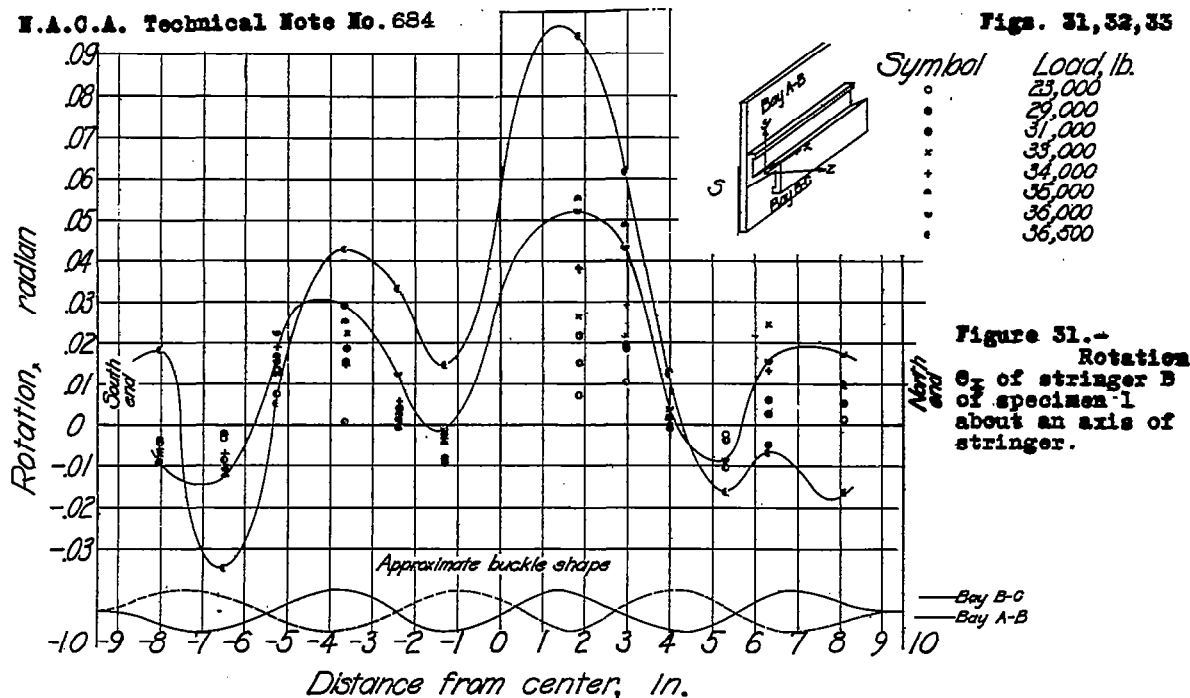




Fig. 34

Figure 34.- Specimen 6 with pointers attached to measure stringer deformations. Load, 18,400 lb.; failure.

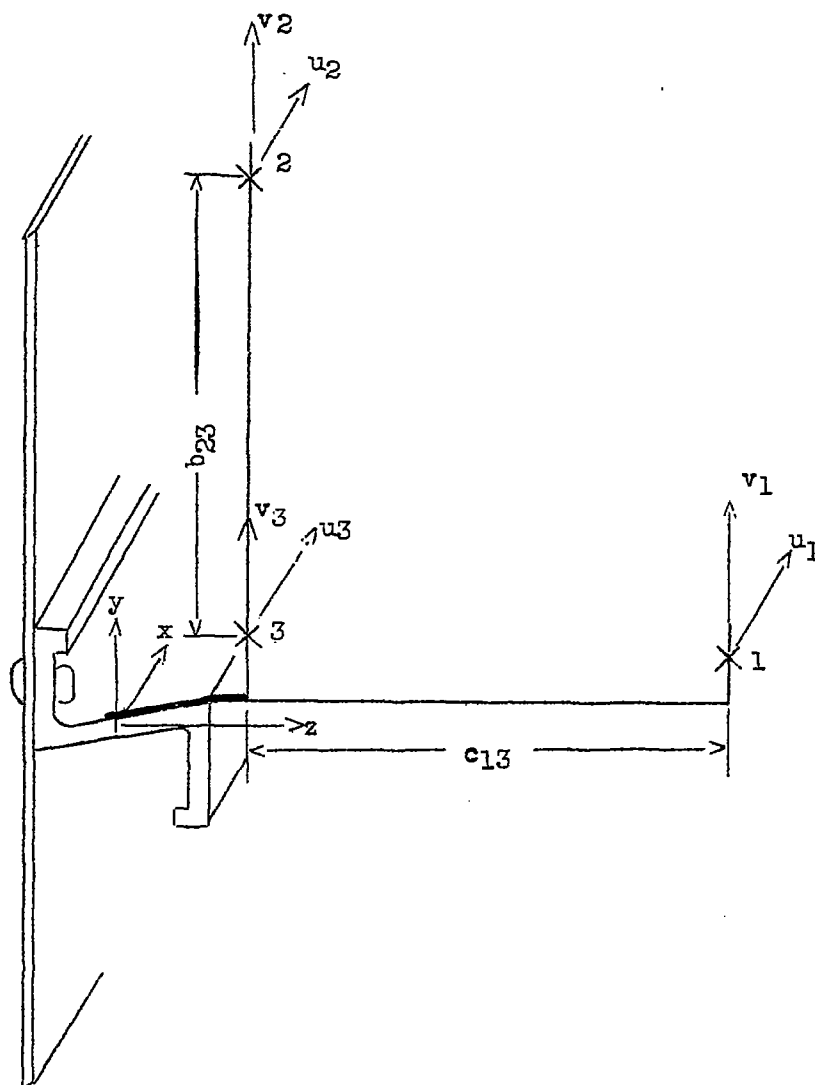


Figure 35.- Diagram of pointers attached to stringers of specimen 6.

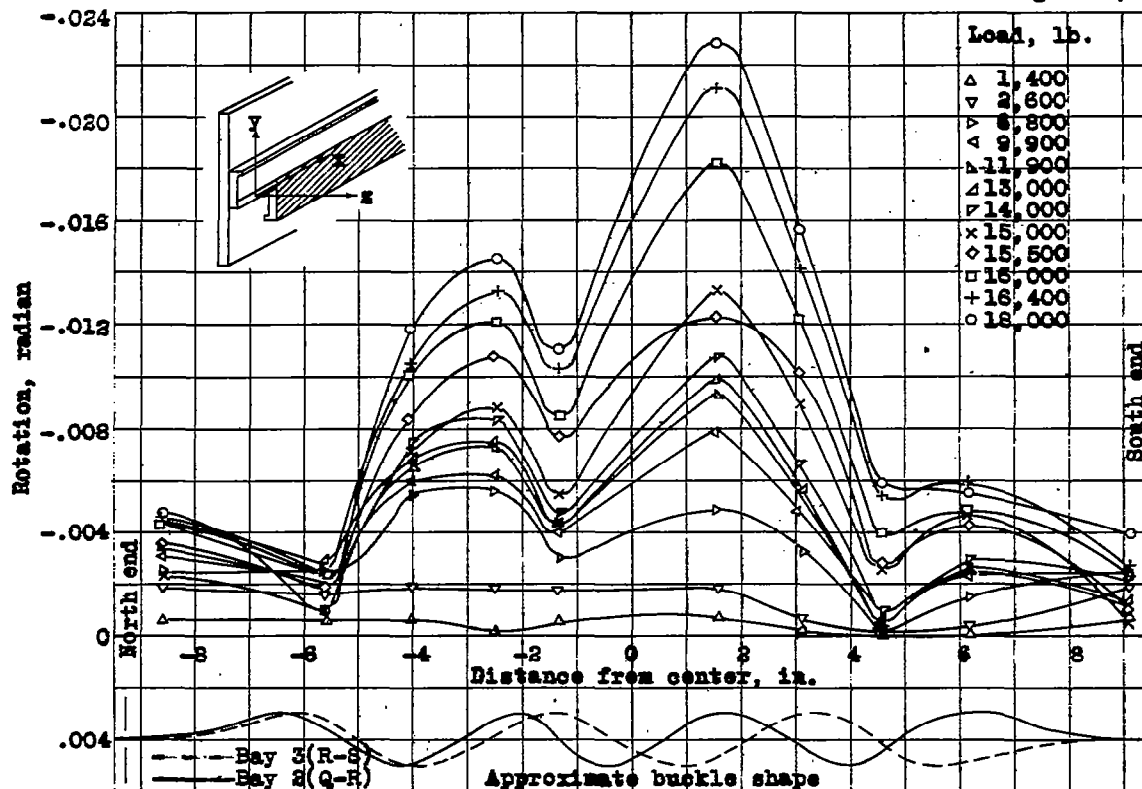


Figure 36.- Rotation θ_x of stringer R of specimen 6 about axis of stringer.

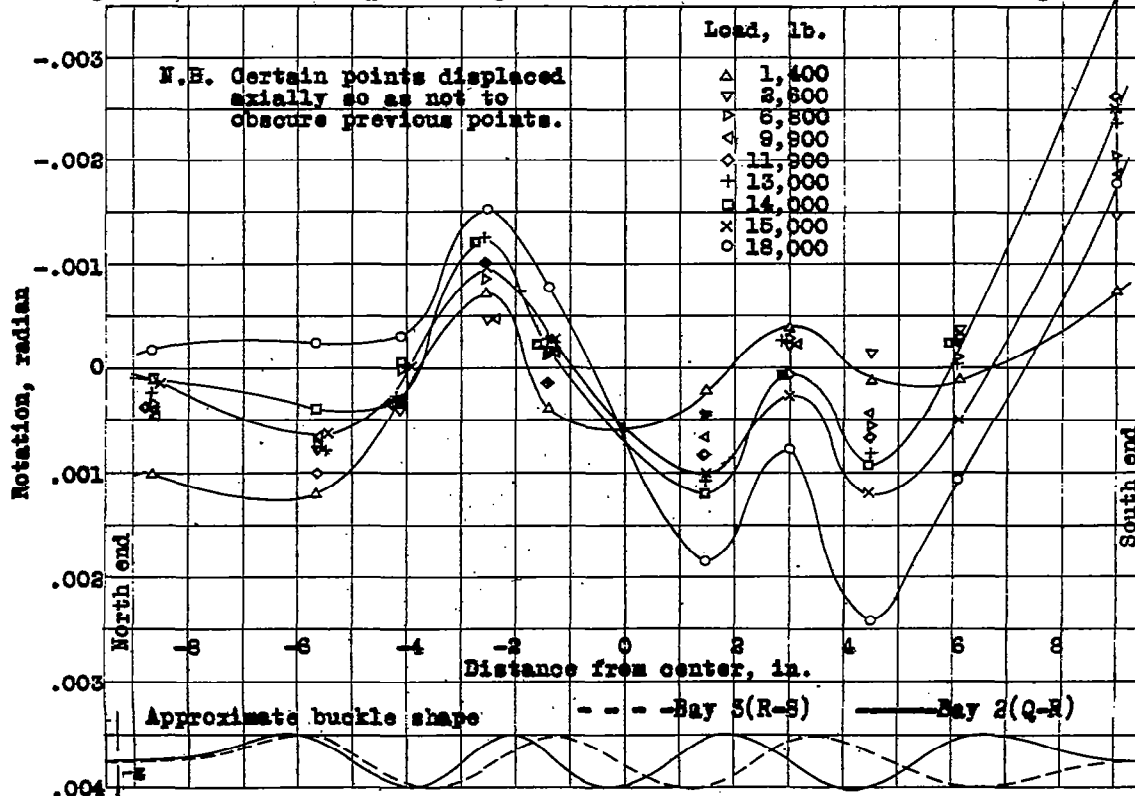
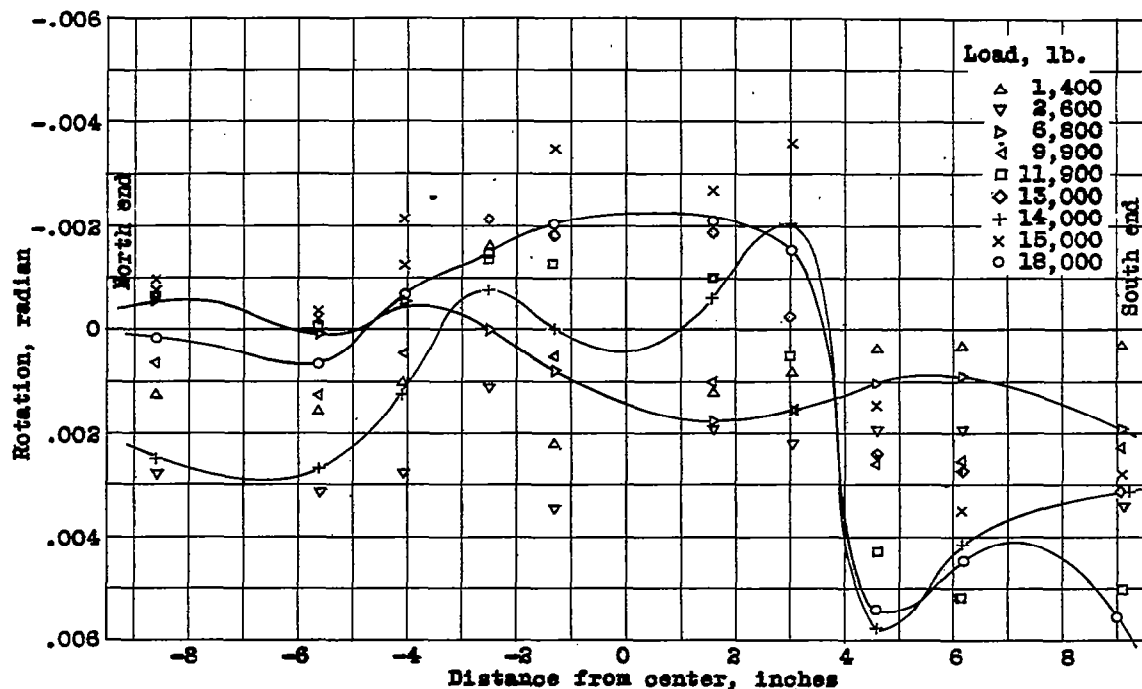
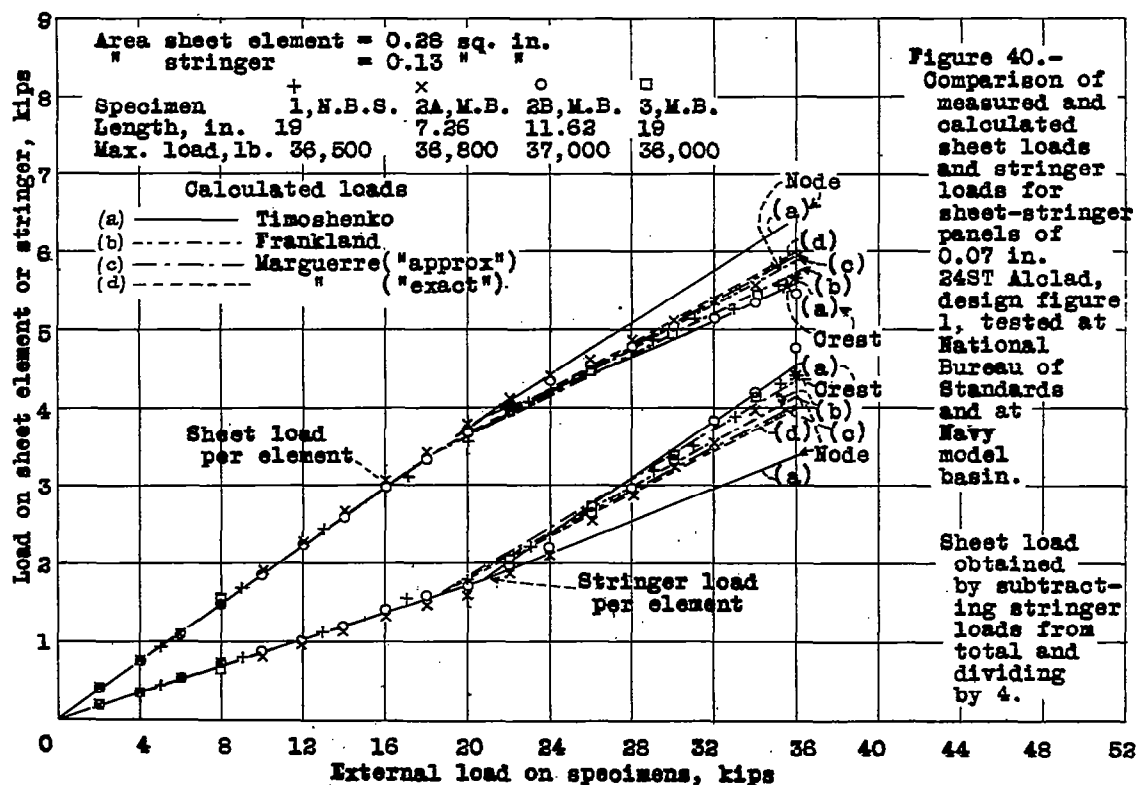


Figure 37.- Rotation θ_y of stringer R of specimen 6 about axis parallel to sheet normal to stringer.

Figure 38.- Rotation θ_z of stringer R of specimen 6 about an axis normal to sheet.

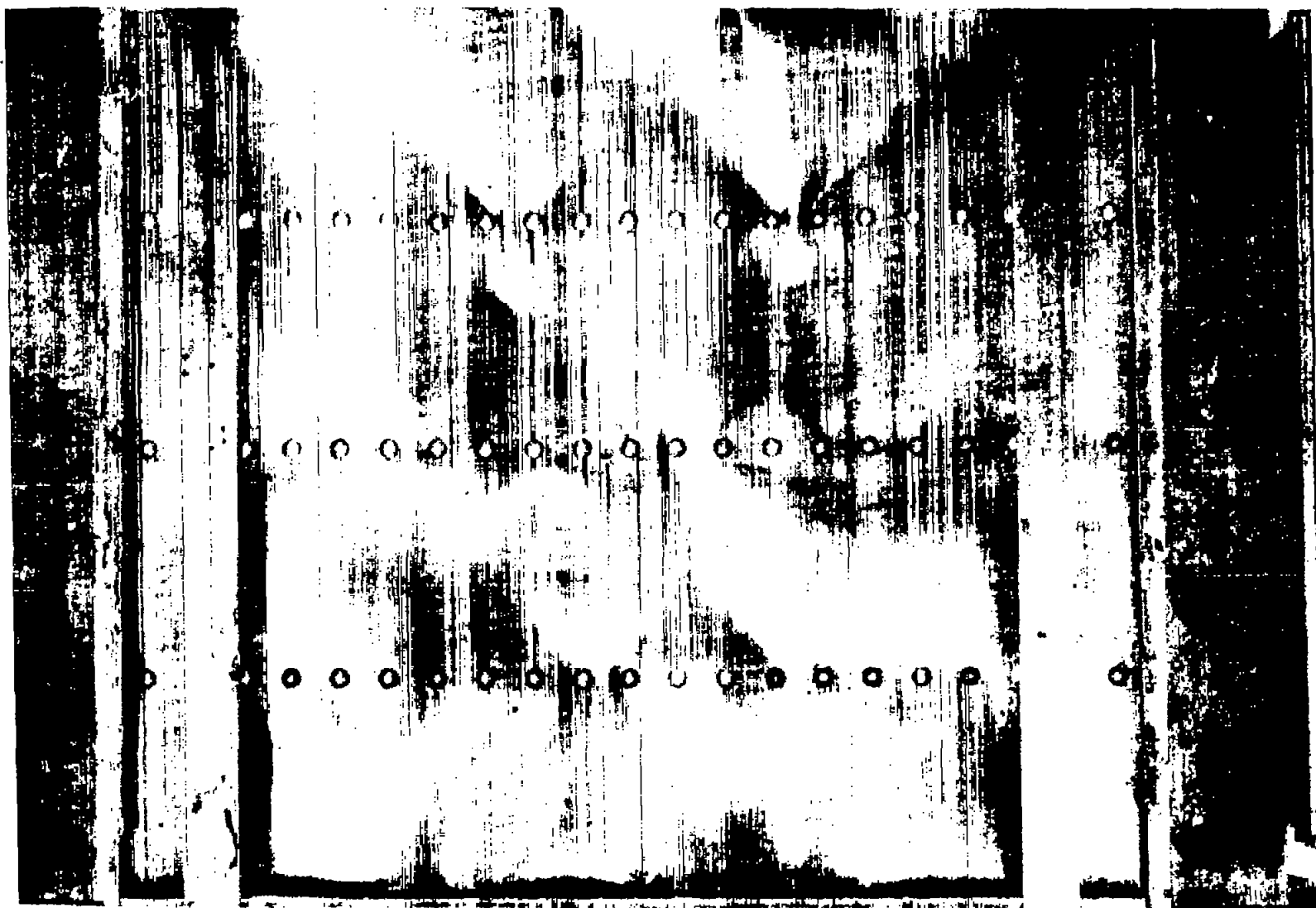


Figure 39.- Specimen 6; sheet side. Load, 18,400 lb.; failure.

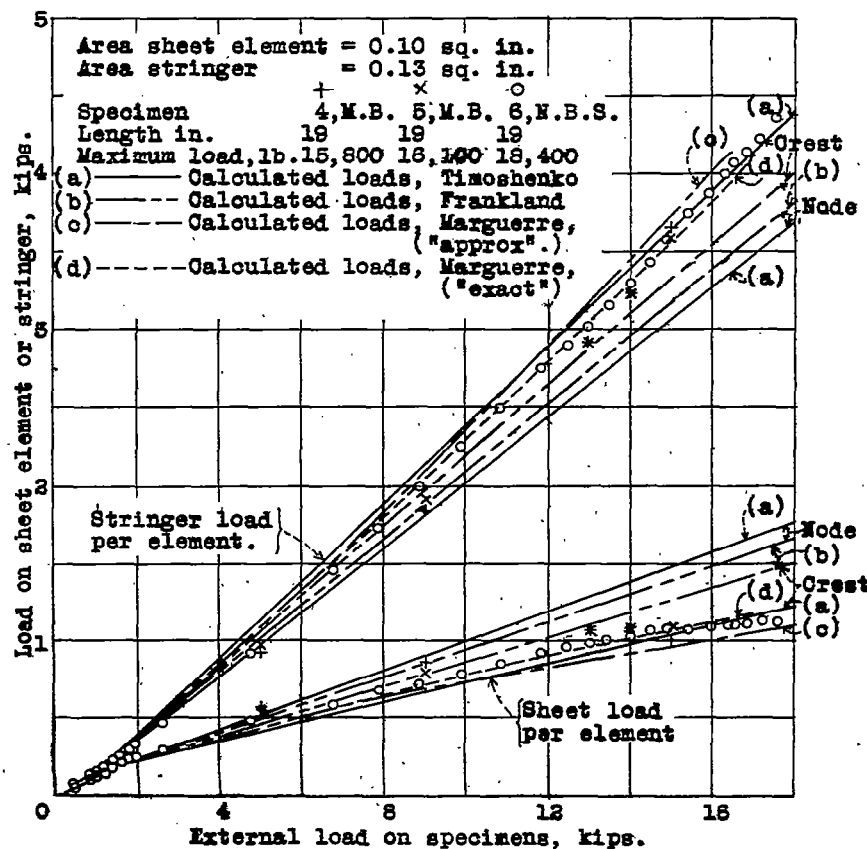
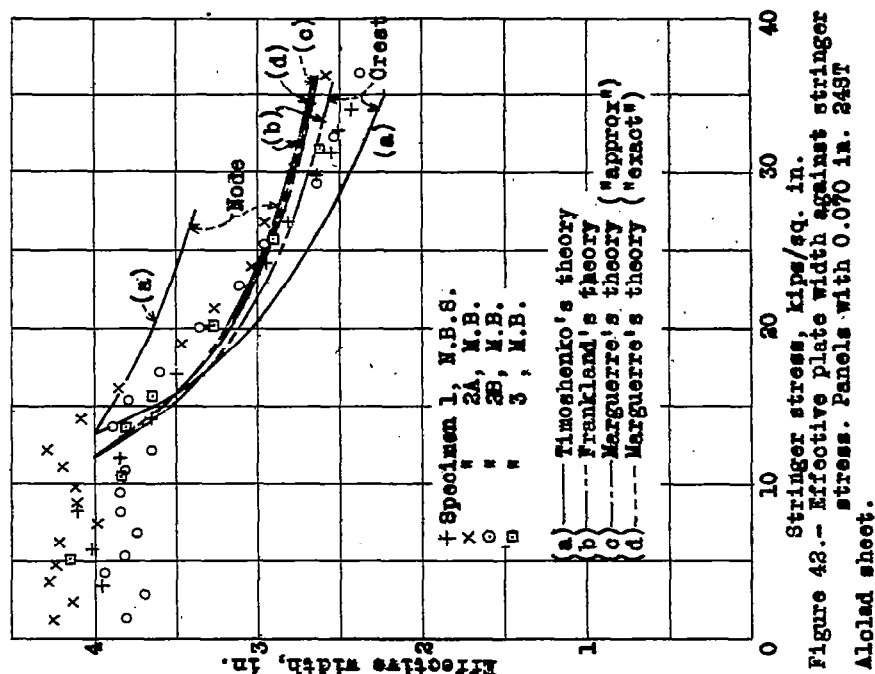


Figure 41.- Comparison of measured and calculated sheet loads and stringer loads for sheet-stringer panels of 0.025 in. 248T Duralumin, design figure 1, tested at National Bureau of Standards and at Navy model basin.

Sheet load obtained by subtracting stringer loads from total and dividing by 4.



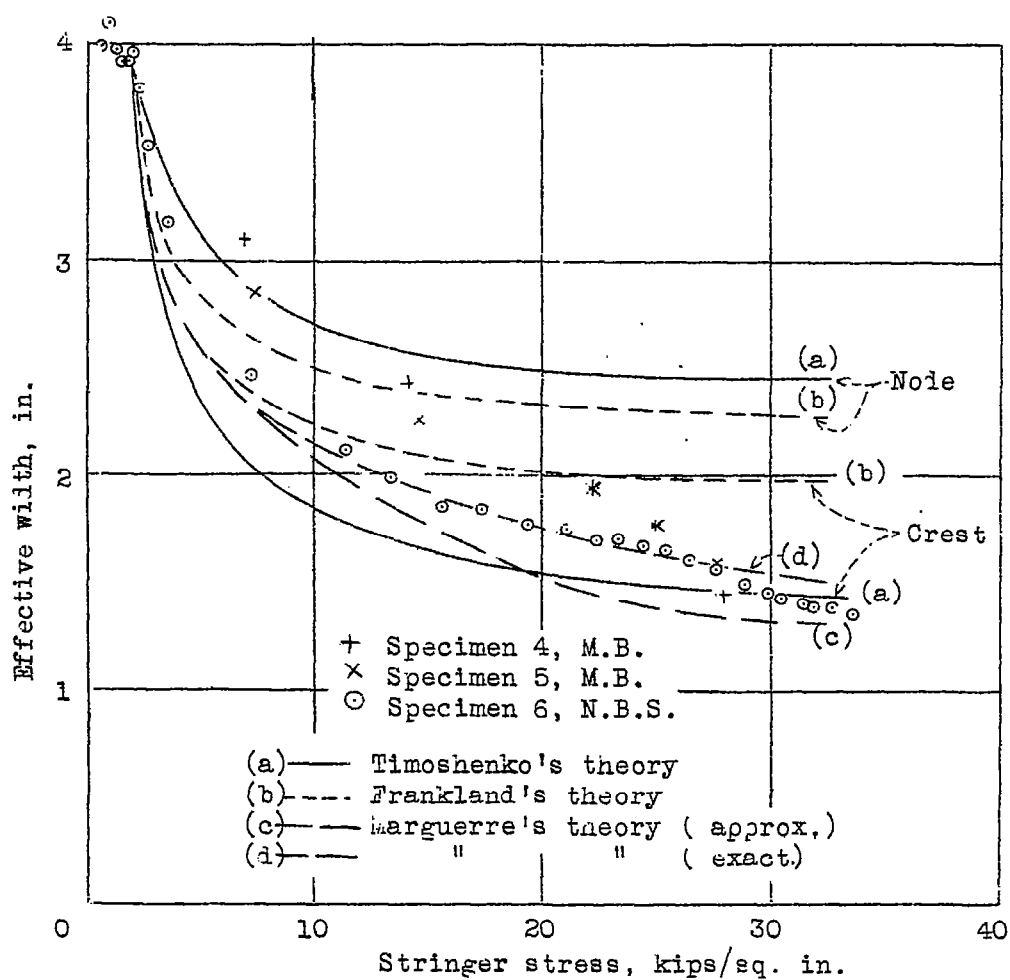


Figure 43.- Effective plate width against stringer stress. Panels with 0.025 in. 24ST sheet.

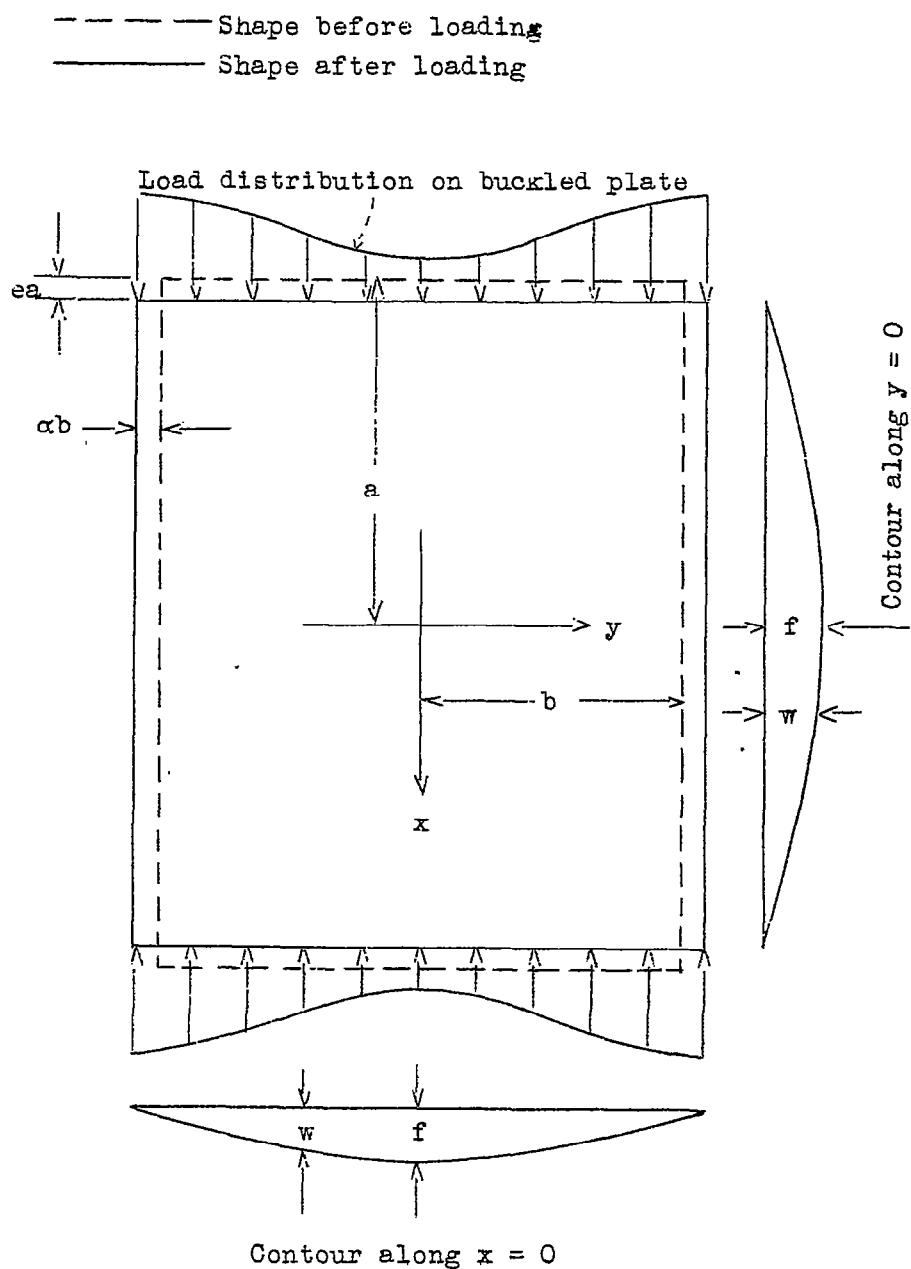


Figure 44.- Diagram showing dimensions and coordinates for buckling of a rectangular plate under compressive load.

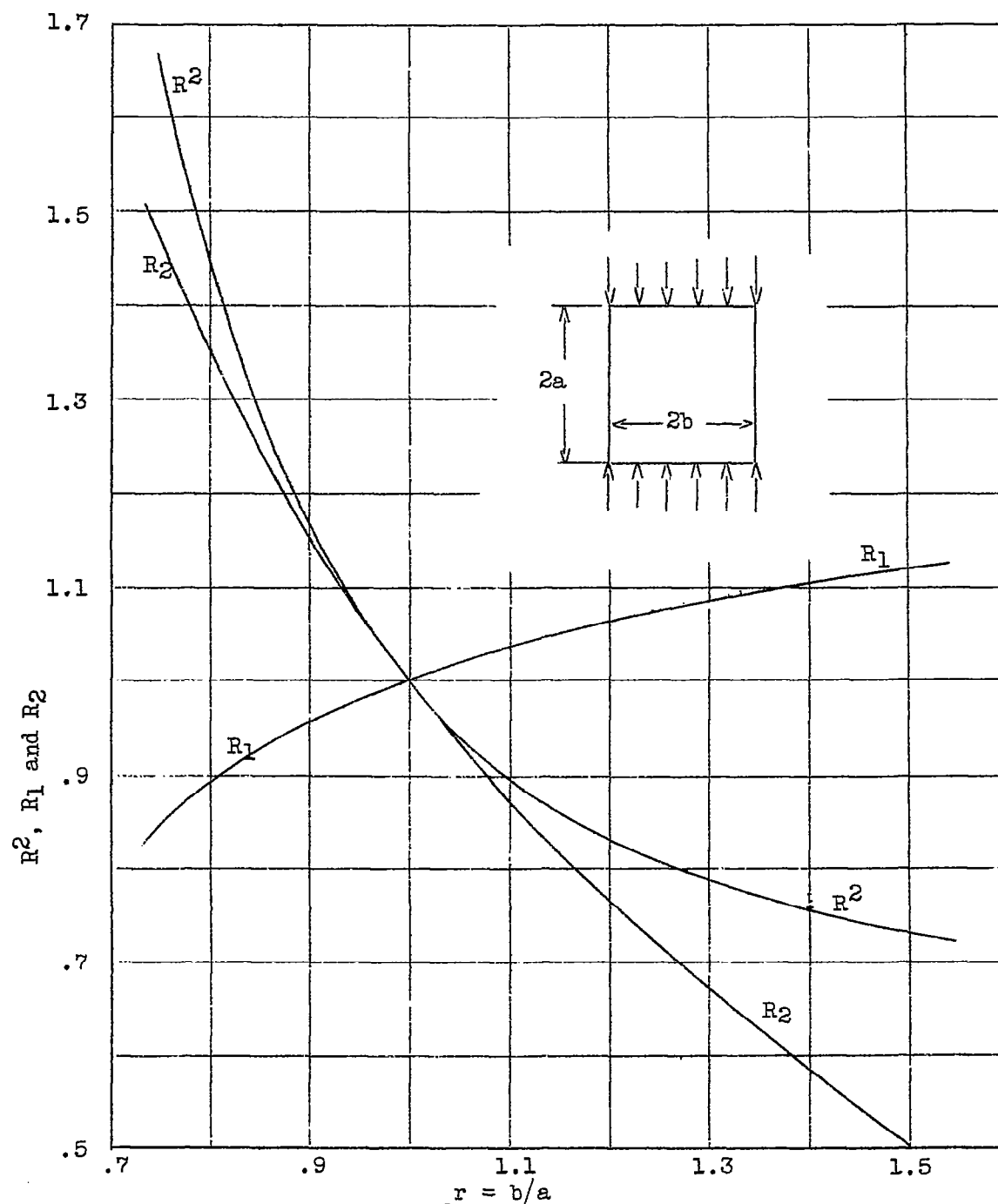


Figure 45.- Variation of R_1 , R_2 and R_2 with the ratio $r=b/a$.
(Timoshenko's theory.)

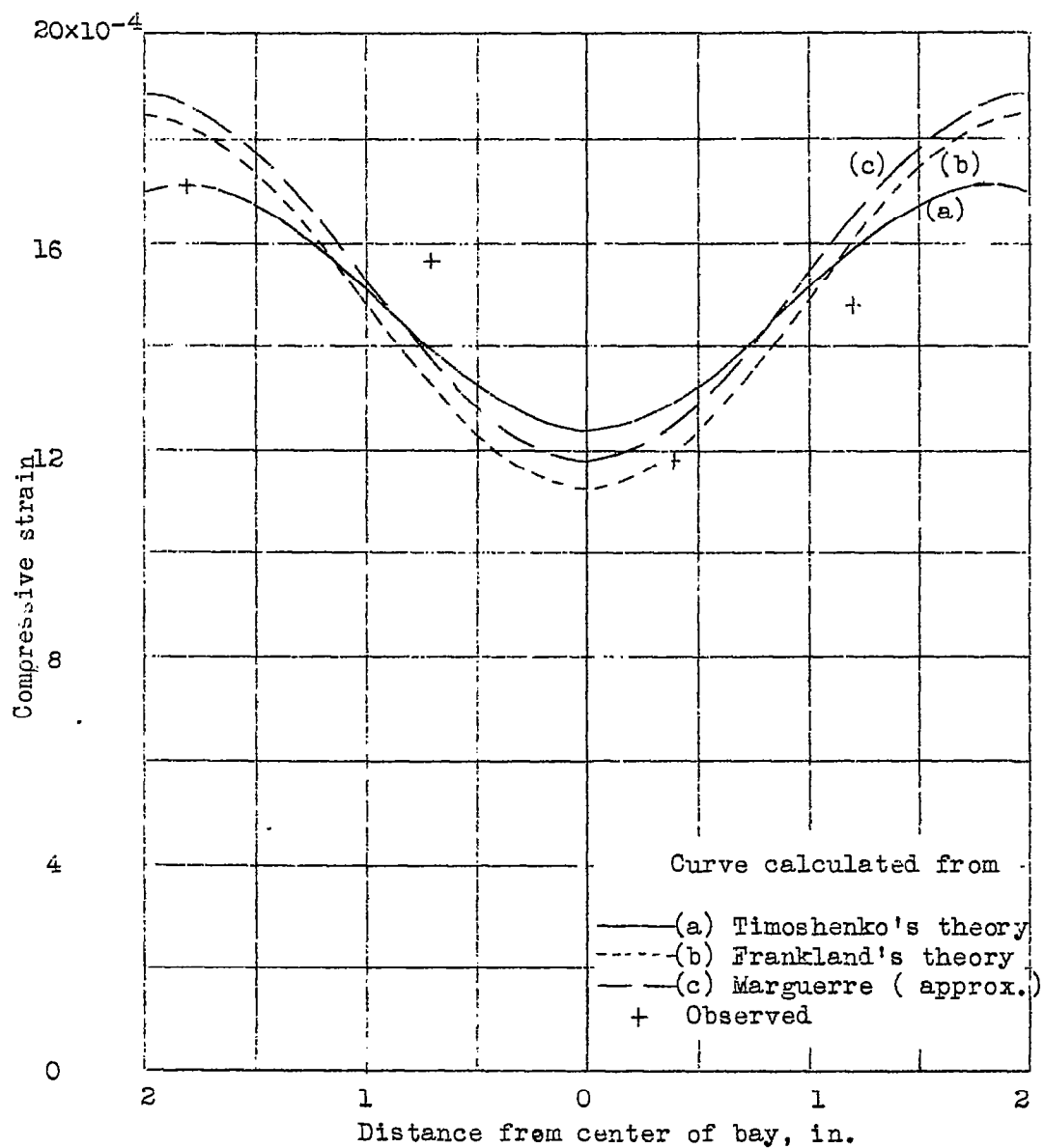


Figure 46.- Compressive strain. Specimen 1. Transverse center-line, 0.070 in. sheet; bay 3; load, 25,000 lb..

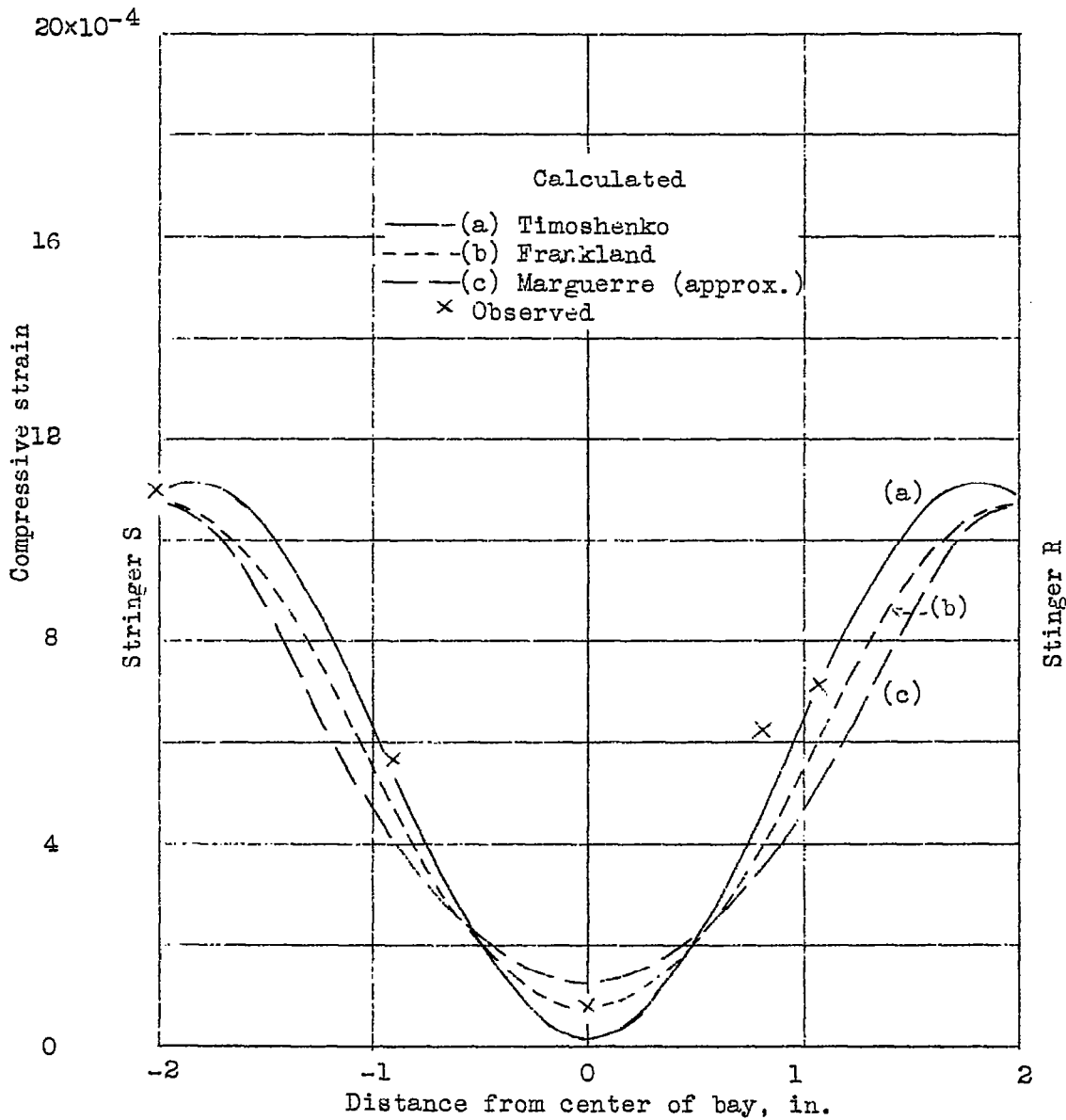


Figure 47.- Axial compressive strain at median fiber on transverse center line. Bay 3; specimen 6; total load, 6,800 lb.

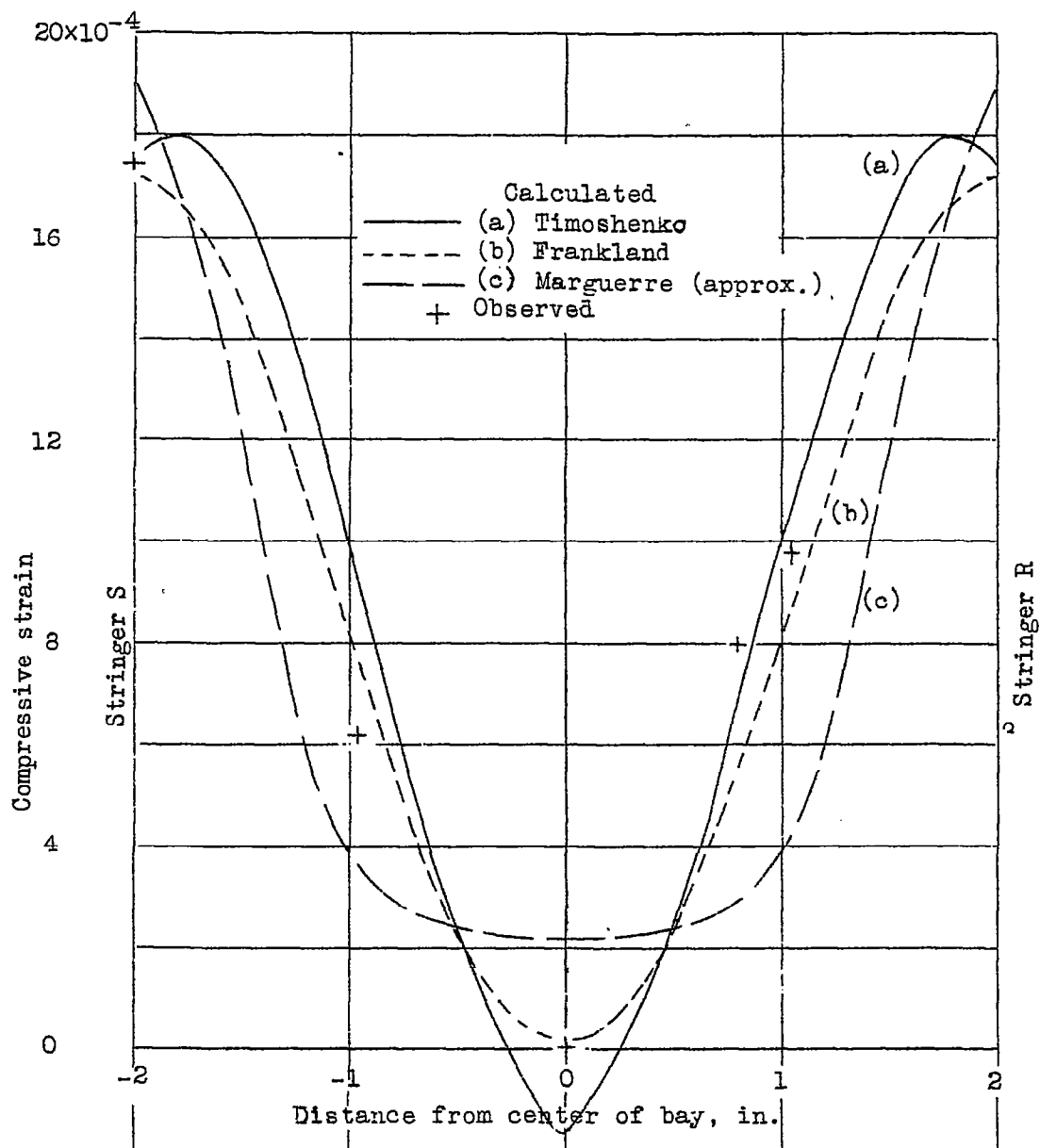


Figure 48.- Axial compressive strain at median fiber on transverse center line. Bay 3; specimen 6; total load, 10,900 lb.

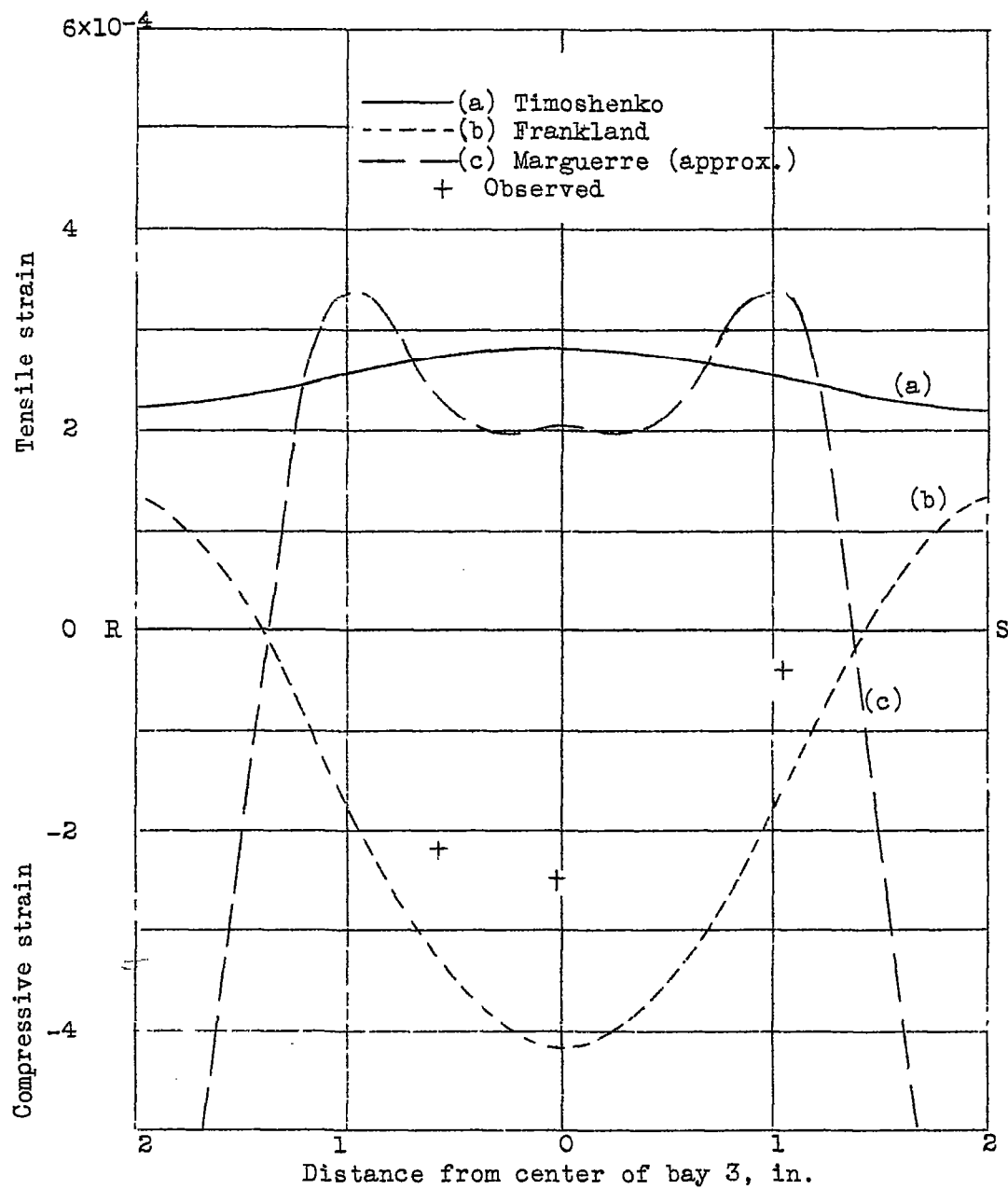


Figure 49.- Transverse strain on transverse center line. Bay 3; specimen 6; load, 10,900 lb.

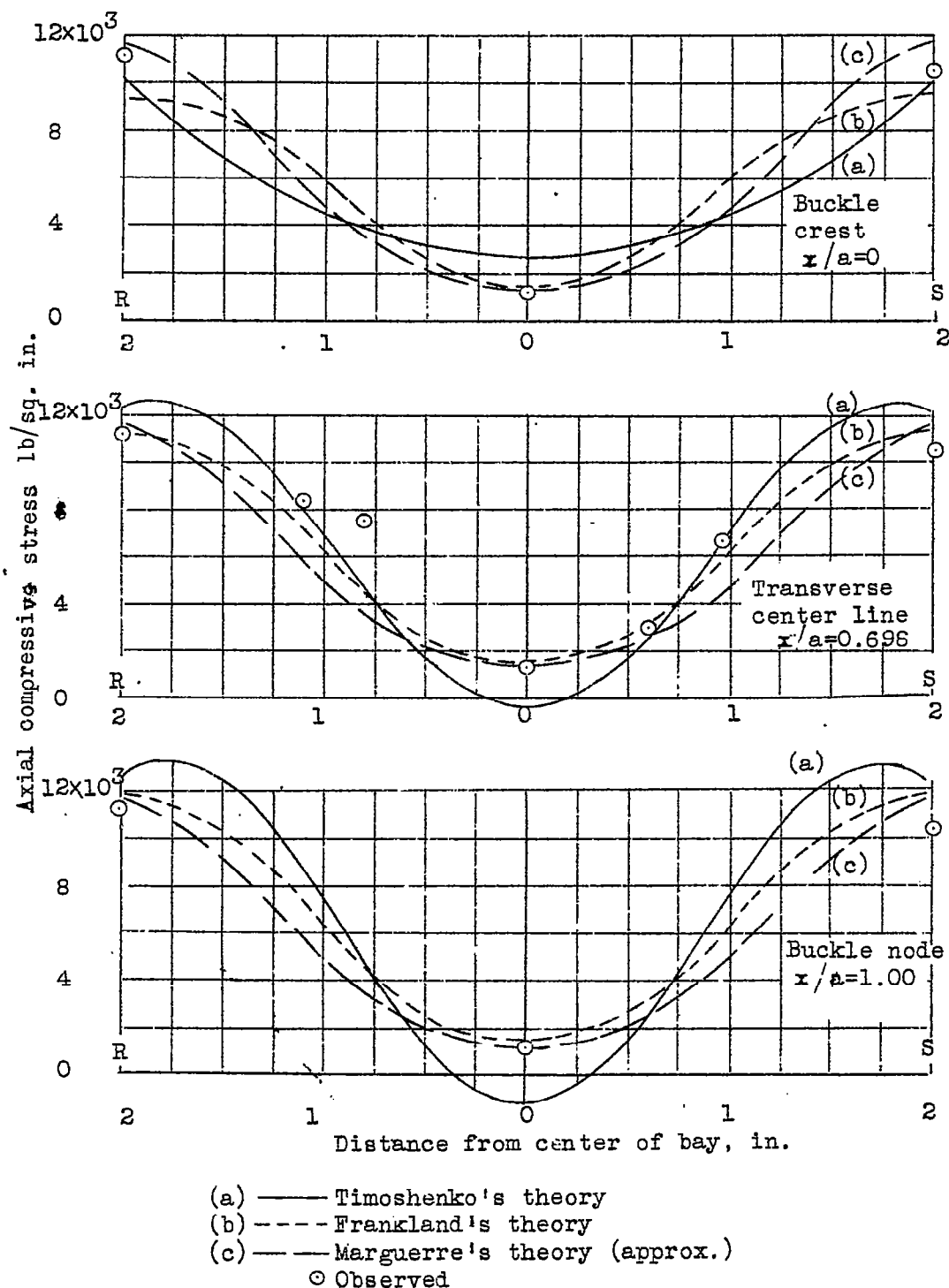


Figure 50.- Distribution of axial stress across sheet. Specimen 6, load, 6,800 lb., bay 3.

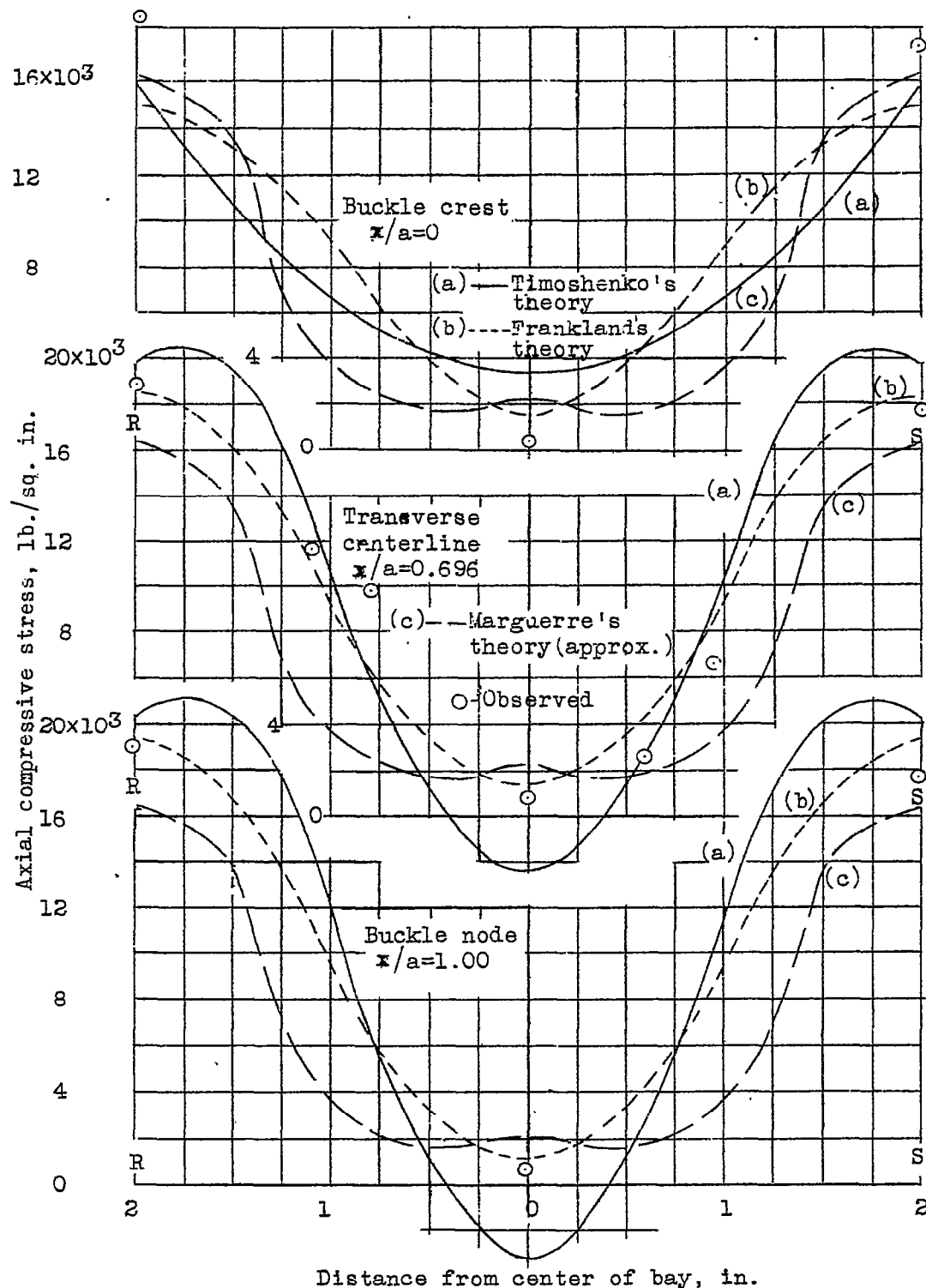


Figure 51.- Distribution of axial stress across sheet. Specimen 6; load, 10,900 lb.; bay 3.

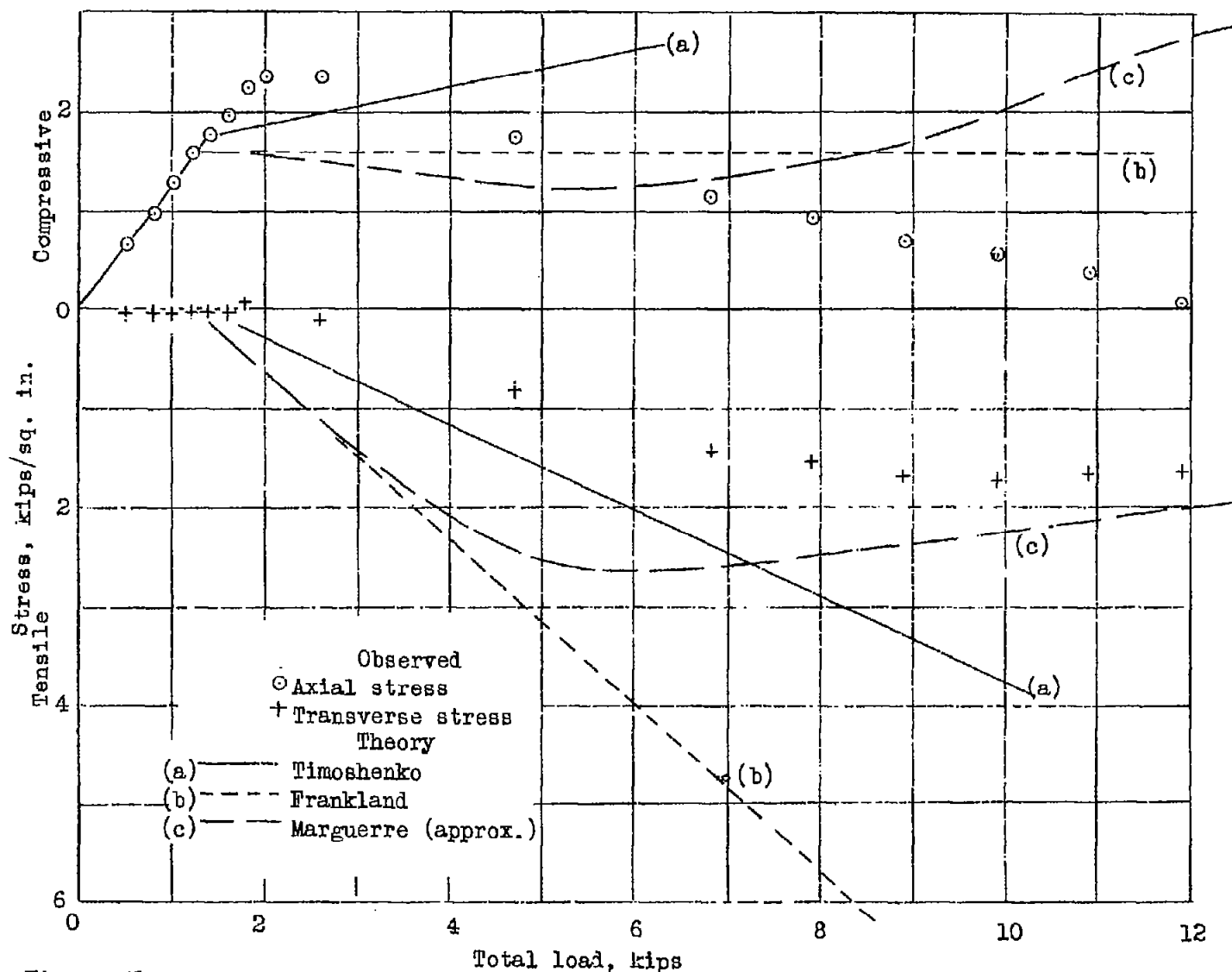


Figure 52.- Axial and transverse stress at crest of buckle. Bay 3, specimen 6.

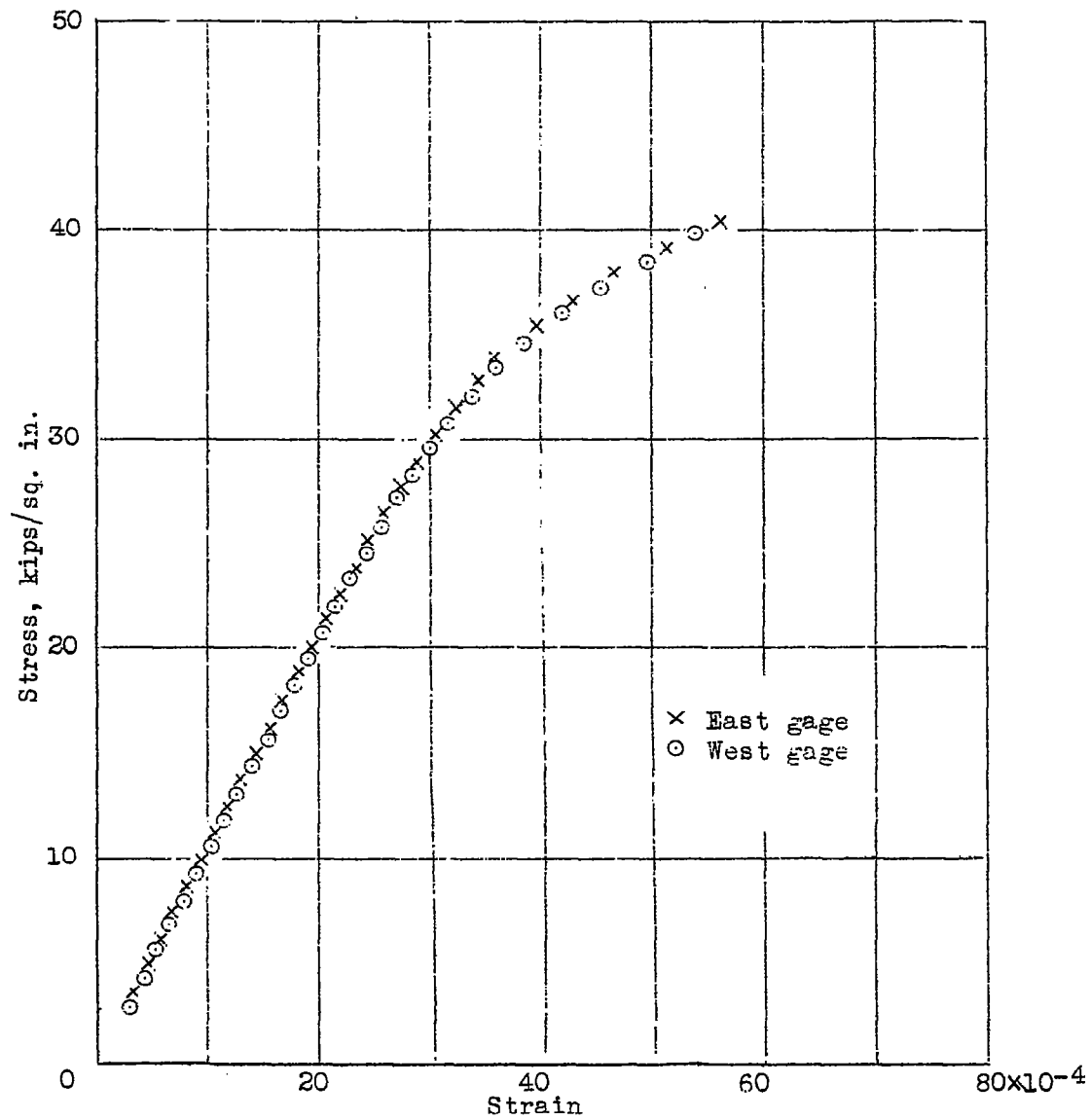


Figure 53.- Compression stress-strain curve of 0.064-in. 24ST Alclad aluminum-alloy sheet loaded in direction of rolling.

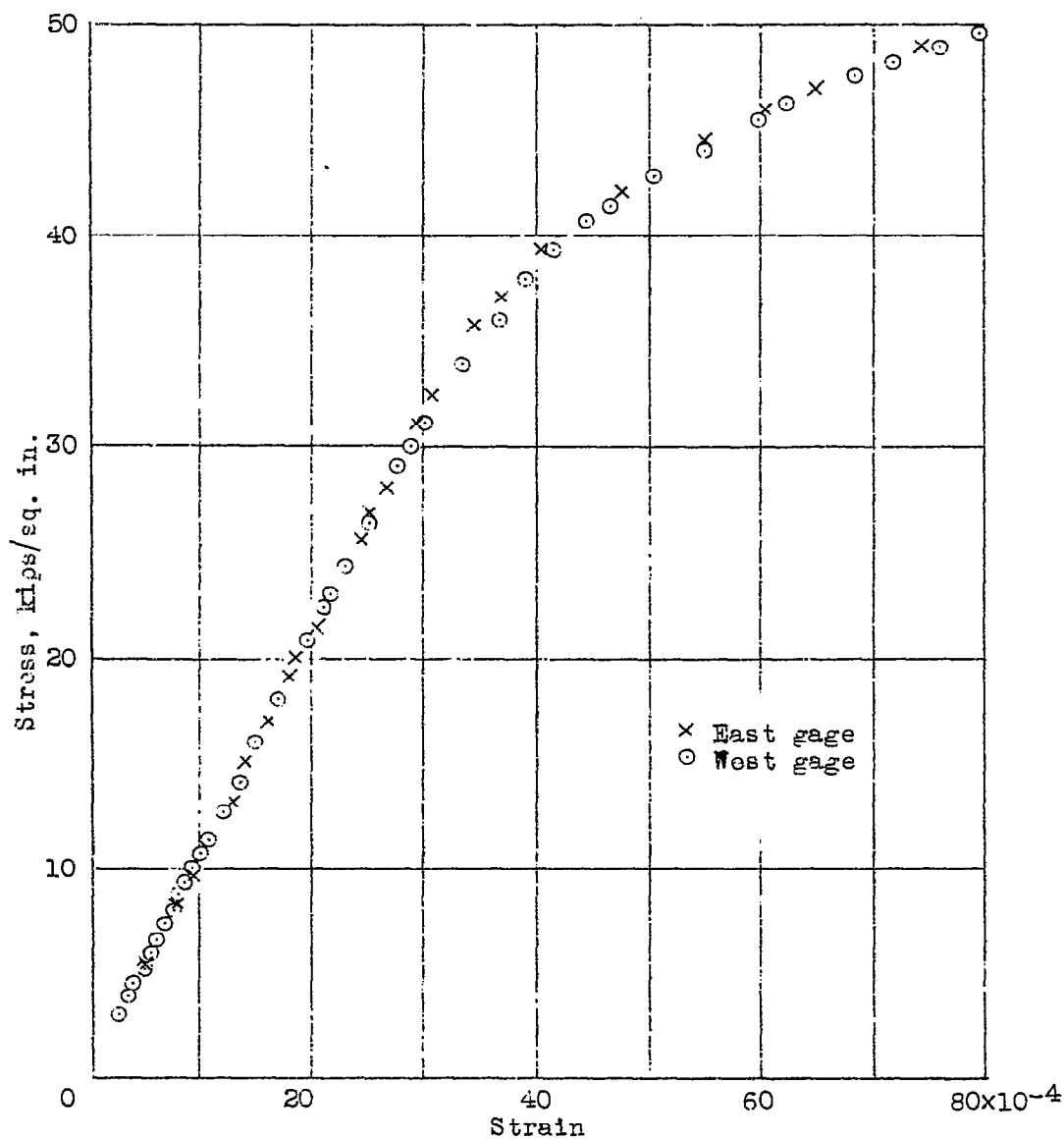
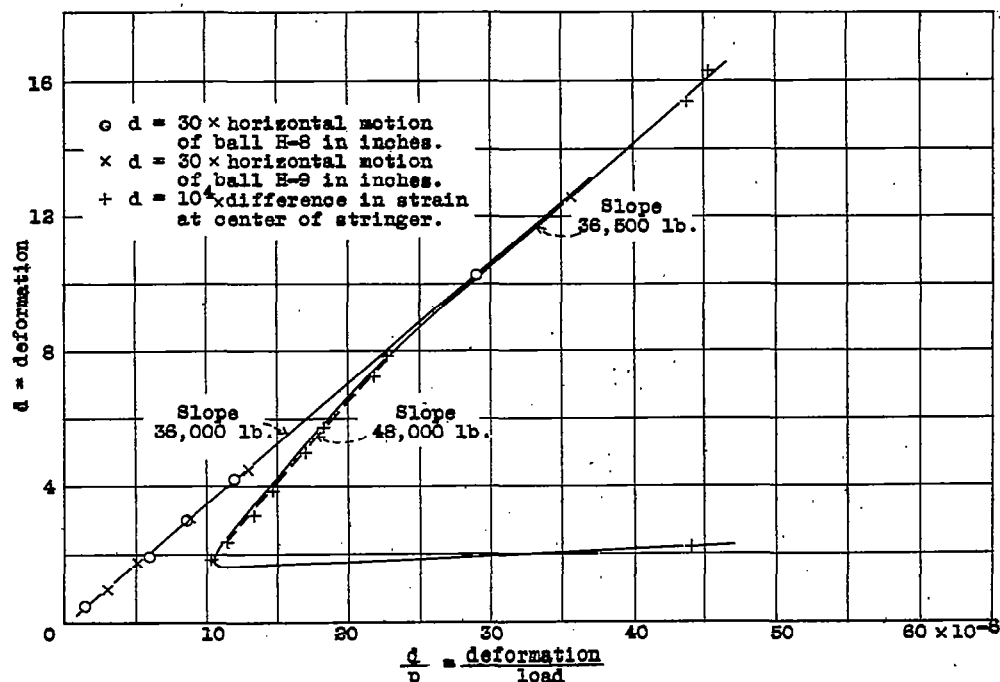
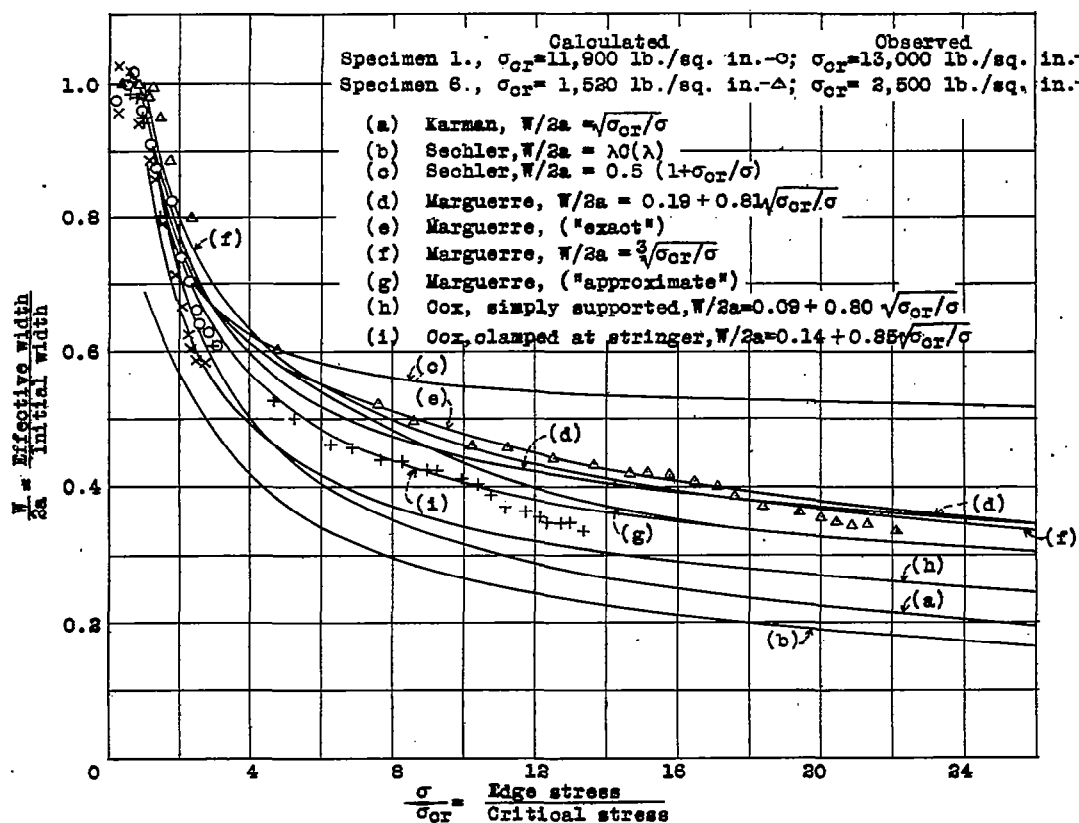
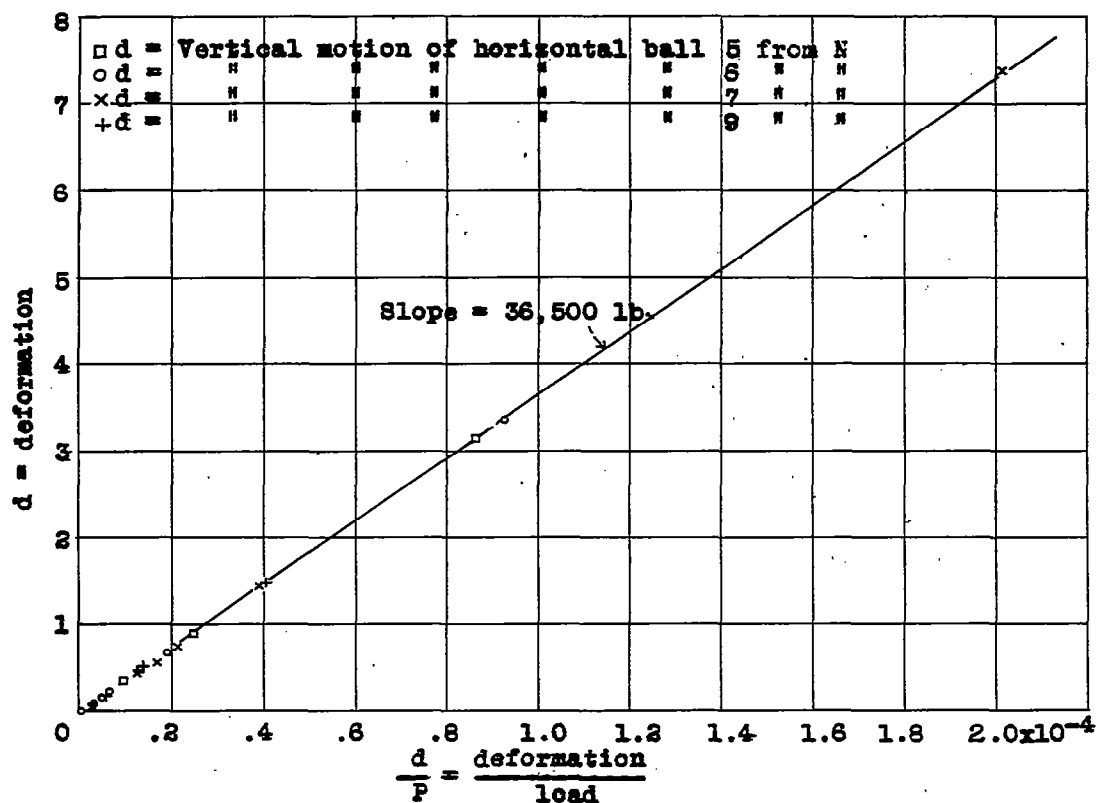


Figure 54.-- Compression stress-strain curve of 0.032 in. 24ST aluminum-alloy sheet loaded in direction of rolling.





Observed buckling load 38,500 lb.
Figure 57.- Southwell's analysis of twisting instability. Stringer A;
Specimen 1.

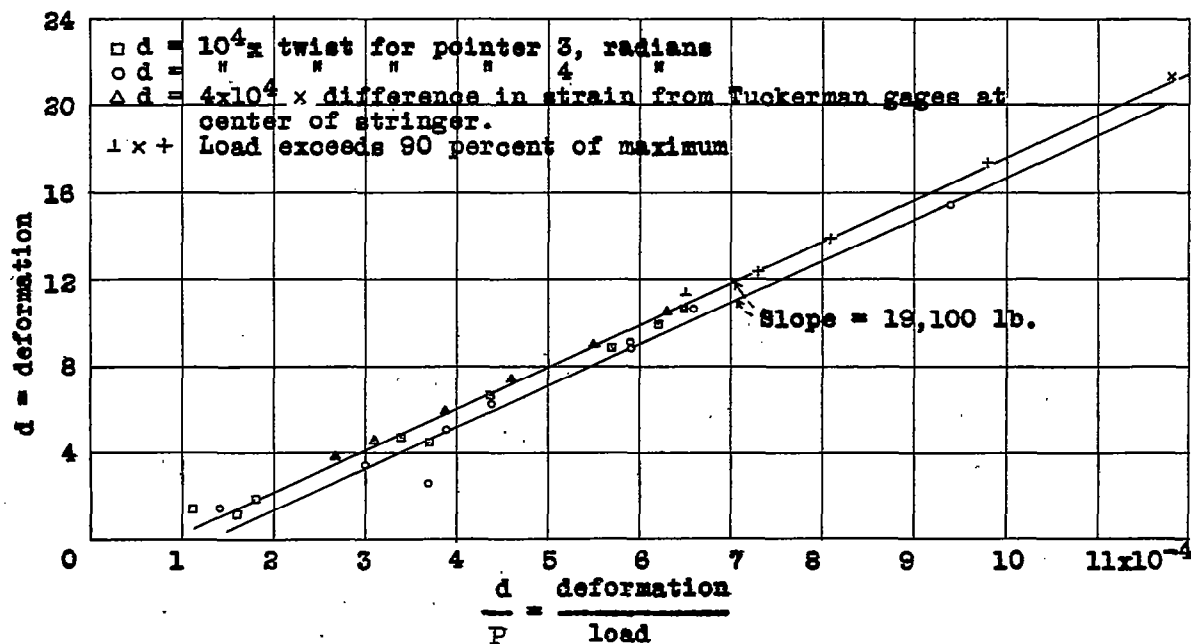


Figure 58.- Southwell's analysis of column instability. Stringer R; specimen 6.

